



UNIVERSIDAD NACIONAL AUTÓNOMA DE MÉXICO
PROGRAMA DE POSGRADO EN ASTROFÍSICA
INSTITUTO DE CIENCIAS NUCLEARES
ASTROFÍSICA TEÓRICA

MODELOS COSMOLÓGICOS Y ASTROFÍSICOS: EL SECTOR OSCURO DEL
UNIVERSO DESCRITO CON CAMPO ESCALAR

TESIS
QUE PARA OPTAR POR EL GRADO DE:
DOCTORA EN CIENCIAS (ASTROFÍSICA)

PRESENTA:
BELEN CARVENTE MENDOZA

TUTOR PRINCIPAL:
DR. DARÍO NÚÑEZ ZÚÑIGA
INSTITUTO DE CIENCIAS NUCLEARES

MIEMBROS DEL COMITÉ TUTOR:
DR. ALDO ARMANDO RODRÍGUEZ PUEBLA
INSTITUTO DE ASTRONOMÍA
DR. JUAN CARLOS DEGOLLADO DAZA
INSTITUTO DE CIENCIAS FÍSICAS

CIUDAD UNIVERSITARIA, CD. MX., JULIO DE 2022



Universidad Nacional
Autónoma de México



UNAM – Dirección General de Bibliotecas
Tesis Digitales
Restricciones de uso

DERECHOS RESERVADOS ©
PROHIBIDA SU REPRODUCCIÓN TOTAL O PARCIAL

Todo el material contenido en esta tesis esta protegido por la Ley Federal del Derecho de Autor (LFDA) de los Estados Unidos Mexicanos (México).

El uso de imágenes, fragmentos de videos, y demás material que sea objeto de protección de los derechos de autor, será exclusivamente para fines educativos e informativos y deberá citar la fuente donde la obtuvo mencionando el autor o autores. Cualquier uso distinto como el lucro, reproducción, edición o modificación, será perseguido y sancionado por el respectivo titular de los Derechos de Autor.

Belen Carvente Mendoza

Modelos cosmológicos y astrofísicos:

el sector oscuro del universo descrito como campo escalar

Tesis de doctorado. Julio de 2022

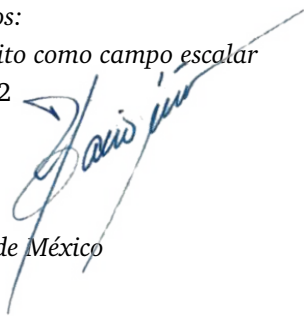
Tutor: Darío Núñez Zúñiga

Posgrado en Astrofísica

Universidad Nacional Autónoma de México

Instituto de Ciencias Nucleares

Ciudad Universitaria, CDMX

A handwritten signature in blue ink, reading "Darío Núñez Zúñiga", is written over the text of the tutor's name and affiliation.

Abstract

While the cosmological content of the Universe have been measured to an amazing accuracy, one of the main question is: Which is the nature of the dark sector? That is, What is the Dark Matter and Dark Energy particle? In this thesis are presented several analyses to incorporate complex scalar fields motivated by potentials coming from particle physics in the context of the dark sector of the Universe. It is presented a general description of the scalar field and the differences between the real and complex fields. Then, it is described the dark matter component of the Universe as a model with two scalar fields, one classical and the other coming from physics beyond the Standard Model of particle physics, exploring via constrains from the effective number of neutrino species the proportions of each field opening the possibility of consider direct and indirect searches for more than one candidate of dark matter. Being an important question the behavior of this dark component, it is presented a scenario with a Subhalo Abundance Matching approach which relates observables from the galaxy with parameters of the halo, letting us to compare the Standard Model of Cosmology, Λ CDM, and several Scalar Field Dark Matter models, allowing us to establish a workable method to study the degeneracy between the suppression of substructures in both types of models. Finally, the exotic matter is explored with a scalar field description. First, in that context, it is presented a Dark Energy model composed by one complex scalar field with a parametric equation of state derived from first principles which allowed us to perform a fitting of some characteristic parameters of the scalar field—for instance, the mass and the autointeraction associated with it—through current observational surveys. Then, we described a solution of the Einstein's equations made of ghost scalar fields which is described by the addition of an angular momentum parameter, named ℓ , providing new analyses of the behavior of the ghost scalar field and a possible description of the dark energy of the Universe.

Along this work, there was described the dark sector of the Universe with several models made of complex scalar fields that were tested with observational survey which allowed us to fit some parameters of the model in question and visualize some of the consequences of any approximation, as the fast oscillation approximation regime.

Keywords — Dark Matter, Dark Energy, Scalar Field, Wormhole, Subhalo Abundance Matching.

Resumen

Si bien el contenido cosmológico del Universo se ha medido con una precisión asombrosa, una de las preguntas principales es: ¿Cuál es la naturaleza del sector oscuro? Es decir, ¿qué es Materia Oscura y Energía Oscura? En esta tesis se presentan varios análisis para incorporar campos escalares complejos motivados por potenciales provenientes de la física de partículas en el contexto del sector oscuro del Universo. Se presenta una descripción general del campo escalar y las diferencias entre el campo real y el complejo. A continuación, se describe la componente de materia oscura del Universo como un modelo con dos campos escalares, uno clásico y el otro proveniente de la Física más allá del Modelo Estándar de partículas explorando, a través de constricciones procedentes del número efectivo de especies de neutrinos, las proporciones de cada campo abriendo así la posibilidad de considerar búsquedas directas e indirectas de más de un candidato a materia oscura. Siendo una cuestión importante el comportamiento de la materia oscura, se presenta un escenario con un enfoque de Coincidencia de Abundancia de Subhalo que relaciona observables de la galaxia con parámetros del halo, permitiéndonos comparar el Modelo Estándar de Cosmología, Λ CDM, y varios modelos de materia oscura de campo escalar, lo cual permitió establecer un método factible para el estudio de la degeneración entre la supresión de subestructura en ambos tipos de modelos. Finalmente, se explora la materia exótica con una descripción llevada a cabo a través de campos escalares. En primer lugar y en este contexto, se presenta un modelo de energía oscura compuesto por un campo escalar complejo con una ecuación de estado paramétrica derivada de primeros principios la cual nos permitió realizar un ajuste de algunos de los parámetros característicos del campo escalar —por ejemplo, la masa y el parámetro de autointeracción asociado con éste— a través de los catálogos observacionales actuales. Luego, describimos una solución de las ecuaciones de Einstein para campos escalares fantasmas descritos a través de la adición de un parámetro de momento angular, llamado ℓ , propocionando nuevos análisis al comportamiento del campo escalar fantasma y una posible descripción de la energía oscura del Universo.

A lo largo de este trabajo se describió el sector oscuro del Universo con varios modelos hechos de campos escalares complejos que fueron probados con sondeos observacionales que nos permitieron ajustar algunos parámetros del modelo en cuestión y

visualizar las consecuencias de considerar aproximaciones, como el régimen de oscilaciones rápidas.

Palabras clave — Materia Oscura, Energía Oscura, Campo Escalar, Agujero de gusano.

Agradecimientos

Podría ser exageradamente breve y agradecer al universo, de forma que no se me escape nadie que haya contribuido activamente en la realización de este trabajo. Intentaré, sin embargo, nombrarles a todas y a todos por la paciencia, amor, financiación, contención, ánimo, correcciones y trabajo conjunto.

Primero, a la UNAM en general y al Posgrado en Astrofísica en particular, por abrirme las puertas de sus institutos, aulas, profesoras y profesores. La educación pública es el único espacio educativo que resulta accesible para las personas que, como yo, pertenecen a la clase media. Al Conacyt por la beca recibida para sostener mis estudios de posgrado. En segundo lugar, a Darío Núñez y Zúñiga, por su dirección paciente y constante durante todo el trabajo realizado. A Aldo Rodríguez Puebla, por la contención en los momentos de crisis, por la sinceridad y el apoyo como profesor, tutor y colaborador. A todos y todas las coautoras de los artículos aquí presentados, cuyas ideas, trabajo y resultados se encuentran plasmados en cada capítulo del trabajo de tesis: Victor Jaramillo, Juan Carlos Degollado, Olivier Sarbach, Celia Escamilla-Rivera, Eréndira Gutiérrez-Luna, Juan Barranco, Catalina Espinoza y Myriam Mondragón. A mi comité sinodal, por aceptar leer mi tesis y hacer valiosas correcciones: Aldo Rodríguez, Celia Escamilla, Myriam Mondragón (de nuevo gracias), Tula Bernal y Argelia Bernal. Para mí fue muy importante que el 80% de ustedes fueran mujeres que han contribuido de manera directa o indirecta a mi trabajo de tesis.

A las mujeres y hombres que han estado conmigo en la cercanía y han combatido a mi lado contra el desgastante síndrome de la impostora y me han ayudado a descubrir que además de científica, soy escritora, amiga y feminista. Espero poderles transmitir mis conocimientos a lo largo del tiempo, porque “la ciencia que no se comunica no es ciencia”. A mis gatos, por estar en cualquier lugar y momento a mi lado, recordándome que necesitamos dormir y comer para seguir siendo entes vivientes. A mi familia, mis profesores y profesoras que me acompañaron durante toda mi educación. Definitivamente todas sus enseñanzas han contribuido activamente a mi forma de hacer y pensar la ciencia.

Contents

1	Introduction	1
1.1	Motivation	1
1.2	Organization of the thesis	2
2	Scalar Field	3
3	Scalar Field Dark Matter	7
3.1	Dark Matter	7
3.2	Scalar field dark matter with two components	8
3.2.1	Scalar field dark matter in particle physics	12
	Axion and axion-like particles	13
	Higgs-like model	17
	Transition from quantum field theory to classical theory.	19
3.2.2	A two scalar field model	23
3.2.3	Cosmological evolution	28
3.2.4	Observational Constrains	32
	Variability on the cosmic ladder	32
	Constraints from N_{eff} and z_{eq}	37
3.2.5	Conclusions	42
3.3	Galaxy–Halo Connection	44
3.3.1	Theoretical framework	45
3.3.2	Suppression relative to CDM from the UV Background	47
3.3.3	Suppression relative to CDM for generic non-CDM models	50
3.3.4	Results	52
3.3.5	Conclusions	59
4	The dark sector of the Universe.	
	Scalar Field Dark Energy	61
4.1	Dark Energy	61

4.2	Complex Scalar Field Dark Energy	62
4.2.1	Complex Scalar Field in an homogeneous background	65
	Friedman equations	65
	The Klein-Gordon equation	66
4.2.2	Dark Energy Solution in the fast oscillation regime	68
	Peculiar branch solution in the fast oscillation approximation	69
	Exact solution for the dark energy term-like	72
	Parametric Equation of State in the late cosmic acceleration approximation	74
4.2.3	Observational constraints	76
4.2.4	Methodology	79
4.2.5	Conclusions	80
4.3	Wormholes	81
4.3.1	Foundations	84
	Metric ansatz	85
	Matter content of the wormhole	85
4.3.2	Stationary Wormhole equations	88
	Qualitative analysis of the solutions	93
	Numerical shooting algorithm	95
	Energy density, mass and curvature scalars	97
4.3.3	Numerical wormhole solutions	99
	0-wormhole	100
	ℓ -wormhole	103
4.3.4	Embedding diagrams and geodesic motion	104
	Geodesic motion	106
4.3.5	Discussion and concluding remarks	110
5	Conclusions	113
	References	115
	Bibliography	135
	List of Figures	137
	List of Tables	141
	Glossary	143

Introduction

1.1 Motivation

While the cosmological content of the Universe have been measured to an amazing accuracy [1], one of the main question is: Which is the nature of the dark sector? That is, what is Dark Matter and Dark Energy? Even more, should we be looking for a single particle or a whole set of “dark” particles. At the present time we have several observations indicating that Dark Matter exists [2, 3, 4, 5] and it is the component of the universe responsible for structure formation and, although there is a main model to describe all that we know as dark matter, there are some differences at small scales between the observations and numerical simulations based on the CDM model. It is well known that most particle dark matter candidates are expected to deviate from the perfectly cold, collisionless fluid and such deviations can be caused by the primordial velocity dispersion, its self-interaction or its quantum nature [6]. Being the dark matter the main responsible for the process of structure and substructure, it is imperative to analyze other candidates that may offer a better description of small-scale structures. The appearance of scalar fields in cosmology has an origin in inflationary models of the early Universe [7, 8, 9, 10], we can implement also the scalar field to explain the other dark component, that responsible for the expansion of the Universe at late times as Dark Energy.

Scalar fields are very important in modern physics, even if they do not exists as the dark sector in fact, the mathematical description used to form models to relieve strong tensions between the observable and the theoretical frames make these scalar fields a possibility worth looking at. Being invariant under coordinate transformations, they are the simplest tensor fields, with order 0. At the moment, and after 40 years of search, the Higgs field is the only scalar field to be detected; discovered in 2012 by the ATLAS and CMS experiments at the Large Hadron Collider, provides the mechanism to endow mass to the particles of the Standard Model of Particle Physics [11].

1.2 Organization of the thesis

Chapter 2

In this section there is a general description of the scalar field, what are the differences between the real and the complex scalar fields and the advantages of each one in terms of the dynamics description.

Chapter 3

This chapter explores the application of the scalar field on the description of the dark matter component. There are two subsections dedicated to different scenarios: first of all, it is presented a model with two classical scalar fields inspired by the Standard Model of Particles mainly differentiated by the mass of the associated particle where it is explored the proportion of each field with constrains from the effective number of neutrino species in order to open the possibility of the search for more than one candidate of dark matter. This work is published at [12]; the second scenario is presented with a Subhalo Abundance Matching model that is based on a statistical approach and the assumption that every galaxy populates a halo of dark matter and, as a consequence, certain observable is related to a parameter of the halo.

Chapter 4

In addition to the Dark Matter, there is another dark component of the Universe that is explored in this chapter: the Dark Energy and other types of exotic matter with a scalar field approach. Then, it is presented a model composed by one complex scalar field which is subjected to observational constrains in order to fit some characteristic parameters of the scalar field through current observational surveys and an equation of state derived from first principles, this model is published in [13]. Additionally, the exotic matter as a scalar field has another possibilities such as a wormhole that, in this case, is described with the addition of an angular momentum parameter, named ℓ . This work is published in [14] and allowed us to analyze the behavior of a ghost scalar field in order to reach new descriptions of this type of fields and a better understanding of the dark energy of the Universe.

Chapter 5

In this section a conclusion of the thesis work is presented.

Scalar Field

” *Baryons, the Standard Model, the everyday stuff?
Us? We are weird, completely abnormal.*

— **Chanda Prescod-Weinstein**

American theoretical cosmologist lead axion
wrangler for the NASA STROBE-X Probe Concept
Study

The last two decades in cosmology and astrophysics research have been an important source of data about the gravitational and evolutionary structure of the Universe [15], which stimulates a demand for approaches beyond the Λ CDM (Lambda Cold Dark Matter), the standard model of cosmological structure formation in the Universe. The physics of the dark sector, roughly 95% of the Universe, has been one of the most intriguing problems of physics. The magnitude of the problem is huge, is there an underlying new physics that describes such dark sector? One cannot discard the existence of new particles with properties that may be exotic in comparison with the current canonical approach to describe this sector.

This is the case for the scalar field, that can be a viable approach to describe the behavior of both components, because it has played an important role in cosmology since its introduction for the first time to explain the inflation phase in the primordial Universe. In the case of dark matter (DM), for instance, some characteristics of the scalar field, such as a nucle cross-section and the cut from the power spectrum at low masses, are particularly interesting features that could solve some of the problems inherent in the cosmological standard model [16, 17]. It is reasonable to presume that dark sector might be describes by a scalar field. In the context of the dark energy, the first suggestions to replace the idea of the cosmological constant were made by Wetterich [18] and Ratra and Peebles [7]; on the other hand, the existence of a scalar field with a very light mass that can have observable consequences in the formation of cosmological structure have been suggested as a viable candidate for dark matter that can potentially solve the well-known problems of the CDM approach (see [19, 20, 21, 22] and references therein).

For a scalar field to behave as a dark component is required to find a scalar potential $V(\varphi)$ with a minimum at some critical value φ_c in which we can define a non-vanishing mass scale m for the associated boson particle via the relation [16]:

$$m^2 \equiv \frac{\partial^2 V(\varphi_c)}{\partial \varphi^2}. \quad (2.1)$$

The simplest possibility of the potential is the quadratic potential

$$V(\varphi) = \frac{1}{2}m^2\varphi^2, \quad (2.2)$$

with the minimum of the potential at the origin. However we cannot discard the presence of higher order, φ^4 , φ^6 , The evolution of the scalar field is described, in the relativistic regime, by the Klein–Gordon equation:

$$\left(\square - \frac{dV}{d|\varphi|^2} \right) \varphi = 0, \quad (2.3)$$

while the non-relativistic regime is described by a Schrödinger-like equation for a wave function ψ . The Eq. 2.1 was one of the first attempts to unify the ideas of quantum mechanics and the theory of special relativity [23] and describes the evolution of a scalar field whose excitations are bosonic particles with zero spin; we have as examples of these particles the π meson, Higgs boson and axions.

The Klein–Gordon equation can be coupled with gravity through the Einstein equations via the Klein–Gordon–equations (KGE), first considered in the context of boson stars which are self-gravitating systems described by complex scalar fields [24, 25]. Even though there exist self-gravitating systems, called oscillatons, described by real scalar fields, they oscillate periodically and, since it is not clear how can be measured these oscillations due to lack of access to the field variable φ , a hydrodynamic approach has been used in several cases for the real scalar field (see, e.g. [26, 16]). Nevertheless, we want to highlight the fact that a scalar field behaves very differently from the behavior of a fluid, so considering these hydrodynamic treatments can result in erroneous interpretations of the variables of a scalar field.

There are a great deal of different approaches to determine the appropriate scalar potential that could adjust to the current cosmological observations, although so far there is no agreement for the correct form. One example is the exponential potential $V(\varphi) = M^4(e^{\alpha\varphi} + e^{\beta\varphi})$ [27] that mimics the dominant density background of Dark Matter but some observational constraints forces the scalar field to never dominate the content of the Universe. Other group of scalar potential has been proposed in order to

have $\rho_\varphi \sim \rho_M$ at $z = 0$, the present, the so-called tracker solutions with potential such as $V(\varphi) \sim \varphi^{-\alpha}$ that reduces the fine tuning and the cosmic coincidence problems but the predicted equation of state does not fit well with the supernovae results. The first attempt to describe the classical evolution of a real scalar with the system of equations KGE and the scalar potential $V(\varphi) \sim \varphi^\alpha$ in an isotropic and homogeneous cosmology was developed by Turner in [19] where $n = 2$ behaves as pressureless matter and $n = 4$ as a radiation. Other scalar potential extensively used to describe the dark sector of the Universe is the quadratic $V(\varphi) = \mu^2|\varphi|^2$, that, in the real scalar case, mimics the cosmological evolution of the Universe predicted by the Λ CDM model [28] but the scalar field undergoes only a matter-like era [29] while the case of a scalar potential with self-interaction, i. e. with the addition of a quartic term to the quadratic scalar field potential $V(\varphi) = \mu^2|\varphi|^2 + \lambda|\varphi|^4$, displays fast oscillations and the field undergoes a radiation-like era followed by a matter-like era [17].

The exact relativistic cosmological evolution of the homogeneous background of a complex self-interacting scalar field described by the KGE system of equations has been considered by [22], in the case of a repulsive interaction, that is a $\lambda > 0$. They showed that the scalar field in this complex case undergoes a stiff-matter era, then the field enters to a radiation-like one, and finally displays a matter-like era. The case of a complex scalar field with a self-interacting potential with $\lambda < 0$ was studied for the first time in [26] and there they found that the scalar field can evolve both the dark components of the Universe: the so-called normal branch where it behaves as a dark matter and a peculiar branch where it mimics the dark energy. The present work is based on the knowledge of the two branches of the quartic potential and it has been applied to the study of a model of two complex scalar fields as dark matter, a single scalar field approach to dark energy and a family of complex and self-interacting ghost scalar fields with an angular momentum-like parameter, the ℓ -wormhole.

The next chapters represent an effort to build a bridge that links some of the results on theoretical Physics with those from the Astronomy, as well as contextualize them in the field of Astrophysics through the scalar field and (astronomical and cosmological) observations. Nowadays, the scalar field is a more often talked about topic in the context of the dark sector of the universe and several recent works in gravitational waves [30] and boson stars [31] suggests that we are close to discerning whether or not these fields exist through observations. So, if the scalar field turns out to be an adequate description of the dark sector of the Universe, we hope that this work will contribute to making this a more noticeable and analyzable possibility in order to answer the key question about the nature of the dark sector.

Scalar Field Dark Matter

” *So important is this dark matter to our understanding of the size, shape, and ultimate fate of the universe that the search for it will very likely dominate astronomy for the next few decades.*

— **Vera Rubin**

American astronomer provider of the first robust evidence of dark matter

3.1 Dark Matter

The existence of dark matter in the universe seems to be one of the most intriguing mysteries of modern cosmology [32] because, in spite of the good agreement between cosmological and astrophysical observations and the theoretical framework constituted by the Λ CDM model, the experimental search of the particle predicted by this hypothesis (the WIMP, weakly interacting massive particle) has been so long and with no results. This pressure exerted on the prevailing hypothesis opens the door to alternative models with predictive ability to explain the behavior of the DM. Scalar field dark matter (SFDM) refers, in general, to the hypothesis that the properties of DM can be represented by a relativistic scalar field φ endowed with an appropriate scalar potential $V(\varphi)$ [16] and, in this chapter are presented two works developing models that take into account scalar fields to describe dark matter that are contrasted against current cosmological observations.

In Section 3.2 it is explored the possibility of incorporating particle physics motivated scalar fields to the dark matter cosmological model [12]. In this landscape, we consider the classical complex scalar field in a certain region in the parameter space of the model which increases the number of neutrino species N_{eff} , in order to be consistent with the observed abundance of light elements produced at Big Bang Nucleosynthesis (BBN). The analyses are performed using one and two scalar fields and the difference

between these models and the priors considered at the edges of the cosmic ladder has been analyzed with the purpose of studying the impact of such models on the Hubble cosmic flow.

In Section 3.3 we use the so called (sub)Halo abundance matching [33, 34], approach to investigate the correlation between galaxies and dark matter halos and its impact of exploring different type of dark matter particles. In particular, we study the potential degeneracy between baryons and dark matter by including the cut at lower masses due to the expected UV background of astrophysical origin and the cut from the power spectrum due the particles different from the standard Λ CDM. Based on [6], we perform an analysis on the star formation histories and abundances of galaxies resulting from the statistical connection of halo and galaxy properties and from different dark matter particles.

3.2 Scalar field dark matter with two components

Introduction

Over the years there has been a remarkable development regarding the studies on the dark matter (DM) component of the Universe. The cosmological observations have been more precise and left no doubt that, within our present understanding of the fundamental interactions, there is in the Universe a component 6.5 times larger than the amount of observed baryonic matter [35] which, except for the gravitational one, has very small interaction with the observable matter and very low electromagnetic emission [36]. Actually, projects as DAMA, CRESST, IceCube and PandaX [37, 38, 39, 40, 41, 42, 43], aimed to the detection of a dark matter particle, have not been able to obtain any detection. We must face the possibility that the interaction of the baryonic or leptonic matter and dark matter, besides the gravitational, be zero. The proposal of modeling the dark matter as a scalar field endowed with a scalar potential of the form

$$V(|\phi|) = \mu^2 |\phi|^2 + \sigma^2 |\phi|^4, \quad (3.1)$$

has grown since the early work discussed in [44] (see also references therein), where it was shown that a real scalar field with a very small parameter, μ , and no quartic term, $\sigma = 0$, could describe a galactic halo and avoid some problems of the standard WIMP model, like the super abundance of satellites predicted by cosmological simulations.

Now a days the proposal has received serious consideration by the community, see for example [45, 16, 46], as several of the benchmarks for a cosmological model have been successfully performed by such model, called ultralight scalar field, as the parameter μ can be related to the mass of the boson particle, m_ϕ , with the expression $\mu = \frac{m_\phi c}{\hbar}$, where c stands for the speed of light in vacuum and \hbar for the reduced Planck's constant, such model has also been called *fuzzy dark matter* [47, 48]. Using this model, it has been possible to reproduce the large scale fiber structure observed in the Universe [49, 50], as well as the observed harmonic structure of the perturbations [51, 52]; the galactic halos and the observed rotational velocity profiles in the galaxies has important developments within this model [53]; the quartic parameter, σ , is interpreted as describing the self-interaction of the field. It is interesting that, if the units of the scalar field, are absorbed in a constant in the Lagrangian, one can consider a scalar field described by a unit-less function and both parameters μ and σ have units of inverse of distance; and as long as the scalar field satisfies the Klein Gordon equation, which is a wave-like description, one can then interpret the parameters as the De Broglie wavelength of the scalar field, λ_ϕ , and the gravitational equilibrium scale [22], allowing us to call such models as *ultra-long wavelength scalar field*. In the manuscript, however, regarding the scalar field we will use the usual unit conventions both to make smoother the passage from the quantum field theory (QFT) to the classical one and to make the cosmological analysis in the usual way, but the idea deserves further studies.

Models considering a complex scalar field for describing the dark matter (and even the dark energy, see [13]) have also been considered and have proved to be excellent models, giving a consistent description of the Friedman homogeneous Universe [22] (we are using the direct transliteration from the Russian name), with a scalar potential as in Eq. (3.1), showing that the μ parameter needs not to be very small, it is enough to demand that $m_\phi > 10^{-21} \text{ eV}/c^2$, due to the presence of the quartic term σ [22, 26] which is strongly constrained in terms of the combination σ^2/μ^4 , proportional to the gravitational length scale that σ defines, which turns out to be ultra-long, of the order of kiloparsecs [22, 26]. These scalar fields are considered completely non-interacting with other types of matter, we will call them *classical scalar fields*. There is a growing conviction not only that scalar fields are very plausible candidates to describe the dark matter present in the Universe, but that objects described by such scalar fields are very plausible to exist in Nature. Models considering a real scalar field have also been considered in large scale Cosmology, see [54] for instance, but they induce the wave oscillation to the spacetime structure, as in the case of the compact objects they form, called *oscillatons* [55], and such oscillation in the scale factor could impose strong constraints on the value of the real scalar field parameters. In this work, we will

consider complex scalar fields which do not present such oscillations in the geometry of the spacetime.

The cosmological model with ultra-long wavelength, classical complex scalar field, is a serious alternative to the standard Cold Dark Matter model, where the dark matter is treated as a pressure-less fluid of WIMPS [36].

Such classical scalar fields, as long as they are considered completely non-interacting with any other field or particle, save via the gravitational interaction, of course, can be incorporated to the Standard Model of particle physics (SM), along with the other dark matter scalar field models such as the axion or the Higgs-like, which, in the classical limit, can be also described as a complex scalar field with a scalar potential as given above but with different values of the parameters μ and σ . One can naturally ask, how much of them, axions or Higgs, can be present along with the classical one without spoiling the successes already obtained by the model which considers only the classical component.

The main goal of this paper is to shed light on this question and, therefore its consequences at cosmological scales. As mentioned above, matter classically described by a complex scalar field with very large values of the mass parameter, of the order of eV , keV , or even hundreds of GeV [56, 57, 58, 59, 60, 61, 62, 63, 64, 65, 66, 67, 68] (corresponds to a wavelength of 10^{-7} , 10^{-10} , 10^{-16} m respectively) could exist in Nature as constituents of dark matter and be part of the general content of the Universe, but how much of an Higgs-like or an axion field could be a component of the observed dark matter? Indeed, there is no reason to consider that the dark matter sector should be described by a single type of matter; we could have the classical as well as other scalar fields included in the computation of the dark matter density. Such considerations could reduce some pressure to the groups in direct search of dark matter, mentioned above, as long as heavier scalar fields, which are the ones usually searched for, might not be the total of the dark matter density and thus, the detection probability reduces in a significant amount. In the present work we will consider that the dark matter sector of the Universe is described by two complex scalar fields.

The passage from a particle physics model with foundations in a quantum field theory to a semiclassical description is often assumed obvious in the literature. For the sake of clarity of the expositions in the following sections we give a brief argument on this matter. In order to study the cosmological implications of such quantum models, a clean path to follow is to first take the classical limit in order to be able to embed the corresponding models classical fields into a gravitational action, by coupling them in a

minimal way to the gravitational field. Next we simply assume that these fields obey semiclassical equations of motion, for the case of the scalar fields considered in this work these would be the Klein-Gordon equation. Finally, we study the cosmological implications of the resulting setups. Of course, in practice it is sufficient to identify the field content of the quantum model and pass directly to the semiclassical equations, but we feel it is important to give a slightly more formal argumentation for this step (we also expand briefly on the classical limit of a QFT in section 3.2.1).

In section 3.2.1 we part from the particle physics and discuss how the axion-like or the Higgs-like particles can be described by a complex scalar field with a scalar potential of the type described above in the semi-classical limit, discussing also the range of values of the parameters of the potential. In section 3.2.2 we describe the homogeneous Friedman model with two such scalar fields and the integration procedure of the field equations. This approach based on [22] will be generalized to solve for the negative self-interaction fully relativistic scalar field, that is, for the one that behaves like dark matter. Then, in section 3.2.3 we present the evolution of certain reference cases for the classical, axion and Higgs-like scalar field models.

After representative single scalar field cases are presented, we will show some of the solutions for the combinations classical+axion and axion+Higgs, where a new parameter k will enter since we need to fix the relative fraction of energy density of each of the fields at late times with respect to the total dark matter.

In section 3.2.4 we present the results of this work, namely, the cosmological effects of considering as part of the matter content the scalar fields described in the previous sections as well as specific cosmological constrains for the two scalar field parameters. In subsection 3.2.4 we examine the variability between the two scalar field models and the priors considered at the edges of the cosmic ladder, namely the H_0 value at early and late times [69], obtaining that they have a clearly different behavior depending on the combination of the two scalar fields taken into account. Although this is not an attempt to solve the tension of H_0 , it will provide us a hint of the behavior of this two scalar field combination in order to know which of that combinations can be fitted through astrophysical observations. Next, in subsection 3.2.4 we present a discussion on how the number of neutrino species N_{eff} together with the requirement of the scalar field to behave as matter at the matter-radiation equality sets a very restrictive condition on the parameters of the model.

In the concluding section 4.2.5 we summarize the more relevant results and a discussion on the implications on direct dark matter detection programs as well as in the cosmological and astrophysical dark matter research.

3.2.1 Scalar field dark matter in particle physics

The Standard Model of particle physics describes the phenomena observed so far in elementary particle physics with very good precision. However, this successful model can only help us to understand about 5% of the total matter in the Universe. It is assumed to be the low energy limit of a more fundamental theory, and must be extended to explain other phenomena like neutrino masses, matter-antimatter asymmetry and even dark matter.

The remaining components in the Universe, called dark matter and dark energy, which make up about 27% and 67% of the total matter in the Universe, respectively [35], do not find an explanation in the framework of the SM but their existence is inferred from its gravitational effects in the astrophysical observations [70, 71]. Beyond the facts relating to the temperature and longevity of the dark matter, we have very little information about its nature and properties. In addition, the lack of experimental evidence in the search for the most popular candidates such as WIMP, sterile neutrinos or dark photons, makes evident the need for new models and search techniques for possible DM candidates. The dark matter may well consist of one or more types of fundamental particles. The simplest fundamental particle is a scalar field (particles with zero spin).

Among the most common candidates to scalar field dark matter (SFDM) in particle physics are axions, axion-like and Higgs-like particles. In particular, we are interested in a model that includes two scalar fields. We will consider here one of the candidates to come from an inert scalar $SU(2)$ doublet, *i.e.* Higgs-like, motivated by some extensions of the SM, where this proposal has been successful [72, 73, 74]. A second candidate may be an axion or axion-like particle coming from particle physics or cosmology [68, 75], and both will be worked along with the classical complex scalar field mentioned in the introduction.

Axion and axion-like particles

The word axion can take on a variety of meanings. The first time was used to name the particle associated to the Peccei-Quinn (PQ) mechanism for preserving Charge-Parity (CP) symmetry in the strong interactions [76, 77, 78]. Legend says that F. Wilczek, who was looking for a name to describe a new pseudo Goldstone boson, while washing clothes, looked at the name of the detergent he was using, *axion* and decided to use that name for the new particle, since he expected it would clean up the problem of QCD with CP symmetry.

Parity (P) is the space reflection operator, i.e. inverts the spatial coordinates, $P : \vec{x} \rightarrow -\vec{x}$ and the charge conjugation operator (C), changes particles into antiparticles without affecting their momenta or spin [79]. In a decay, the combined transformation CP changes particles to antiparticles and the sense of longitudinal polarization is reversed. If, the rate for one decay and its conjugate are the same, we have that the CP symmetry is conserved.

In quantum field theory, the term axion applies to any pseudoscalar Goldstone boson of the spontaneous breaking of one global chiral symmetry that is broken at some scale f_a . Such particles need not solve the strong CP problem or couple to gluons [75]. This means their mass could take any value and be very weakly coupled which makes them difficult to detect experimentally. These Goldstone bosons that do not acquire a mass from radiative corrections of Quantum Chromodynamics (QCD) are also called axion-like-particles (ALPs).

In string theory the term axion can refer either to matter fields, or to pseudoscalar fields associated to the geometry of compact spatial dimensions [68]. From now on, we will use the word axion to refer to a pseudoscalar field in any of the theories mentioned above.

The axion acquires mass from QCD chiral symmetry breaking, and can be calculated in chiral perturbation theory [77, 68],

$$m_a \approx 6 \times \mu\text{eV} \left(\frac{10^{12}\text{GeV}}{f_a} \right). \quad (3.2)$$

This expression is a model-independent statement. The axion decay constant f_a is related to vacuum expectation value v_a , that breaks the Peccei-Quinn symmetry $f_a = v_a/N_{DW}$. N_{DW} is an integer that characterizes the vacuum of axion models called *color anomaly*, also known as the *domain wall number* [80, 81]. We can infer from the

Eq. (3.2), that if f_a is large enough, the axion can be highly light and stable which, added to the very weak interaction with the rest of matter, makes an excellent DM candidate [68, 81, 75].

We will focus on the QCD axion models where there are in general three types:

- The Peccei-Quinn-Weinberg-Wilczek (PQWW) axion, which introduces one additional complex scalar field only.
- The Kim-Shifman-Vainshtein-Zakharov (KSVZ) axion, which introduces heavy quarks as well as the Peccei-Quinn scalar.
- The Dine-Fischler-Srednicki-Zhitnitsky (DFSZ) axion, which introduces an additional Higgs field as well as Peccei-Quinn scalar.

In these three types, the Lagrangian of each model is taken to be invariant under a global $U(1)$ symmetry, that is spontaneously broken at one scale f_a by the potential, $V(\varphi) = \lambda_{\text{QCD}} (|\varphi|^2 - f_a^2/2)^2$ where φ is the Peccei-Quinn field and takes a vacuum expectation value (*vev*) $\langle \varphi \rangle = f_a/\sqrt{2}$. In the PQWW model, $f_a \approx 250$ GeV, this scale is accessible to experimental search and given the absence of signals, this axion is excluded by collider experiments. In KSVZ and DFSZ models the decay constant is a free parameter and can be made large enough such that they are not excluded.

After the global $U(1)$ symmetry breaking at some scale f_a , one angular degree of freedom appears as $\langle \varphi \rangle e^{i\Phi_a/f_a}$. The field Φ_a , is the axion and it is a pseudo Nambu-Goldstone boson of this broken symmetry.

At the classical level the Lagrangian is invariant under chiral rotation, which leads to the shift symmetry of the axion field, $\Phi_a \rightarrow \Phi_a + \text{const}$. But at quantum level non-perturbative physics becomes relevant, e.g. instantons switch on at some particular energy scale Λ_a and break the shift symmetry $\Phi_a \rightarrow \Phi_a + \text{const}$, inducing a potential for the axion. However, the potential must respect the residual discrete shift symmetry, $\Phi_a \rightarrow \Phi_a + 2n\pi f_a/N_{\text{DW}}$, for some integer n , which remains because the axion is still the angular degree of freedom of a complex field.

The axion potential generated by QCD instantons is,

$$V_a(\Phi_a) = \Lambda_a^4 \left[1 - \cos \left(\frac{N_{\text{DW}} \Phi_a}{f_a} \right) \right], \quad (3.3)$$

where Λ_a is the non-perturbative physics scale, N_{DW} is the domain wall number and f_a the PQ symmetry breaking scale. If $N_{\text{DW}} > 1$, there appear domain walls that can

quickly dominate the energy density of the early Universe, which is incompatible with standard cosmology and can be avoided if N_{DW} is taken equal to unity [80, 68].

On the other hand, if we consider only small displacements from the potential minimum $\Phi_a < f_a$, we can expand it as a Taylor series, whose approach to second order is $V(\Phi_a) \approx \frac{1}{2}\Lambda_a^4\Phi_a^2/f_a^2$. We identified the mass term $\frac{1}{2}m_a^2\Phi_a^2$, with $m_a^2 = \Lambda_a^4/f_a^2$.

We will adopt as potential for axion, in subsequent analyses on axion as a dark matter candidate, only the first and second term of the Taylor series around the minimum potential, this is,

$$V_a(\Phi_a) = \frac{1}{2} \left(m_a^2 \Phi_a^2 - \frac{1}{12} \frac{m_a^2}{f_a^2} \Phi_a^4 \right). \quad (3.4)$$

The axion mass is protected from quantum corrections, since these all break the underlying shift symmetry and must come suppressed by powers of f_a . For the same reason, self-interactions and interactions with SM fields are also suppressed by powers of f_a . Regarding the self-interactions, we can easily obtain an expression for them by means of an expansion of the cosine potential to higher orders. This renders an axion model with a light (less than meV), weakly interacting, long-lived particle. These properties are protected by a underlying symmetry, so the axion provides a natural candidate to DM model [75].

Some values for the decay constant could be lie around the fundamental scales of particle physics such as Grand Unified Theory (GUT) scale $f_a \sim 10^{16}$ GeV. Given the lack of knowledge at high-energies¹ structure of particle physics and the difficulties in obtaining well-defined measurements of the initial conditions in inflationary cosmology, there are no strong reasons to prefer any particular value for f_a . But usually $f_a \lesssim M_{\text{pl}} \sim 10^{19}$ GeV, since it is not obvious how to make a model of such an axion without a full understanding of quantum gravity [68, 62, 75].

A cosmological populations of axions can be produced by various mechanisms, but the main ones are: decay of parent particle, decay product of topological defect, thermal population from the radiation bath and vacuum realignment [68].

In the case of decay of parent particle, a massive particle with m_X , is coupled to axion and decays. In all cases $m_X > m_a$ and their decay produces a population of relativistic axions. If the decay occurs after the axions decoupled from the SM then they remain relativistic throughout the history of the Universe and become dark radiation [75].

¹By high-energies we mean any symmetry breaking scale $\gtrsim 1$ TeV.

In the case of decay product of topological defect, two scenarios need to be considered: whether the Peccei-Quinn phase transition occurs during or after inflation.

The breaking of global symmetries leads to the formation of topological defects. A broken $U(1)$ creates axion strings and if $N_{DW} > 1$, domain walls appears too [80]. If PQ symmetry is broken during inflation, topological defects and their decay products are diluted by the expansion of the Universe and can be ignored.

In the second stage, after inflation, the PQ symmetry is broken when the radiation temperature drops below f_a . The breaking of the global symmetry gives rise to topological defects and the string decay produced axions. The axion field begins oscillating when $m_a \sim H$, this axions are dominated by the low-frequency modes, making them non-relativistic and contributing as CDM to the cosmic energy budget [68].

If axions are in thermal contact with the standard model radiation, these are created and annihilated during interactions among particles in the primordial soup. The axions established in this way are called thermal axions. Initially, axions are in equilibrium with the thermal bath of particles, but later become decouple at temperature T_D . Thermal axions are relativistic if $T_D > m_a$. Once decoupled the axion population is merely diluted and redshifted by the expansion of the Universe [81], then the axions become non-relativistic when its temperature is less than m_a . For $f_a > 10^9$ GeV, the thermal axion lifetime exceeds by many orders of magnitude the age of the Universe [81], but behave cosmological in a manner similar to massive neutrinos, and contribute as hot DM [68] suppressing cosmological structure formation.

In the case of misalignment production, we need to consider the equation of motion for the axion after non-perturbative effects, $\ddot{\Phi}_a + 3H(t)\dot{\Phi}_a + m_a^2\Phi_a = 0$. It is the equation of a simple harmonic oscillator with $3H(t)$ time dependent friction. $H(t)$ is the Hubble parameter. When $H > m_a$, the axion field is overdamped and it is frozen by Hubble friction, this means that the expansion of the Universe slows the axion field down ($\dot{\Phi}_a = 0$) and we get a coherent state of axions at rest [68].

The misalignment production of axions is non-thermal and through this mechanism, even very light WIMPs can be Cold Dark Matter [81].

Axion and ALPs could be located through axion-photon conversion in external electric (\vec{E}) or magnetic (\vec{B}) fields [82], described by the Lagrangian

$$\mathcal{L}_{A\gamma\gamma} = g_{A\gamma\gamma}\Phi_a\vec{E}\cdot\vec{B}, \quad (3.5)$$

where $g_{A\gamma\gamma}$ is the diphoton coupling constant. Pseudoscalar-ALPs and scalar-ALPs could be created when a beam of linearly polarized photons propagates in a transverse magnetic field \vec{B} . If an optical barrier is placed downstream to the beam, all unconverted photons will be absorbed while ALPs would traverse the optical barrier. By applying a second magnetic field in the regeneration domain beyond the wall, the inverse process can convert the ALPs back into photons, which can be subsequently detected [58]. This type of arrangement is called Light-Shining-through-Walls (LSW) experiment and the best current limit has been achieved by the OSQAR (Optical Search for QED Vacuum Birefringence, axions and Photon Regeneration) experiment, with the exclusion limits $|g_{A\gamma\gamma}| < 3.5 \times 10^{-8} \text{ GeV}^{-1}$ at 95% confidence limits, obtained in vacuum for $m_a \lesssim 0.3 \text{ meV}$ [58]. Other exclusion limits for pseudoscalar and scalar axion-like-particles can be found in [63, 83, 64, 65, 66, 84, 67, 59, 56].

In addition to the possible connection to DM, two hints from astro-particle physics strengthen the axion-like particles existence: the anomalous excessive cooling of stars and the anomalous transparency of the Universe to very high energy gamma rays. The cooling excess can be attributed to ALPs, produced in the hot cores that abandoning the star unimpeded, contributing directly to the energy loss [85, 86, 87]. The anomalous transparency can be explained if a part of the photons are converted into light spin zero bosons in astrophysical magnetic fields. The ALPs can travel through cosmological distances unhindered, due to their weak coupling to normal matter. A part of such light bosons are in turn reconverted into high-energy photons and could be detected [88, 89].

Higgs-like model

The Lagrangian density of the Standard Model can be explicitly divided into gauge, fermion, Higgs and Yukawa sectors. The Higgs part is $\mathcal{L}_\varphi = (D^\mu\varphi)^\dagger D_\mu\varphi - V(\varphi)$, where $\varphi = \begin{pmatrix} \varphi^+ \\ \varphi^0 \end{pmatrix}$ is a Higgs scalar, transforming as a doublet of $SU(2)$, φ^\dagger is its adjoint. φ^+ and φ^0 are charge and neutral complex fields and D_μ is the gauge covariant derivative. $V(\varphi)$ is the Higgs potential, the combination of $SU(2) \times U(1)$ invariance and renormalizability restricts V to the form

$$V(\varphi) = \mu^2\varphi^\dagger\varphi + \lambda(\varphi^\dagger\varphi)^2. \quad (3.6)$$

For $\mu^2 < 0$ there will be spontaneous symmetry breaking and the nonzero *vev* of neutral component φ^0 will generate the W and Z masses. The λ term describes a quartic self-interaction $\lambda(\varphi^\dagger\varphi)^2$ of the Higgs field. Vacuum stability requires $\lambda > 0$ [79].

A very useful proposal to explain some particle physics open questions, such as the small mass of the neutrinos [90], the fermionic mixing [91, 92] and dark matter [72, 73, 74] is the extension of the Higgs sector of the SM, which consists of the introduction of new symmetries, plus the addition of scalar singlets and/or doublets in \mathcal{L}_φ . After the break of the electroweak symmetry, the extra scalar fields acquire mass and are known as Higgs-like particles.

Particularly, dark matter can be explained with inert Higgs scalars, i.e. that do not acquire a *vev*, are stable and cannot decay to SM particles. The stability is usually achieved by introducing an extra Z_2 discrete symmetry [57].

We will adopt for our study a model with an inert Higgs doublet (an equivalent analysis can be done considering a singlet complex scalar field), besides the usual SM one,

$$\Phi_h = \begin{pmatrix} \Phi^+ \\ \Phi^0 \end{pmatrix} = \frac{1}{\sqrt{2}} \begin{pmatrix} \Phi_1 + i\Phi_2 \\ \Phi_3 + i\Phi_4 \end{pmatrix}, \quad (3.7)$$

where Φ^+ and Φ^0 are the charged and neutral complex components of the field Φ_h , respectively, which can also be expressed in terms of their real parts, Φ_i , $i = 1, 2, 3, 4$; whose potential is of the form,

$$V_h(\Phi_h) = m_h^2(\Phi_h^\dagger\Phi_h) + \frac{\lambda_h}{2}(\Phi_h^\dagger\Phi_h)^2, \quad (3.8)$$

where we will choose $m_h^2 > 0$ [72, 92] and none of the components acquire a vacuum expectation value. We are assuming that the coupling between the inert doublet and the SM Higgs is very small. The DM candidate must come from the neutral complex component, Φ^0 . It is known from DM experimental searches that this type of matter must be electromagnetically neutral, since the mediator of electromagnetic interaction is the photon and the dark matter is considered to be transparent to light.

In general, the mass of the Higgs-like DM candidates depend largely on the model, for example if they have couplings to the SM fields. But the mass constraints in the experimental search for extra Higgs fields usually lies around the order of GeV. The most recent mass limits for a variety of models with extra neutral Higgs bosons can be found in [56, 60, 61].

The DM candidate, among the massive states coming from the doublet Φ_h , will be the neutral lightest and stable particle (whose decay is protected by some symmetry).

The consistency of a Higgs-like dark matter model can be checked with the dark matter relic abundance [61]. According to the WIMP paradigm, the dark matter candidate has weak interactions with the SM particles and was in thermal equilibrium in the early stages of the history of the Universe. Subsequently, the interaction rate of the DM fell below the Hubble expansion rate causing the freeze-out of the DM [93].

To avoid any confusion, we want to make it clear that in the following, when referring to Higgs particles, we refer to Higgs-like particles (Φ_h), they are different from the SM Higgs doublet (φ).

Axions, axion-like and Higgs-like particles are excitations of quantum fields, however, the interest in this work is to analyze the behavior of these particles on a cosmological scale, where the DM candidates are treated in a classical way. Thus, we need to make a transition from quantum to classical theory. This transition can be studied within the framework of an effective action. This topic is described in the next sub-section.

Transition from quantum field theory to classical theory.

Consider a QFT with lagrangian density $\mathcal{L} = \mathcal{L}_0 + \mathcal{L}_{\text{int}}$. For the purpose of this section it is sufficient to consider the example of one scalar field $\phi(x)$. In the context of a microscopic theory, it is very important to determine the Scattering matrix or S -matrix, since its knowledge allows one to compute observable quantities like annihilation/scattering amplitudes for particles including e.g. DM candidates, that can be compared to observations of indirect/direct DM detection experiments.

We can compute the S -matrix in terms of the n -point Green's functions of the theory:

$$G(x_1, x_2, \dots, x_n) = \langle \Omega | T (\phi(x_1) \cdots \phi(x_n)) | \Omega \rangle, \quad (3.9)$$

with $|\Omega\rangle$ the vacuum of the interacting theory and T denotes the time-ordering operator. In the path integral formalism these functions are encoded in the generating functional $Z[J]$ through the expression:

$$G(x_1, x_2, \dots, x_n) = (-i)^n \frac{\delta}{\delta J(x_1)} \frac{\delta}{\delta J(x_2)} \cdots \frac{\delta}{\delta J(x_n)} Z[J] \Big|_{J=0}, \quad (3.10)$$

where $J(x)$ is an external source² and the derivation is functional. The path integral representation of $Z[J]$ is given by:

$$Z[J] = N^{-1} \times \int D\phi \exp \left\{ i \int d^4x (\mathcal{L}(\phi(x)) - \phi(x)J(x)) \right\}, \quad (3.11)$$

with $N = \int D\phi \exp\{iI[\phi]\}$ and $I[\phi] = \int d^4x \mathcal{L}(\phi(x))$. In cases where there are no interactions, the path integral can be evaluated in closed form taking the free generating functional as:

$$Z_0[J] = \exp \left\{ -\frac{i}{2} \int J(x) \Delta_F(x-y) J(y) d^4x d^4y \right\}, \quad (3.12)$$

where $\Delta_F(x-y)$ is the free Feynman propagator.

If interactions are present, no closed form of the generating functional is known. However, in this case $Z[J]$ satisfies the differential Schwinger-Dyson equation:

$$-i(\square + m^2) \frac{\delta Z[J]}{\delta J(x)} - \mathcal{L}'_{\text{int}} \left(-i \frac{\delta}{\delta J(x)} \right) Z[J] = J(x) Z[J], \quad (3.13)$$

where m is the scalar field mass. The term \mathcal{L}' denotes the differentiation of \mathcal{L}_{int} with respect to ϕ and evaluated on $\phi \rightarrow -i \frac{\delta}{\delta J(x)}$; the functional differentiation with respect to $J(x)$ acts on $Z[J]$. The solution to the above equation (up to a normalization factor) can be expressed formally in terms of the free generating functional as:

$$Z[J] = \exp \left\{ \left[i \int d^4x \mathcal{L}_{\text{int}} \left(-i \frac{\delta}{\delta J(x)} \right) \right] \right\} Z_0[J]. \quad (3.14)$$

The exponential in this equation is expressed as a power series in the coupling constant. This procedure is equivalent to the Feynman diagram perturbation theory, thus $Z[J]$ generates all diagrams including disconnected ones.

There is a generating functional $W[J]$, which generates only connected Feynman diagrams (or connected Green's functions). The connected generating functional $W[J]$

² $J(x)$ is a number of functions of spacetime which transform in such way that $\sum J(x)\phi(x)$ is an invariant [94].

relation to Z is through exponentiation (switching to normal units to make explicit Planck's constant):

$$Z[J] = e^{\frac{i}{\hbar}W[J]}. \quad (3.15)$$

The effective action $\Gamma[\bar{\phi}]$ from W using the Legendre transformation is

$$\Gamma[\bar{\phi}] = W[J] - \int d^4x \frac{\delta W[J]}{\delta J(x)} J(x), \quad (3.16)$$

here the following notation has been introduced:

$$\frac{\delta W[J]}{\delta J(x)} \equiv \bar{\phi}, \quad (3.17)$$

where $\bar{\phi}$ is called the average (or classical) field. $\Gamma[\bar{\phi}]$ generates single particle irreducible connected diagrams. This is a simple example of a working analogy where the effective action is the analogue of the Gibbs potential in equilibrium statistical mechanics in the presence of coupling to an external source or J -reservoir.

The usefulness of the effective action has been shown extensively in the literature [94], we will concentrate on its loop expansion for this work. As shown in Ref. [95], the effective action can be expressed as a series expansion in loops where the n -loop term is proportional to \hbar^n :

$$\Gamma[\bar{\phi}] = I[\bar{\phi}] + \frac{1}{2}i\hbar \ln \det(i\mathcal{D}^{-1}) + \mathcal{O}(\hbar^2), \quad (3.18)$$

where \mathcal{D} is the propagator for a “modified” action, i.e. the action for the original theory expanded around the average field but keeping only terms of second and higher order. For our present purposes, it suffices to notice that in the limit $\hbar \rightarrow 0$ the effective action reduces to the tree level action $I[\bar{\phi}]$, as expected. Thus, the classical limit of a given theory corresponds to the 0-loop term in the quantum effective expansion. It is thus natural to take, for example, the expression for the tree level potential of a given particle physics quantum model and couple the corresponding classical fields to gravity as a starting point for an analysis in the context of a cosmological model.

Regarding the quartic parameters, the ones in the classical action will match the zeroth-order quantum parameters in the effective expansion. Furthermore, if we assume that quantum corrections are small, the quartic couplings have to lie within the interval $-4\pi < \lambda < 4\pi$, to ensure perturbative unitarity at the quantum level. Then, the

following question arises: Can the physical values of the quartic couplings in the scalar potential, constrained from particle physics, have consequences on the cosmological parameters? We will show that in the Higgs-like case, the interval for λ implies that this field belongs to the cosmological non self-interacting regime.

The dark matter candidates we have reviewed here, axion, axion-like and Higgs-like, are considered as real scalar fields in the classical limit. However, a more general and appropriate approach in the cosmological framework is to take them as complex scalar fields. Since the halos formed by complex scalar field are stationary gravitational solitons known as boson stars, which are stable [96] compact objects. On the other hand, the halos in the case of a real scalar field, known as oscillatons [97], are metastable oscillating solutions.

In the case of a Higgs-like particle, it is not entirely correct to say that the classical limit is a real scalar field; as it happens, in this particular case this limit is a complex scalar field. The transition from a real quantum field to a complex classical field can be understood as follows.

Consider a generic doublet of $SU(2)$, denoted by

$$H = \begin{pmatrix} H^+ \\ H^0 \end{pmatrix} = \frac{1}{\sqrt{2}} \begin{pmatrix} H_1 + iH_2 \\ H_3 + iH_4 \end{pmatrix}, \quad (3.19)$$

where H^+ and H^0 are charged and neutral complex components of the Higgs field, respectively. The DM candidate must come from H^0 , as described in the subsection 3.2.1. In the quantum scenario, in a first stage, some mechanism at a high energy scale (for instance, the breaking of a symmetry) will give mass to the components H_i , $i = 1, 2, 3, 4$ and in principle, the masses of the components of H^0 will be equal $m_3 = m_4$, because all these fields form part of the same $SU(2)$ doublet (see Eq. (3.8)).

In a second stage, the electroweak symmetry is spontaneously broken and the SM particles acquire mass. In addition m_3 and m_4 can acquire radiative corrections, generating an inequality in masses leading to a decay of the heavy particle to the light particle, obtaining only one particle (a real scalar field) as DM candidate.

However, in the classical limit, radiative corrections cannot be detected due to their quantum nature, so the equality $m_3 = m_4$ is preserved, giving us two DM candidates, which can be included as components of a complex scalar field.

3.2.2 A two scalar field model

We consider two cosmological scalar fields that contribute to the energy and matter density of the Universe. From this point forward we will assume that both are complex and obey the classical field equations, according to the discussion in the previous section. These fields gravitate via minimal coupling given by the action,

$$S = \int d^4x \sqrt{-g} \left(\frac{c^4}{16\pi G} R + \mathcal{L}_{\Phi_1, \Phi_2} \right), \quad (3.20)$$

where

$$2\mathcal{L}_{\Phi_1, \Phi_2} = -\nabla^\mu \Phi_1^* \nabla_\mu \Phi_1 - \nabla^\mu \Phi_2^* \nabla_\mu \Phi_2 - V(\Phi_1, \Phi_2). \quad (3.21)$$

Varying Eq. (3.20) with respect to the metric $g_{\mu\nu}$ gives

$$R^\mu_\nu - \frac{1}{2} R \delta^\mu_\nu = \frac{8\pi G}{c^4} T^\mu_\nu, \quad (3.22)$$

with

$$T^\mu_\nu = g^{\mu\eta} \partial_{(\eta} \Phi_1^* \partial_{\nu)} \Phi_1 + g^{\mu\eta} \partial_{(\eta} \Phi_2^* \partial_{\nu)} \Phi_2 - \frac{\delta^\mu_\nu}{2} \left[g^{\alpha\beta} \partial_\alpha \Phi_1^* \partial_\beta \Phi_1 + g^{\alpha\beta} \partial_\alpha \Phi_2^* \partial_\beta \Phi_2 + V(\Phi_1, \Phi_2) \right]. \quad (3.23)$$

The variation with respect to the fields Φ_1 and Φ_2 gives the following equations of motion:

$$\square \Phi_1 - \frac{dV}{d|\Phi_1|^2} \Phi_1 = 0. \quad (3.24)$$

$$\square \Phi_2 - \frac{dV}{d|\Phi_2|^2} \Phi_2 = 0. \quad (3.25)$$

We assume that in addition to the scalar field, we have radiation r , baryons b and dark energy Λ , but these components do not interact with the scalar field. In the

homogeneous case, the solution to the Einstein equations (3.22), is the Friedman-Lemaître-Robertson-Walker metric:

$$ds^2 = -c^2 dt^2 + a(t)^2 (dr^2 + r^2 d\Omega^2), \quad (3.26)$$

where we have taken the $t = \text{constant}$ hyper-surfaces ($k = 0$) case, where we consider a flat Universe. The tt component of Eq. (3.22) becomes

$$H^2 = \frac{8\pi G}{3c^2} [\rho_r(t) + \rho_b(t) + \rho_\Lambda(t) + \rho_{\Phi_1, \Phi_2}], \quad (3.27)$$

here, $H := \dot{a}/a$ is the Hubble parameter, and ρ_x corresponds to the energy density associated to the energy momentum tensor of $x = r, b, \Lambda$ components and

$$\rho_{\Phi_1, \Phi_2} = \frac{1}{2c^2} |\partial_t \Phi_1|^2 + \frac{1}{2c^2} |\partial_t \Phi_2|^2 + \frac{1}{2} V(\Phi_1, \Phi_2). \quad (3.28)$$

In addition to the density of the scalar field, a ‘‘pressure’’ term can be defined as

$$p_{\Phi_1, \Phi_2} = \frac{1}{2c^2} |\partial_t \Phi_1|^2 + \frac{1}{2c^2} |\partial_t \Phi_2|^2 - \frac{1}{2} V(\Phi_1, \Phi_2), \quad (3.29)$$

and a corresponding equation of state w can be defined as the ratio of density to pressure.

Now, if we concentrate on the case where the potentials are separated for each field $V(\Phi_1, \Phi_2) = V_1(\Phi_1) + V_2(\Phi_2)$, the equations of motion also separate. In this case we have $\rho_{\Phi_1, \Phi_2} = \rho_1 + \rho_2$ and $p_{\Phi_1, \Phi_2} = p_1 + p_2$, with $\rho_1 = \frac{1}{2c^2} |\partial_t \Phi_1|^2 + \frac{1}{2c^2} V_1(\Phi_1)$ and similarly for the other density and pressures. In terms of these quantities, the equations of motion for the scalar fields imply the following relations,

$$\partial_t \rho_1 + 3H(\rho_1 + p_1) = 0. \quad (3.30)$$

$$\partial_t \rho_2 + 3H(\rho_2 + p_2) = 0. \quad (3.31)$$

Before starting with the technical details on the integration of the coupled complex system of differential equations (3.24), (3.25) and (3.27), we need to specify the particular form of the scalar potentials. From now on we will return to natural units.

As discussed in the previous sections, we will consider three scalar potentials, two of them taken from dark matter scalar fields models hypothetically fundamental and the third, associate to a scalar field model purely motivated by cosmology.

As described in the subsection 3.2.1, QCD non-perturbative effects after the Peccei-Quinn symmetry breaking, at some scale f_a , provide a potential for the axion Φ_a . A simple choice for this, is the instanton potential in Eq. (3.3), which turns out to be a very commonly used potential, if a specific form of self-interaction for the axion is required [98, 99, 68].

We will assume that this potential is valid during all the evolution of the Universe. Although axions are described by a real scalar field in the quantum relativistic field theory, at low-energy, axions can be described more simply by a classical non-relativistic effective field theory with a complex scalar field [98]. So that we exchange $\Phi_a \rightarrow |\Phi_a|$ in (3.3).

In this analysis we are interested in studying slight deviations from the non-interacting scalar field dark matter model. So, let us consider small displacements of the complex field around the minimum of the potential, $|\Phi_a| \ll f_a$. Then, we can make the expansion of (3.3) as in (3.4), $V_a(\Phi_a) = 2(m_a f_a)^2 (|\Phi_a|^2 / (2! f_a^2) - |\Phi_a|^4 / (4! f_a^4) + \dots)$. Notice that, in this expression we have included an extra 2 factor to be consistent with the Lagrangian of a complex scalar field (3.21) and for simplicity, we will take just the first and second terms of the expansion,

$$V_a(\Phi_a) = m_a^2 |\Phi_a|^2 - \frac{m_a^2}{12 f_a^2} |\Phi_a|^4. \quad (3.32)$$

We identify the positive self-interaction parameter $\lambda_a/2 = m_a^2/(12 f_a^2)$, which we will use later. The Eq. (3.32), corresponds to the first potential considered in the subsequent analyses. Recall that in the low density regime, $|\Phi_a|$ is small compared to f_a and thus, the dynamical behavior is captured by the first terms in the potential [100].

The second scalar potential we will be considering, corresponds to a very massive scalar field that appears in the Higgs-like model. As stated in 3.2.1, classically the relevant part of the model could manifest itself as a single complex scalar field.

We assume that this component will be one of the components of dark matter and that it could be modeled in the classical regime by a complex scalar field with the potential³ (3.8).

³The Lagrangian of a complex scalar field in QFT usually does not have the overall 2 factor as in the gravitation references cited here, which coincides with the convention used in this sections (see Eq. (3.21)). The $1/2$ term in the λ_h term is considered in order to compare directly with the quantum theory, since under the change $\Phi_h \rightarrow \sqrt{2}\Phi_h$ the Lagrangian of the Higgs-like field becomes $\mathcal{L} = -\nabla^\mu \Phi_h^* \nabla_\mu \Phi_h - m_h^2 |\Phi_h|^2 - \lambda_h |\Phi_h|^4$.

Typically the mass term m_h is in the GeV region and due to perturbative analysis the self-interaction, lies within $-4\pi < \lambda < 4\pi$ as mentioned in section 3.2.1.

The third single scalar field model introduced to the analysis is one with unrestricted a priori values on mass and self-interaction, in this sense we refer to it as *classical*. We consider this as a (mainly) classical model in which the connection to fundamental physics is somewhat “free”. The parameters of mass and self-interaction are allowed to vary throughout the spectrum of values as long as they are consistent with cosmological and astrophysical observations. We are interested in the (positive) self-interacting case, that has been shown to be necessary according to [22]. The potential for this field is (3.1), where $\phi = \Phi_c$, $\mu = m_c$ and $\sigma^2 = \frac{1}{2}\lambda_c$.

All three scalar potentials of the single scalar field models have the same structure, however, we distinguish them by cases given the allowed values of their parameters. The properties of each case are listed in Table 3.1.

Tab. 3.1: Single and double scalar field models described in section 3.2.2. Top: Three single scalar field models with their free parameters and the validity intervals of m and λ parameters. The representative cases are the specific values of the parameters explored in this work. Bottom: Three possible double scalar field models with the corresponding combinations at the description. The k constrain is referred to the minimum fraction of the energy density of the lightest field at the present ($a = 1$) with respect to the total dark matter density. The viability of the models is reported in the last column with two different meanings in the *viability* term for the single models: the (i) column refers to the $\text{BBN}+z_{\text{eq}}$ analysis described on section 3.2.4, while the column (ii) denotes the viability from a relic density point of view for the scalar field models reported at the cited works.

SINGLE MODEL	Free parameters	m	λ	Representative cases (m, λ)	Viability	
					(i)	(ii)
Axion (Φ_a)	f_a	$5.69 \left(\frac{10^9 \text{ GeV}}{f_a} \right) \text{ meV}$	$-m_a^2/(6f_a^2)$	$(5.7 \times 10^{-13} \text{ eV}, -5.4 \times 10^{-82})$	×	✓ [68]
Higgs (Φ_h)	m_h, λ_h	$\sim 100 \text{ GeV}$	$(-4\pi, 4\pi)$	$(100 \text{ GeV}, 1)$	×	✓ [61]
Classical (Φ_c)	m_c, λ_c	$\lesssim 1 \text{ eV}$	> 0	$(3 \times 10^{-21} \text{ eV}, 4.2 \times 10^{-86})$	✓	NA
DOUBLE MODEL	Description			k constrain	Viability	
I	Classical + Higgs			$\gtrsim 0.423$	✓	
II	Axion + Higgs			×	×	
III	Classical + Axion			NA ⁴	✓	

Starting from these cases, the analysis is carried out on combinations of these. However, for simplicity we will explore only two of the three possible combinations, the classical+Higgs and the axion+Higgs. It will be shown that both models have the capability to modify the expansion of the Universe throughout BBN, however it will turn out that the presence of the classical $\lambda > 0$ scalar field is required. Therefore the third possible case (classical+axion), together with the first, contain a set of values in their parameters consistent with this analysis, however this model has four free parameters and we will leave the full analysis for a future work.

The first model considers a Higgs-like scalar field in combination with an classical field. The equations of motion for this case have only three free parameters: the mass and self-interaction of the classical and the fraction of it with respect to the Higgs at $a = 1$, namely k (defined below). The Higgs field is in the weakly self-interacting regime [26], which implies that the field at a homogeneous level behaves similar to the cold dark matter fluid because it always oscillates rapidly. The second model will be the axion+Higgs combination which has one scalar field related free parameter, f_a . In the Table 3.1 we summarize this models. And as mentioned, the combination axion+classical will not be explored in this work. We will show that the axion field, at most, passes through a matter-like and stiff matter eras and not through the radiation-like era as the $\lambda > 0$ case, even so its stiff era may affect expansion sufficiently to influence BBN.

3.2.3 Cosmological evolution

Now, with the specific form of the scalar potentials, we are able to continue with the integration of the evolution equations. We consider the procedure done by Li et al. in [22] for one complex scalar field. In order to do this, we are going to force both fields to be matter-like at the present time, this means that both of them must be in the fast-oscillation regime, i.e. their complex phase time derivative (ω), must be greater than the Hubble rate: $\omega/H \gg 1$. The integration will be made backwards in terms of the variable a (and not t), starting at $a = 1$, therefore going back in time the fields will come out of the fast oscillating regime but at different times.

In the standard one-field case, the solution is obtained in two parts given that in the fast oscillation an approximation is needed due to the difficulties of numerical integration. In the two-field case, we must split the domain of a in three, introducing an intermediate section in which one of the fields still oscillates rapidly but the other

one is already in transition to the slow oscillation regime. Three sets of differential equations must be taken into account, with adequate initial (or matching) conditions.

Introducing the variables $A_1 = \rho_1 - p_1$, $A_2 = \rho_2 - p_2$ and $B_1 = m_1^2 \partial_t |\Phi_1|^2$, $B_2 = m_2^2 \partial_t |\Phi_2|^2$ the full system composed of the two (complex) Klein-Gordon equations and the Friedman equation become:

$$\dot{a} = aH_0 \sqrt{\frac{\Omega_r}{a^4} + \frac{\Omega_b}{a^3} + \Omega_\Lambda + \frac{\rho_1}{\rho_{\text{crit}}} + \frac{\rho_2}{\rho_{\text{crit}}}}. \quad (3.33)$$

$$\frac{d\rho_1}{da} = -3 \frac{2\rho_1 - A_1}{a}, \quad (3.34)$$

$$\frac{dA_1}{da} = \pm \frac{B_1}{\dot{a}} \sqrt{1 + \frac{2\lambda_1}{m_1^4} A_1},$$

$$\text{(If } \lambda_1 > 0, \text{ take the upper signs. If } \lambda_1 < 0 \text{ both signs are possible.)} \quad (3.35)$$

$$\frac{dB_1}{da} = -3 \frac{B_1}{a} + 2m_1^2 \frac{1}{\dot{a}} \left[2(\rho_1 - A_1) - \frac{m_1^4}{2\lambda_1} \left(\sqrt{1 + \frac{2\lambda_1}{m_1^4} A_1} \mp 1 \right)^2 \right]. \quad (3.36)$$

And similarly for the second field. This was showed in the one-field, positive self-interaction case by [22]. The negative self-interaction \pm possibility is explained below.

Since the equations (3.33–3.36) are solved in terms of a , the Friedman equation is purely algebraic.

Clearly, the initial condition (at $a = 1$ since we are integrating backwards) for the density of this components are the values Ω_i which are well known numbers constrained by observations. In the same way, the density parameter for dark matter, Ω_{dm} fix the total energy density $\rho_1 + \rho_2$ at $a = 1$, therefore we write

$$\rho_1(a = 1) = k \Omega_{\text{dm}} \rho_{\text{crit}}, \quad (3.37)$$

$$\rho_2(a = 1) = (1 - k) \Omega_{\text{dm}} \rho_{\text{crit}}, \quad (3.38)$$

for $0 \leq k \leq 1$, where $\rho_{\text{crit}} = 3H^2/(8\pi G)$ being H the Hubble parameter and G the gravitational constant. This is the only initial condition needed for the fields, since the full system (3.34–3.36) reduces to a set of equations in the fast oscillation regime, given below, which as said before, are feasible to solve and ensure that the scalar fields behave like cold dark matter at late times:

$$p_1 = \frac{m_1^4}{9\lambda_a} \left(1 \mp \sqrt{1 + \frac{3\lambda_1}{m_1^4} \rho_1} \right)^2, \quad (3.39)$$

$$\frac{d\rho_1}{da} = -3 \frac{\rho_1 + p_1}{a}. \quad (3.40)$$

The same equations (3.39) and (3.40) will be applied to the field Φ_2 exchanging $1 \rightarrow 2$. The same rule showed near Eq. (3.35) for the \pm signs applies.

This regime was also derived in [26] where the solutions were studied in more depth for both the positive and negative self-interaction cases. However, in the case of negative self-interaction, special care must be taken, since there exist two solutions, both with negative pressure. We have chosen the one with increasing pressure, and therefore a candidate for dark matter. This corresponds to the so-called normal branch in [26], where in equations (3.35), (3.36) and (3.40) the upper sign is taken in the \pm expressions.

This division into two branches for the case of negative self-interaction can be extended to the limit of slow oscillations also by means of a simple \pm , as indicated in the previous equations. This extension will allow us to obtain the full solution for the negative λ case, at least in the normal branch.

Going back in cosmic time, there must be a value for the scale factor at which the fast oscillation regime stops to be valid in one of the fields. At this point, defined by a_e , we have to solve the complete system of equations (3.34–3.36) given the following matching initial conditions (see [22]): The density and pressure variables are evaluated at a_e , thus determining initial values for the density and the variables A in the complete set of equations, while the new variable B , must take the value

$$B_1(a_e) = -H(a_e) \frac{\rho_1(a_e) + p_1(a_e)}{\sqrt{1 - 2 \frac{\lambda_1}{m_1^4} (\rho_1(a_e) - p_1(a_e))}} \left(2 + \frac{1}{\sqrt{1 - 3 \frac{\lambda_1}{m_1^4} \rho_1(a_e)}} \right), \quad (3.41)$$

and similarly for B_2 .

We solve the equations using a fourth-order Runge-Kutta method⁵. The problem is solved in three parts, as we discussed earlier. We monitor the end of fast oscillation of

⁵RK4 is the most commonly used Runge Kutta method to find the solution of an ODE initial problem of first order. See [101] and references therein.

the fields using the equation for the pulsation in terms of the energy density in the fast oscillation regime,

$$\omega_a = m_a \sqrt{\frac{1}{3} - \frac{2}{3} \sqrt{1 - \frac{3\lambda_a}{m_a^4} \rho_a}}, \quad (3.42)$$

making the switch to the full system when $\omega/H \sim 10^3$ because according to numerical experimentation, at this point the fast oscillation limit is still valid and at the same time the full system can be solved with computationally reasonable resolutions on a . A similar value is used in [22] as the threshold which states the marginal case where the scalar field has fully morphed into CDM at matter–radiation equality.

Before proceeding with the cosmological constraints, we show typical solutions for the negative and positive self-interaction single scalar field models in Table 3.1. Then we report representative solutions of the two scalar field models of Table 3.1.

In Figure 3.1 we present the plots for the equation of state and the fraction of energy for the following single scalar fields. We have chosen to show some representative cases in each model. For example, for the axion field we take two values of the f_a , first the Planck scale $f_a = 10^{19}\text{GeV}$ whose mass and self-interaction, according to the formulas in Table 3.1, are $(m_1, \lambda_1) = (5.7 \times 10^{-13}\text{eV}, -5.40 \times 10^{-82})$, second the grand unified theory scale (GUT), with $f_a = 10^{16}$ corresponding to $(m_1, \lambda_1) = (5.7 \times 10^{-10}\text{eV}, -5.40 \times 10^{-70})$.

Then for the Higgs model, we choose a representative case with parameters $(m_1, \lambda_1) = (100\text{GeV}, 1)$. Actually for the allowed range of λ_h the field will always be in the fast oscillation regime. In the extensive study made in [26] it was shown that below certain threshold in the parameters, the scalar field will be in the so-called non self-interacting regime. Which can be shown is always the case for the Higgs model, given the big value for the mass and the restriction on λ_h . In other words, taking different (allowed) values for λ_h and even lowering 9 orders (or raising any order) m_h give indistinguishable solutions between them and also indistinguishable from ΛCDM . In Figure 3.1 we use the same red line in the top panel, to describe the equation of state of the Higgs as well as the one of the fluid standard CDM.

We note that for the axion fields, the transition from stiff $w = 1$ to matter-like $w = 0$, occurs later as the scale f_a increases. However, for the Planck scale axion this is still not enough to noticeably change the density fractions of the components of the Universe in this particular range for a between 10^{-14} and 1, this is the reason that in the plot

for Ω_x , bottom panel in Figure 3.1, we use the same dashed black line to describe standard CDM as well as the axion and the Higgs models. Important differences in the density parameters (including at BBN), are obtained for f_a above the Planck scale; e.g. for a mass term of the order $m_a \sim 10^{-20}$ eV whose scale of symmetry breaking is $f_a \sim 10^{26}$.

Other reference case of interest is the fiducial model in [22], obtained as a classical positive self-interaction scalar field that satisfy some cosmological constrains involving BBN value of the effective number of neutrinos and the behavior of the field at z_{eq} . This is a model with parameters $(m_1, \lambda_1) = (3 \times 10^{-21}$ eV, 4.2×10^{-86}).

In the top panel of Figure 3.2 we present the fraction of energy for the two scalar field model constituted by the classical and the Higgs fields, that we name Model I, with two different contributions of each scalar field. The scalar field parameters for the representative case potted at the top panel of Figure 3.2 are given in Table 3.1. We can see the evolution of the dark matter density of the Model case I with a solid line and the contribution of the individual scalar fields with translucent lines. All the other contributions are plotted in dashed lines. Finally, at the bottom panel of Figure 3.2 is plotted the fraction of energy of the Model II, assembled with an axion field and a Higgs field with the values of m and λ provided on Table 3.1 for the representative cases.

3.2.4 Observational Constrains

Variability on the cosmic ladder

The tension between H_0 values between early Universe predictions and local cosmology model-independent measurements has revealed the great importance of building solid techniques that combine data sets which can determine late time cosmological parameter values [102]. For instance, Baryonic Acoustic Oscillations (BAO) measurements alone do not determine cosmological parameters; but they can be combined with the CMB anisotropies power spectrum and luminosity distances measured from SNeIa to provide cosmological parameters in the context of different cosmological scenarios. The cosmic distance ladder refers to the sequence of different methods that are used in Astronomy to measure distances to space objects. At the bottom of the ladder we can find the objects whose distance can be directly measured, like parallax. On the other hand, the extragalactic distance scale is a set of techniques to determine the distance

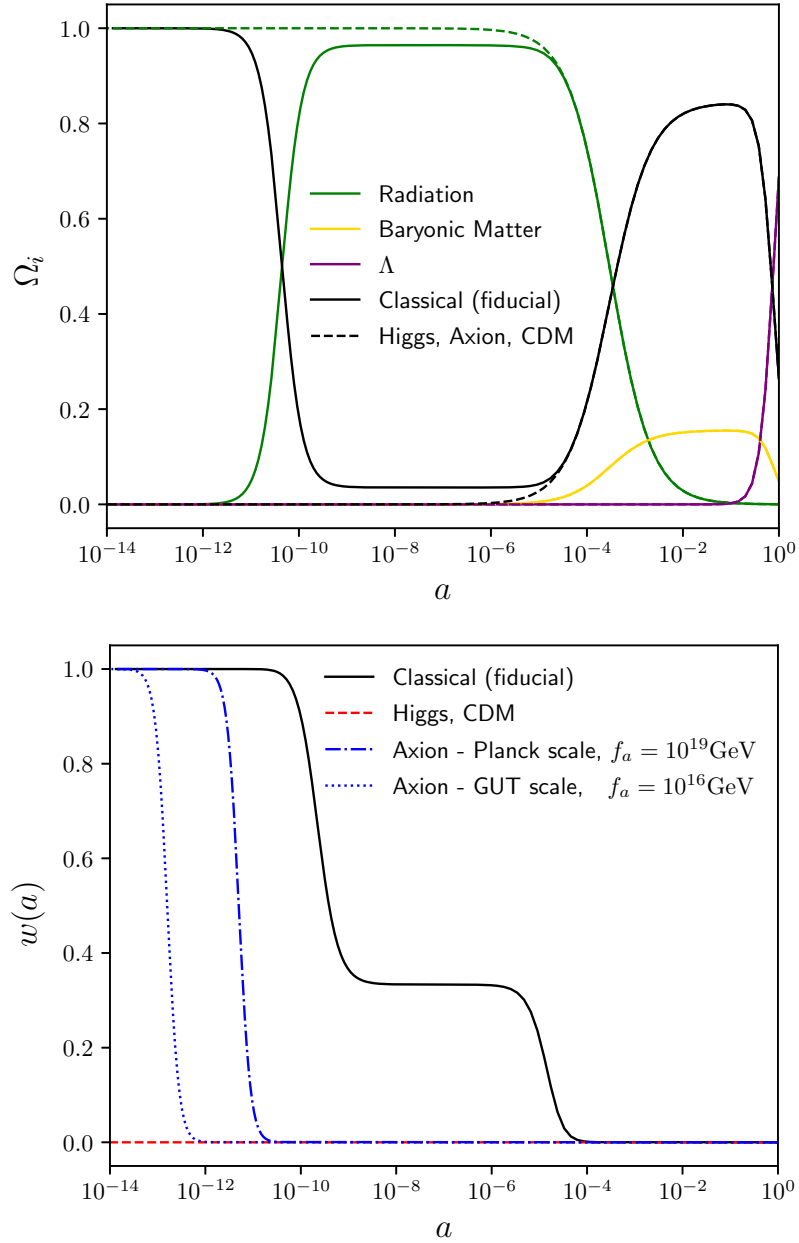
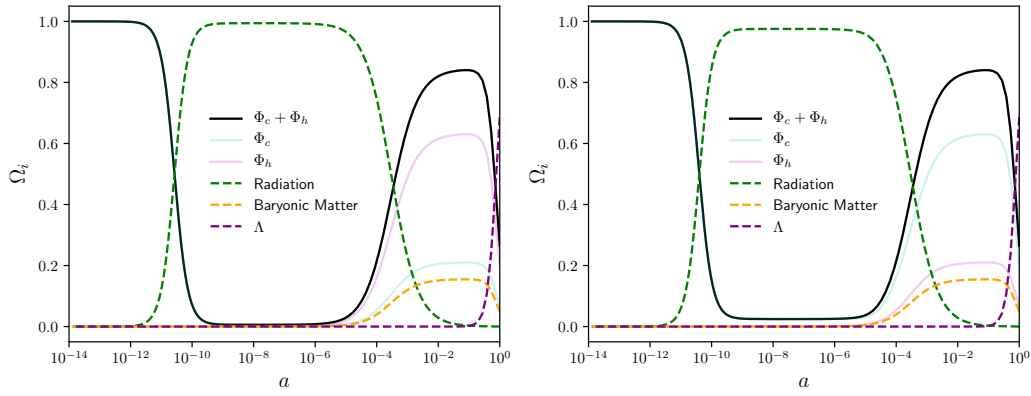
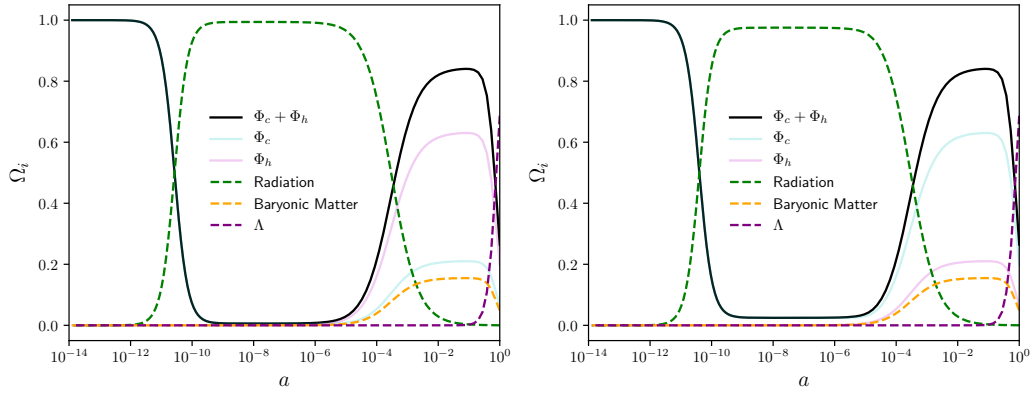


Fig. 3.1: Single scalar field representative cases of Table 3.1. Top panel: All solid lines correspond to the classical positive self-interaction fiducial cosmology [22]. The dashed lines are the reference CDM Universe, which happens to coincide in this plot to the Higgs and axion (GUT, Planck) cases. Bottom panel: Equations of state. While the positive self-interaction classical field undergoes three phases, the negative self-interaction case undergoes two and the Higgs field remains indistinguishable from standard cold dark matter.



(a) Two scalar field model I. Density fractions for $k = 0.25$

(b) Two scalar field model I. Density fractions for $k = 0.75$



(c) Two scalar field model II. Density fractions for $k = 0.25$

(d) Two scalar field model II. Density fractions for $k = 0.75$

Fig. 3.2: Evolution of the density parameters of the Universe. All solid lines correspond to the scalar field dark matter model with two components and the dashed lines represent the rest of the density contributions. Top panel: Two scalar field model I. Bottom panel: Two scalar field model II.

of cosmological bodies beyond Milky Way, for instance, that for which SNeIa can be used.

In this section we compute the variation of our model and the priors considered at the edges of the cosmic ladder. Although this is not an attempt to solve the tension of H_0 , it will provide us a hint of the behavior of this two scalar field combination:

- I: Classical+Higgs,
- II: Axion+Higgs,

see Table 3.1, in the direction of know which of that combinations can be fitted through astrophysical observations. In order to perform such analysis we considered the following:

1. An early H_0 prior: using the cosmological model Λ CDM and the Planck Collaboration [35] data with the corresponding $H_0 = 67.04 \pm 0.5 \text{ km s}^{-1} \text{ Mpc}^{-1}$. We denote this prior as PL18.
2. A late H_0 prior: from the measurement of the Cepheid amplitudes at late times with the corresponding $H_0 = 74.03 \pm 1.42 \text{ km s}^{-1} \text{ Mpc}^{-1}$ [103]. We denote this prior as R19.

Following this recipe would give us a percentage rate of the differences between the models described above and the scale factor at which these deviations take place.

We solved the system of equations (3.33-3.36) as explained before and compute the corresponding cosmological evolution for the Classical, axion-like and Higgs-like scalar fields at different contributions of each one, characterized by the η parameter, for each case analyzed and with the two different H_0 priors mentioned above. Then we compare this evolution of the dark matter fractional densities Ω_{DM} with that of our model, noticing that the main difference, characterized by the slope on the upper plots in Figure 3.3, has a dependence on the η parameter. That is, the larger the parameter, the slope shifts to the right. This movement can be quantified if we compute

$$\Delta = \frac{\Omega_{\text{DM}}(\eta = 0.25) - \Omega_{\text{DM}}(\eta = 0.75)}{\Omega_{2\text{SFDM}}}, \quad (3.43)$$

where $\Omega_{2\text{SFDM}}$ is the density fraction of the two scalar fields and Ω_{DM} is the density fraction computed with PL18 and R19, i.e, Δ_{I} is referred to the case I and Δ_{II} corresponds to the case II. As we can see in Figure 3.4, the quantification on the shift due to the difference of the η parameter is bigger in the model I compared with model II,

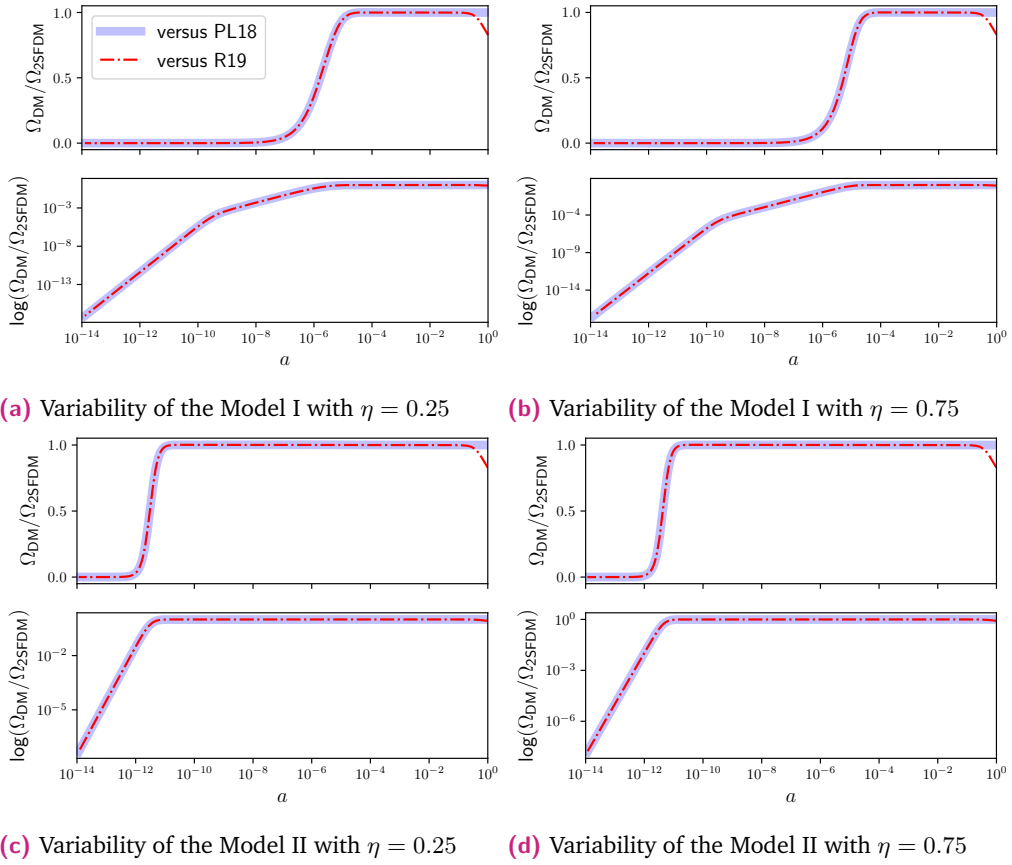


Fig. 3.3: Variability of our model, labeled as 2SFDM, with respect to Planck 2018 (PL18) and Riess et al (R19) H_0 priors in (a) the case I (Classical+Higgs) for $\eta = 0.25$ and (b) for $\eta = 0.75$. (c) The variability in the case II (axion+Higgs) for $\eta = 0.25$ and (d) for $\eta = 0.75$. The values for the free model parameters are in Table 3.1

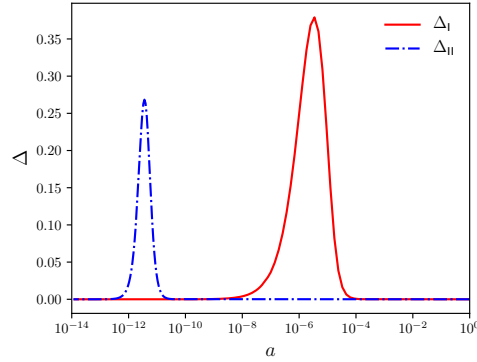


Fig. 3.4: Quantification (Eq. 3.43) of the shift on the slope of the variability (see Figure 3.3) of the models I and II. The maximum relative difference in the density fraction between $\eta = 0.25$ and $\eta = 0.75$ for the Classical + Higgs model computed with R19 relative to the density fraction of the two scalar field model, occurs at $a \sim 10^{-6}$ (red solid line); while for the axion + Higgs model this occurs earlier, at $a \sim 10^{-12}$ (blue dashed line). This behavior is the same for the density fraction when PL18 is used and shows that the model I is more sensitive to the current energy density fraction than the model II.

showing that the model constituted by classical and Higgs fields is more sensitive to the current energy density fraction of a lighter scalar field than the model made of axion and Higgs scalar fields. Furthermore, we can notice that, without taking into account the variation on the η parameter, the differences between the values of the dark matter density fraction with PL18 and R19 priors and the density fraction $\Omega_{2\text{SFDM}}$ of our model occur in an earlier Universe on the model II than in the model I. See, e.g. Figure 3.3 (a) and (c).

Constraints from N_{eff} and z_{eq}

Among the parameters that determine the production of light elements at BBN we have the expansion rate H . This is a period where every component other than radiation is subdominant, therefore the presence of extra relativistic degrees of freedom, beyond the Standard Model implies a modification to H with respect to its ΛCDM profile. This can be quantified inside the effective number of neutrino species N_{eff} as a contribution to the ΛCDM value N_{eff}^0 through a parameter known as number of equivalent neutrinos ΔN_ν , although its source does not necessarily come from a neutrino. It is defined by

$$\Delta N_\nu = \frac{\rho_\xi}{\rho_\nu}, \quad (3.44)$$

where ρ_ν is the energy density of the standard model neutrino (per neutrino specie) and ρ_ξ is the energy density of the additional relativistic fields in consideration, this contribution could correspond to the positive self-interaction (classical) scalar field or to the negative self-interaction axion field for those cases when the energy contribution is important in order to modify H , that is, when they behave as radiation and/or stiff matter during BBN. With the previous definition, the total radiation energy density divided by the photon energy density, ρ_r , is

$$\frac{\rho_r}{\rho_\gamma} = 1 + \frac{\rho_\nu}{\rho_\gamma} (3 + \Delta N_\nu). \quad (3.45)$$

If it is assumed that neutrinos are completely decoupled from the electromagnetic plasma at the electron-positron annihilation, the temperature of the photons increases with respect to that of the neutrinos by $(T_\nu/T_\gamma)^3 = 4/11$. Now, the density ratio $\rho_\nu/\rho_\gamma = 7/8(T_\nu/T_\gamma)^4$, implies that

$$\frac{\rho_r}{\rho_\gamma} = 1 + \frac{7}{8} \left(\frac{4}{11} \right)^{4/3} N_{\text{eff}}, \quad (3.46)$$

with

$$N_{\text{eff}} = N_{\text{eff}}^0 \left(1 + \frac{\Delta N_\nu}{3} \right); \quad N_{\text{eff}}^0 = 3 \left[\frac{11}{4} \left(\frac{T_\nu}{T_\gamma} \right)^3 \right]^{4/3}. \quad (3.47)$$

Where in this case $N_{\text{eff}}^0 = 3$. However if it is not assumed that the neutrinos are completely decoupled when the electron-positron pairs annihilate, then $N_{\text{eff}}^0 = 3.046$ [104].

The total N_{eff} enters through H to the equations that determine the primordial light element abundances (solved by BBN codes) and if for example the lepton asymmetry is neglected, the BBN primordial abundances can be confronted with astronomical observations of the abundances of (mainly) deuterium D [105] and the isotope ${}^4\text{He}$ [106]. This constraints on the observed elements can be traduced in constraints over N_{eff} as well as Ω_b [107, 108].

The 2015 reference [108], obtained $N_{\text{eff}} = 3.56 \pm 0.23$ or

$$\Delta N_\nu = 0.5 \pm 0.23. \quad (3.48)$$

This value certainly excludes the possibility of a new neutrino as well as the standard N_{eff}^0 case. Nevertheless the parameters of a complex scalar field with positive λ can be

constrained to be consistent with this measurement as showed by Li et al. [22, 109] if a time dependent $\Delta N_\nu(a)$ is assumed rather than a relatively late time fixed value. The constrain (3.48) is applied through BBN, between the neutron to proton freeze-out and the first nuclei production, at $a_{n/p}$ and a_{nuc} respectively.

In our numerical analysis, if Φ_1 is not subdominant at BBN, the constrain (3.48) is implemented with the formula,

$$N_{\text{eff}} = \frac{N_{\text{eff}}^0}{2} \left(1 + \frac{\Omega_1}{\Omega_r} + \sqrt{\left(1 + \frac{\Omega_1}{\Omega_r} \right)^2 + \frac{\Omega_1}{\Omega_r} \frac{32}{7} \left(\frac{11}{4} \right)^{4/3} \frac{1}{N_{\text{eff}}^0}} \right), \quad (3.49)$$

which is a result of inserting ρ_γ from (3.46) into (3.47) along with the definition (3.44) and $\rho_\nu = \Omega_r - \Omega_\gamma$, notice that in this expression, Ω_r contains the γ and ν contributions only, which are evolved separately from Φ in the code.

Additional to the BBN constraints discussed so far, there is a need to make the relativistic and stiff matter scalar field solutions reach a matterlike behavior in w at the latest in the matter-radiation equality $z_{\text{eq}} \approx 3365$. This condition is imposed in the code by setting $w(z_{\text{eq}}) < 0.001$.

The results of this BBN+ z_{eq} analysis for the single $\lambda_1 > 0$ scalar field, was reported first by Li et al. in [22] and later an update was made within their work [109]. We recover their result:

$$m \gtrsim 5 \times 10^{-21} \text{ eV}, \quad (\text{single } \lambda > 0) \quad (3.50)$$

$$8 \times 10^{-4} \text{ eV}^{-4} \lesssim \frac{\lambda_1}{m_1^4} \lesssim 10^{-2} \text{ eV}^{-4}. \quad (3.51)$$

If we repeat this analysis now including the single scalar axion case, we should be able to obtain a constrain on the single parameter f_a particularly for the cases with big values of this parameter, which as showed in the previous section, are the models that affect expansion the most. It should be mentioned that the general $\lambda < 0$ case cannot be solved in all the cases, particularly in those where the slow oscillation regime appears closer to $a = 1$ and the square root arguments in (3.35) and (3.36) become

negative at certain point a_i which corresponds to a place where the scalar field “turns on” [26]. Luckily, numerical experimentation on solutions for the axion field (where the mass and self-interaction have a specific dependence on f_a) shows that this is never the case and no discontinuities in the Einstein equations appear.

However, the situation occurs when the stiff matter stage of the axion affects $N_{\text{eff}}(a)$ very drastically, and not in the “stepped” way in which it happens for the $\lambda > 0$ case. If the limits are kept to 1σ in Eq. (3.48) there is no value of f_a for which $N_{\text{eff}}(a)$ is kept inside this limits, not even at 2σ . It happens that if the $N_{\text{eff}}(a)$ enters into the limits (3.48) in $a_{\text{n/p}}$ at the beginning of nucleosynthesis, it no longer enters at the end of it, at a_{nuc} , and vice versa.

Therefore, the single axion model is discarded in relation to this cosmological constrain.

It is possible to repeat this analysis for the two scalar field cases. We are interested in exploring Model I and Model II (Table 3.1). Both of them include the Higgs-like field, which as has been said is similar to CDM fluid regardless of the specific values that m_h and λ_h assume. Therefore, in Model I we have a three parameter model and in Model II we have just two parameters.

- Model I. We fix the value of η , (i.e. the fraction of the energy density of Φ_c at $a = 1$ with respect to total dark matter density, (3.37)), and explore the existence of possible values of m_1 and λ_1 consistent with the 1σ BBN+ z_{eq} analysis. The case $\eta = 1$ coincides with the single case constraints in (3.50,3.51). If we begin to decrease the value of η , the range of the parameters consistent with the constrain decrease in size, as shown in Figure 3.5, until a critical value is reached, after which no value is allowed. This constrain on η , gives

$$\eta \gtrsim 0.423 . \quad (3.52)$$

That is, an upper bound of $\sim 58\%$ for the Higgs (or $w = 0$ fluid) component can be considered in order to be consistent with this constrains. In the critical case, where η takes values near 0.423, we have that the $(m, \lambda/m^4)$ parameter space narrows to the values $m \gtrsim 2 \times 10^{-21} \text{eV}$ and $\lambda/m^4 \sim 3 \times 10^{-2} \text{eV}^{-1}$.

- Model II. In this simpler case, a joint analysis over η and f_a can be made. We find that no $1 - \eta$ ratio of the Higgs field is capable of smoothing the $N_{\text{eff}}(a)$ evolution dictated by the axion, during BBN. And since the Higgs field has a contribution to N_{eff} of 0 with respect to N_{eff}^0 , this two fields case (like the single axion case),

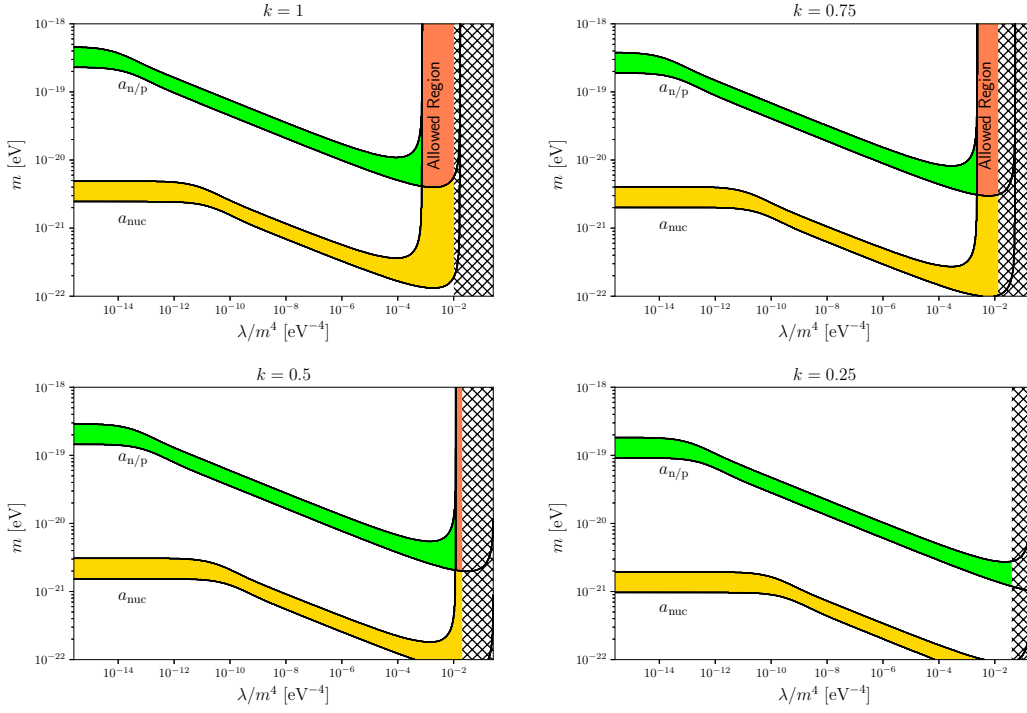


Fig. 3.5: Constraints from z_{eq} and N_{eff} within 1σ for the two scalar field Model I. η is the fraction of the classical field with respect to the total dark matter components. The crosshatched region that appears on the right side of all figures, represents the values of the scalar field parameters not allowed by the z_{eq} constrain. The green and yellow bands are the allowed regions from the N_{eff} constrain, (3.48), at $a_{n/p}$ and a_{nuc} respectively. The red band is the region of the parameter space that is consistent with both the z_{eq} and N_{eff} , throughout BBN, constraints.

is discarded in the sense that there is no set of parameters such that (3.48) is satisfied. Relaxing the constrain to 2σ in (3.48) no allowed values are found either.

- Model III. The classical ($\lambda > 0$) + axion case has 4 relevant free parameters and a higher complexity. It is found that for all axions with $f_a < 10^{19}\text{GeV}$, for which the equation of state is 0 before the start of BBN, as showed in section 3.2.3, the axion scalar field behaves effectively as a $w = 0$ fluid for the purposes of this restriction, and therefore the same restriction as for case I would apply here. A complete analysis of this case will be reported elsewhere.

3.2.5 Conclusions

In this work we presented a straightforward analysis to incorporate scalar fields derived from models coming from physics beyond the Standard Model of particle physics (BSM) in the Cosmological evolution. The usual Cosmological models which incorporate scalar fields to describe the dark matter component of the Universe, have been successful in building a serious alternative to the well known CDM model. These type of proposals consider a scalar field that does not interact in any way, except via the gravitational interaction, with the rest of the matter in the Universe; we have denoted these fields as *classical*.

The combination of some scalar fields coming from BSM with the classical scalar field proposal, demands a clear description and discussion of the interpretation of the transition from a quantum field theory to a wave function satisfying the Einstein-Klein-Gordon system of equations. In order to do this transition we used the effective action perturbative expansion, where we identified the zeroth order term with the classical field, which we then reparametrized as a complex scalar field.

The BSM fields that we analyzed were the Higgs-like and axion-like fields (clearly the SM Higgs boson itself, being the mass mediator, can not be used to describe the dark matter), and included them along with the classical one considering that the dark matter is composed of two such fields. Then, both of these fields would contribute to the dark matter relic density observed today, i.e. 0.26, and we explore which proportions of each field today are consistent with BBN at the early Universe.

To start, we considered the case of only one BSM field, taken as a complex classical field as explained in sub-section 3.2.1. We found that in the case of a single Higgs-like

DM, it is not possible to increase N_{eff} in a significant way during BBN, notice that this is the same case as in ΛCDM . On the other hand, the axion and axion-like fields increase N_{eff} abruptly without the possibility of satisfying the constraint during all the period of BBN.

Neither it is possible to find allowed values consistent with this constraint for the BSM parameters in the case where both fields are combined in any proportion. On the other hand, to produce a cosmological model that remains consistent with constraints satisfied by the single classical scalar field, we can consider up to 58% of Ω_{DM} to be a Higgs-like field if the remaining 42% is the classical one. The combination of a classical with an axion-like field turns out to have four free parameters which prevent us to perform a brief survey of the parameters and make a full analysis in the lines of the present work. However, we can say in advance that a combination of a classical field together with an axion or axion-like field, will have a set of parameters for the scalar field where this restriction is satisfied, specifically for $f_a < 10^{19}$ GeV.

We want to stress out the results regarding the Higgs-like scalar field. The searches on direct [37, 38, 39, 40] and indirect [41, 42, 43] detection of dark matter usually take into account one DM candidate, which comprises 100% of the relic density. Our result opens the possibility to take into account in the direct and indirect searches more than one candidate to DM, which contribute to the relic density in different proportions, and thus modify the expected fluxes in the experimental analysis. This fact has to be taken into account in the design of the experiments and in the interpretation of their results.

Furthermore, according to BBN and z_{eq} analysis, a large part of Ω_{DM} in our two field models, is required to be the classical complex scalar field, which has zero interaction with the rest of the matter, beyond the gravitational one. In order to understand more of its properties, different types of experiments have to be developed. For instance, the distribution of the complex scalar field in the vicinity of a black hole, so called black hole wigs [110], has a very particular density distribution which, in turn, affects the dynamics of light and observable matter in such vicinity in a characteristic way. It is important to look, as discussed and done in [111] for instance, for possible observable (gravitational) consequences of one type or another of dark matter model, in order to be able to discard or make more robust a given proposition for describing that quarter of the total density of the Universe which we call dark matter.

3.3 Galaxy–Halo Connection

At the present time, the paradigm of galaxy formation is based on the assumption that dark matter plays a fundamental role in the galaxy formation process, since galaxies form out of the condensation of cold gas within a dark matter halo. Although the nature of dark matter is still a mystery, the current standard model in cosmology and the halo structure formation, the so-called Λ CDM, has been very successful for describing the distribution of the matter from the galactic to the large-scale Universe. However, this model presents different problems at small-scales related to the N-body simulations such as the “missing satellites” [112], the “cusp-core” [113], the “too big to fail” [114] and the “plane of satellites” [115, 116] problems. Nevertheless, the current hydrodynamical simulations, with a more sophisticated knowledge of baryonic physics, exhibit the importance of the effect of stellar and radiative feedback in galaxies suppress star formation, that is, given the UV background at the reionization epoch of the Universe, not all dark matter haloes eventually host a galaxy [117, 118, 119, 120]. In addition, recent results have shown that non-circular motions in disk galaxies are able to mimic the presence of kiloparsec-scale density ‘cores’, when none are actually present [121]. That is, understanding the baryon physics for galaxy formation at all scales and non-circular motions when considering the evidence of a potential satellite problem or for dark matter cores is mandatory in order to understand whether the current cosmological model is in tension with current observations. In this section we focus on including the effects of a UV background in order to test the impact on the galaxy-halo connection and on the nature of the dark matter particle.

In this section it is performed an analysis of the parameters of a scalar field dark model within a semi-empirical approach of the Galaxy–Halo connections. The idea behind this connections is to use simple rules to populate dark matter haloes and subhaloes with galaxies that would be consistent with the observed distribution of galaxy surveys. There are several ways to doing this. In this work we will focus on the Subhalo Abundance Matching (SHAM) which matches the cumulative Galaxy Stellar Mass Function (GSMF) to the cumulative Halo Mass Function (HMF) to obtain, at the same time, a correlation between galaxy stellar mass and halo (and subhalo) mass [see e.g., 122, 123, 124, 125, 126]. However, the importance of the galaxy–halo connection not only relies on determining accurate models that match observations, but also relies on using it as a phenomenological tool to understand the average growth of galaxies [125]. In this sense, the work presented here shows that the connection between halo and galaxy parameters is important and can explain the galaxy formation history at

both high and low masses, if the process of the stellar and radiative feedback is taken into account [127].

3.3.1 Theoretical framework

The (sub)halo abundance matching (SHAM) is a simple and yet powerful statistical approach for connecting observable properties of galaxies to haloes [see e.g. for a review, 126] by assuming that every halo host a galaxy. In its simplest form, given some halo property (usually halo mass or maximum circular velocity), the halo number density and the galaxy number density are matched in order to obtain the connection between haloes and the galaxies that they host.

If we assume that halo mass M_{halo} is the halo property that correlates best with stellar mass, we can model the GSMF of galaxies by defining $\mathcal{H}(M_*|M_{\text{halo}})$ as the probability distribution function that a halo of mass M_{halo} hosts a galaxy of stellar mass M_* . Then, the intrinsic GSMF, $\phi_{gI}(M_*)$, as a function of stellar mass is given by [125]:

$$\phi_{gI}(M_*) = \int \mathcal{H}(M_*|M_{\text{halo}}) \phi_{\text{halo}} d \log M_{\text{halo}}, \quad (3.53)$$

where ϕ_{halo} denotes the total number density of haloes and subhaloes within the mass range $\log M_{\text{halo}} \pm d \log M_{\text{halo}}/2$. Here M_{halo} is interpreted as the virial mass, M_{vir} , for distinct haloes and M_{peak} , the peak value of virial mass at or before accretion, for subhaloes. So

$$\phi_{\text{halo}}(M_{\text{halo}}) = \phi_{\text{vir}}(M_{\text{vir}}) + \phi_{\text{sub}}(M_{\text{peak}}). \quad (3.54)$$

However, the GSMF inferred from observations, ϕ_{obs} , through the estimation of stellar masses of galaxies can be represented as the convolution of ϕ_{gI} [125]:

$$\phi_{\text{obs}}(M_*) = \int \mathcal{G}(M_*/x) \phi_{gI}(x) d \log x. \quad (3.55)$$

Then, employing Eqs. 3.64-3.55, the stellar-to-halo mass relation is given by:

$$\phi_{\text{obs}}(M_*) = \int P(M_*|M_{\text{halo}}) \phi_{\text{halo}}(M_{\text{halo}}) d \log M_{\text{halo}}. \quad (3.56)$$

When it has been established the galaxy-halo connection via the Eq. 3.55, we can use the growth of dark matter haloes in order to determine the rate at which the cosmological baryonic arrival material reaches the interstellar medium (ISM) of a

galaxy. Then, when needed conditions are satisfied, some of the baryonic material will be transformed into stars, so we can use the growth of dark matter haloes (that can be measured from the extended Press–Schechter formalism [128] when one uses the Markovian random walks to infer the halo mass functions, or more accurately by using high-resolution N-body cosmological simulations of dark matter) to predict the M_* of the galaxy that they host as a function of different redshifts z , and thus the galaxy star formation histories (SFHs) [125]:

$$\text{SFR}(z|M_{\text{vir},0}, z_0) = \frac{f_{\text{in situ}}}{1-R} \left[\frac{\Delta M_*(z|M_{\text{vir},0}, z_0)}{t(z) - t(z + \Delta z)} \right], \quad (3.57)$$

where $M_{\text{vir},0}$ is the final mass of the halo at the redshift of observation z_0 , $f_{\text{in situ}}$ is the fraction of mass acquired through star formation (in contrast with the *ex-situ* build of galaxies via galaxy mergers, R is the fraction of mass that returns as gaseous material into the interstellar medium and $\Delta M_*(z|M_{\text{vir},0}, z_0)$ is the amount of stellar mass the galaxy will grow between $t(z)$ and $t(z + \Delta z)$. In addition, we can calculate the cosmic star formation (CSFR), $\dot{\rho}_{\text{obs}}$ [125]:

$$\dot{\rho}_{\text{obs}}(z) = \int \langle \text{SFR}(M_{\text{halo}}) \rangle \Theta(M_{\text{halo}}) \phi_{\text{halo}}(M_{\text{halo}}) d \log M_{\text{halo}}. \quad (3.58)$$

Although abundance matching is a conceptually simple and yet powerful method to connect galaxies and haloes at the sense described above [129], and the quantities derived from this approach often agree for galaxies in haloes more massive than $\sim 10^{10} M_{\odot}$ [126], at lower mass haloes it is not clear whether the assumptions of SHAM are still valid [130]. It has been shown that simulations that model the evolution of matter (baryons and dark matter) only subject to gravity do not produce the same abundance of haloes as hydrodynamic simulations that include the ejection of baryons from low-mass haloes via supernova feedback at the reionization epoch [131, 117]. Moreover, both effects will tend to suppress the formation of galaxies at the very small scales. On the other hand, different type of dark matter particle will produce an impact at the small-scale galaxy formation physics. A non-cold dark matter cosmology, such as fuzzy or axion-like dark matter, that typically presents a suppression of the power spectrum below $\sim 10^{10} M_{\odot}$, will inhibit the formation of galaxies in low-mass dark matter halos [131]. The above, shows that there exists a degeneracy related to the lack of small-scale galactic structures: Does galaxy formation is suppress due the presence of a UV background in a Λ CDM model or is it the result of a cut in the power spectrum from a non-cold dark matter particle?

3.3.2 Suppression relative to CDM from the UV Background

As we discussed in Section 3.3.1, at dwarf galaxy scales with haloes up to $\sim 10^{10} M_{\odot}$, CDM simulations appear to overpredict the structure formed in comparison to observations [131], e.g.,:

- The abundance of haloes with maximum circular velocity $v_{\max} \sim 35 \text{ km s}^{-1}$ is a factor of ~ 10 with respect to the one measured by ALFALFA⁶,
- The dynamics of satellites do not match with the simulations in the so-called cusp–core problem, and
- The stellar-to-total mass ratios calculated from the abundances fail to match those of individual dwarf galaxies.

As we will see below, some of these tensions can be alleviated by assuming that a UV background. Here, the term *alleviate* is referred to dilute the overprediction of substructure since these tensions are extremely complex and extensively studied with a number of vast answers (see [132] and references therein). During the epoch of reionization, the gas temperature is raised to the order of $\sim 10^4 \text{ K}$ [133]. As Tassis et al. found [134], the global star formation rate, at reionization epoch, was significantly reduced and the stellar feedback boosts this effect. Ergo, the stellar population has an imprint of the epoch of reionization (EoR).

The problems referring to the overabundance of (sub)haloes mentioned above, can be alleviated, then, if we included the impact of the UV background on the baryons, which is expected to impact the formation of galaxies at small scales in three ways [131, 117]:

1. In simulations, the interstellar gas is expelled from haloes, while intergalactic gas does not accrete in the presence of ionizing radiation.
2. The satellite galaxies are more sensitive to ram pressure stripping because it removes gas from low-mass satellite galaxies.
3. The haloes with a lower mass and shallower potential well caused by the loss of baryons, leads to diminished accretion of baryons and of dark matter.

⁶The Arecibo Legacy Fast ALFA survey is an extragalactic HI survey to conduct a census of the local HI universe over a cosmologically significant volume.

In order to include the above into models of galaxy formation and evolution, or as in our case, in semi-empirical models of galaxy formation we use the result based on the hydrosimulations of [117].

Initially, we assume that before the EoR the baryon fraction in the Universe, $f_b \equiv M_b/M$, is: $\langle f_b \rangle \equiv \Omega_b/\Omega_0$. But, after reionization, f_b drops down as a function of halo mass [117]. The function that describes such behavior is reported in [135]:

$$f_b(M, z) = \langle f_b \rangle \left\{ 1 + (2^{\alpha/3} - 1) \left[\frac{M}{M_c(z)} \right]^{-\alpha} \right\}^{-3/\alpha}, \quad (3.59)$$

where $M_c(z)$ is a characteristic mass at which the formation of galaxies is heavily suppress, [117] This is a biparametric function with a fitted $\alpha = 2$ established in [117] and the characteristic mass M_c [133]:

$$\frac{M_c(z)}{10^{10} h^{-1} M_\odot} = \left[\frac{\tau(z)}{1+z} \right]^{3/2} \left[\frac{\Delta_c(0)}{\Delta_c(z)} \right]^{1/2}, \quad (3.60)$$

where $\tau(z)$ represents the evolution of the minimum virial temperature required by the halos to continue cooling in the presence of the ultraviolet background:

$$\tau(z) = 0.73 (1+z)^{0.18} \exp[-(0.25z)^{2.1}]. \quad (3.61)$$

Additionally, the redshift-dependent characteristic virial overdensity $\Delta_c(z)$ [136] is given by:

$$\Delta_c(z) = \frac{178 + 82x(z) - 39x^2(z)}{1 + x(z)}, \quad (3.62)$$

$$x(z) = -\frac{(1 - \Omega_m)a^3}{\Omega_m + (1 - \Omega_m)a^3}, \quad (3.63)$$

where a is the cosmic expansion factor. Inspired in [131], we propose to modify the Eq. (3.64) multiplying the GSMF by the baryon fraction (3.59) and contrast the results with observations from the GAMA project [137] as we can observe in Fig. 3.10:

$$\phi(M_*) = \int f_b \mathcal{H}(M_*|M_{\text{halo}}) \phi_{\text{halo}} d \log M_{\text{halo}}. \quad (3.64)$$

In order to describe the mean SHMR, we adopt the parametrization [124, 125]:

$$\langle \log \mathcal{M}_* \rangle = \log(\epsilon M_0) + g(x) - g(0), \quad (3.65)$$

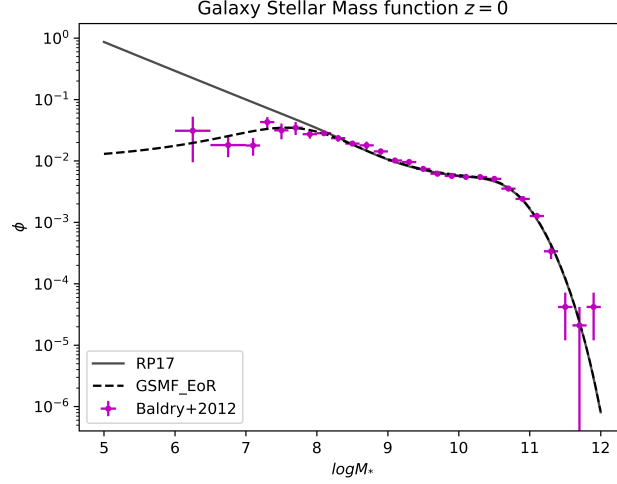


Fig. 3.6: The Galaxy Stellar Mass Function (GSMF) at $z = 0$. The black solid line represents the GSMF as in the Eq. (3.64) [125]; the black dotted line, in contrast, shows the GSMF with the baryon suppression at EoR; the violet points are the observations of the GAMA project for $z < 0.06$ [137].

where

$$g(x) = \delta \frac{(\log(1 + e^x))^\gamma}{1 + \exp(10^{-x})} - \log(10^{-\alpha x} + 1) \quad (3.66)$$

and $x = \log(M_{\text{vir}}/M_0)$. Every parameter is redshift-dependent z and the only parameter free to be adjusted is α :

$$\alpha(z) = \alpha_0 + \mathcal{P}(\alpha_1, \alpha_2, z) \mathcal{Q}(z), \quad (3.67)$$

where

$$\mathcal{P}(x, y, z) = y z - \frac{x z}{1 + z}, \quad (3.68)$$

$$\mathcal{Q}(z) = \exp\left(-4/(1 + z)^2\right). \quad (3.69)$$

Then the SHMR was modified as:

$$\langle \log \mathcal{M}_* \rangle_{\text{EoR}} = f_b(M_{\text{vir}}, \beta_1, \beta_2) \langle \log \mathcal{M}_* \rangle + \frac{1 - f_b(M_{\text{vir}}, \beta_1, \beta_2)}{\log M_{\text{vir}}}, \quad (3.70)$$

where the sigmoid function f_b is given by:

$$f_b(M_{\text{vir}}, \beta_1, \beta_2) = \frac{1}{1 + \exp(-\beta_1(\log M_{\text{vir}} - \beta_2))}. \quad (3.71)$$

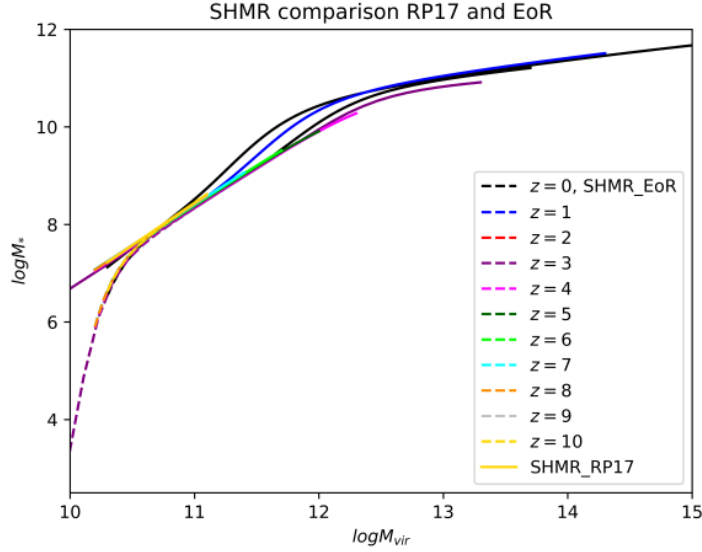


Fig. 3.7: Stellar-to-halo mass relation modified according to equation 3.70 with the baryonic suppression (dashed lines) in comparison with the SHMR without the baryonic suppression [125]

This modification is compared with the expression without the baryonic suppression in the Figure 3.7.

Nevertheless, over the last two decades, a breakthrough has been set our observational understanding on the evolution of GSMF, as well as the evolution of the SFR and the cosmic star formation cSFR [120], in particular in some types of Star-Formation galaxies (SFGs) that obey a tight SFR- M_* relation. In this sense, we explore the suppression relative to CDM from the UV background by using the redshift evolution of the far-ultraviolet (FUV) luminosity functions combined with the evolution of the GSMF of SFGs inspired by [138].

3.3.3 Suppression relative to CDM for generic non-CDM models

Another possible solution that we want to explore to the small-scale problem of the Λ CDM cosmology is to relax the nature of the dark matter, i.e., going beyond the standard CDM paradigm and explore the so-called “non-cold” dark matter (nCDM) candidates, that are well motivated by particle physics theories. Some of these candidates were explored in this work in the previous section 3.2, for instance: sterile neutrinos [139, 140, 141] or axion-like particles [47, 45, 142]. Different scenarios

lead to different shapes in the suppression of the power spectrum [48] and most of the constraints from structure formation data refer to a very specific shape of the small-scale power suppression, namely, that of the thermal warm dark matter. However, a lot of viable nCDM candidates do not have thermally distributed momenta, which may lead to non-trivial suppressions in their power spectra. The suppression of the gravitational clustering in these models can be parametrised via the transfer function $T(k)$ [6]:

$$T(k) \equiv \sqrt{\frac{P_X(k)}{P_{\text{CDM}}(k)}} \simeq \left(1 + (\alpha k)^\beta\right)^{-\gamma}, \quad (3.72)$$

where k is the comoving wave number, $P_X(k)$ and $P_{\text{CDM}}(k)$ are the nCDM and CDM power spectrums, respectively. Stücker et al. [6] found that several nCDM models can be reduced to only two free parameters by fixing $\gamma = 5$, namely:

- a) Resonant Sterile Neutrinos. A suitable lepton number asymmetry in the early universe can resonantly enhance the active-sterile transitions (Shi-Fuller mechanism) and yield spectra that are more likely to be in agreement with data [143, 144]
- b) Decay Sterile Neutrinos. This mechanism relies on the decay of a hypothetical particle in the early universe, whose properties translate into those of the resulting keV sterile neutrino; one example of this production mechanism is that of a singlet scalar particle which may either thermalise (freeze-out) or not (freeze-in) [139, 145].
- c) Fuzzy Dark Matter. Also called ultra-light dark matter, consists of condensed scalar field with associated masses of $m \sim 10^{-22}$ eV such that their wave behavior becomes relevant at astrophysical scales. This model is considered, to first approximation, without self-interaction, and only one free parameter, the Dm mass [146, 22].
- d) Effective Theory of structure formation (ETHOS). Consists of an attempt to formulate an effective theory of cosmic structure formation, to map virtually any particle physics model to the constraints from astrophysics and cosmology, in particular we are interested in the transfer functions studied in [147].

Additionally, if we re-express the parameter α in terms of the half-mode comoving wave number that indicates the scale where $T(k)$ is suppressed by a factor of 2, k_{hm} :

$$\alpha = \frac{\left(2^{1/5} - 1\right)^{1/\beta}}{k_{hm}}, \quad (3.73)$$

the models stated above can be described by the parameters k_{hm} which controls the cutoff scale and β , that regulates the steepness of that cutoff.

The suppression of the halo and subhalo mass functions relative to CDM can be reliably and inferred in the intermediate suppression regime, $n_X(M)/n_{\text{CDM}}(M) > 5\%$. In this section, we will introduce a generic expression for this relative suppression that it is suitable for use in future studies to predict the mass function for generic non-cold dark matter models. Stücker et al. in [6] showed mass function suppression ratios:

$$f(M) \equiv n_X(M)/n_{\text{CDM}}(M), \quad (3.74)$$

and in [148] was suggested a fitting of the mass-dependent abundance suppression ratio, $n_X(M)/n_{\text{CDM}}(M)$ with a function of the form:

$$\frac{n_X(M)}{n_{\text{CDM}}(M)} \simeq \left(1 + \left(a \frac{M_{hm}}{M} \right)^b \right)^c, \quad (3.75)$$

where the half-mode mass is defined by [149]:

$$M_{hm} \equiv \frac{4\pi}{3} \rho_0 \left(\frac{\pi}{k_{hm}} \right)^3, \quad (3.76)$$

where, in turn, ρ_0 is the critical density of the universe and the three free parameters a , b and c will be fitted via MCMC (Markov chain Monte Carlo) with a model that includes the baryonic suppression relative to the UV background detailed on section 3.3.2 applied to a nCDM model. Moreover, the relation between a , b , c and the parameter β can be approximated through the power law [6]:

$$a \left(f^{1/c} - 1 \right)^{-1/b} = \mu_f \cdot \beta^{\nu_f}, \quad (3.77)$$

where μ_f and ν_f depend on the value of the suppression ratio f given by equation (3.75). So, if the three parameters a , b , c are fitted, we can adjust also the parameter β that is related directly with the nature of the particle of a nCDM model.

3.3.4 Results

In order to study the possible degeneracy between the baryon suppression coming from the EoR because UV background and that for nCDM models as a result of the cutoff on the power spectrum, we compare 4 models:

Model	β	$M_{hm} [M_{\odot}/h]$
Resonant Sterile Neutrinos	2.26	9.38×10^8
	2.01	1.23×10^9
	2.14	4.80×10^9
	2.19	7.62×10^9
Decay Sterile Neutrinos	2.72	2.53×10^8
	2.72	2.94×10^8
	2.62	7.54×10^8
	2.51	1.24×10^9
Fuzzy DM	5.41	1.93×10^8
	5.34	5.28×10^8
	5.27	1.34×10^9
	5.29	3.51×10^9
ETHOS	3.43	4.76×10^8
	2.93	5.05×10^8
	2.12	1.03×10^9
	1.11	5.70×10^9

Tab. 3.2: Values of β and M_{hm} of Eq. (3.72) given by [6] for several non-cold dark matter models taken from [48]. The γ parameter was fixed as $\gamma = 5$.

1. CDM Model.
2. CDM + photoionization Model.
3. nCDM Model.
4. nCDM + photoionization Model.

As a starting point, we use the best fit model from Rodriguez-Puebla (work in progress) to the CDM Model. Briefly, they developed a highly consistent model in which galaxies growth within the merger trees of dark matter halos as well as their central super-massive black holes. In order to constrain the model, the authors used a Bayesian scheme [150] to fit to a large battery of observations, including: the galaxy stellar mass function from $z \sim 0 - z \sim 10$; the evolution of the star formation rate-stellar mass relation from $z \sim 0 - z \sim 8$; the cosmic star formation history; the size-mass radius from $z \sim 0 - z \sim 6$, and the quasar luminosity function $z \sim 0 - z \sim 6$. In addition, this models has been show to reproduce correctly the clustering properties of the galaxies (Rodriguez-Puebla et al. in prep. and Kakos et al. in prep.) as well as the observed counts on the far Infrared (Nava et al. in prep.). Thus, once we have established our fiducial CDM model, we now repit our fit by fixing our best fit parameters to the CDM Model and this time by fitting the far-ultraviolet luminosity function only and for the

cases 2-4. Notice that the Rodriguez-Puebla model is for galaxies where they can be accurately described by the Λ CDM model. Below we present our results.

In Fig. 3.8 we show the best fit model for the FUV luminosity function to a compilation of 21 observational studies (see Table 1 in [138] for details). Notice that for higher redshift galaxies $z \gtrsim 4$ determinations of the faint slope of the UV LFs may be over-estimated due to magnification bias [151]. The vertical lines corresponds to James Webb Space Telescope (JWST) prediction limits [152] estimated assuming the use of the F200W filter estimated for an investment comparable to CANDELS-W (labeled as *deep*) and a Hubble Ultra Deep Field HUDF-like survey on a cluster field with $10\times$ magnification (designated as *deep 10-x*) from gravitational lensing from a massive galaxy cluster, for more details, see [151].

In Fig. 3.10 we show the best fit model for the Galaxy Stellar Mass Function. We compare our model for the GSMF, with different authors based on local and high redshift measurements [137, 138, 153, 154, 155, 156, 157].

Additionally, for the nCDM + photoionization Model, we fitted the parameters a , b , c , M_{hm} to

$$a = 2.50 \tag{3.78}$$

$$b = 0.96 \tag{3.79}$$

$$c = -0.50 \tag{3.80}$$

$$M_{hm} = 9.40 \times 10^9, \tag{3.81}$$

that, according to the section 3.3.3, is used to fit the value of the parameter $\beta = 1.88$. If we compare this results with the Table 3.2, there is no precise match with any of the models proposed and studied by [6] due, possibly, to the existent degeneracy between the suppression coming from the UV background and that expected from the cutoff to the power spectrum of the nCDM model. However, we can note that the fit of β and M_{hm} is consistent with the resonant sterile neutrino model, see Table 3.2 Nevertheless, we observe that in Figures 3.8-3.10 there is a clear difference between the four models explored here at low masses, which represents an advance in the possible differentiation between models when the observations can reach deeper into the masses. In addition, more simulations and characterizations as the ones performed by [6] are needed in order to increase the spectrum of models to be tested.

Luminosity function ϕ_{FUV}

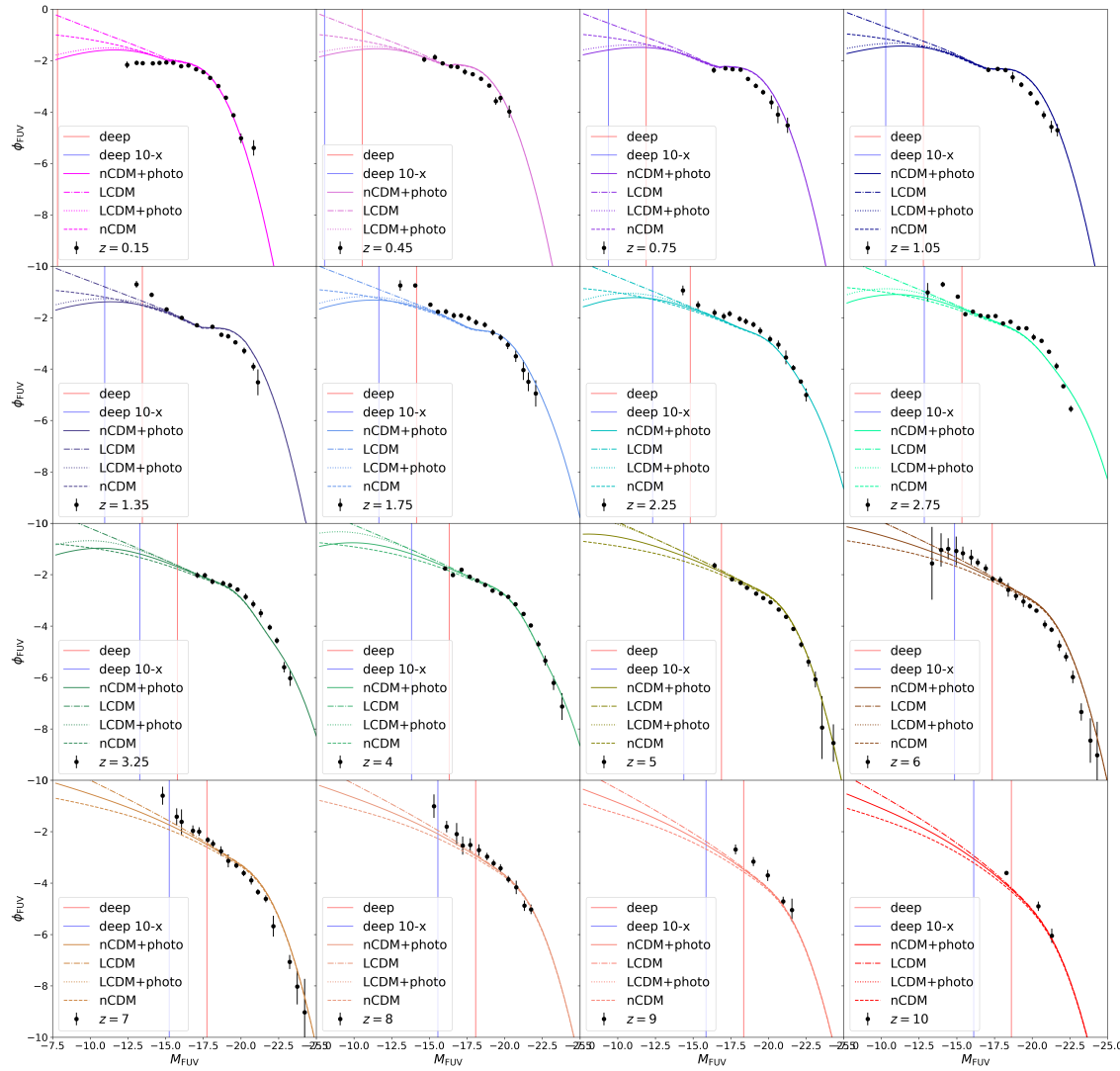


Fig. 3.8: Luminous Function (FUV) at different redshifts $z \in (0.15, 10)$

Luminosity function quotient $\phi_{FUV,i}/\phi_{CDM}$

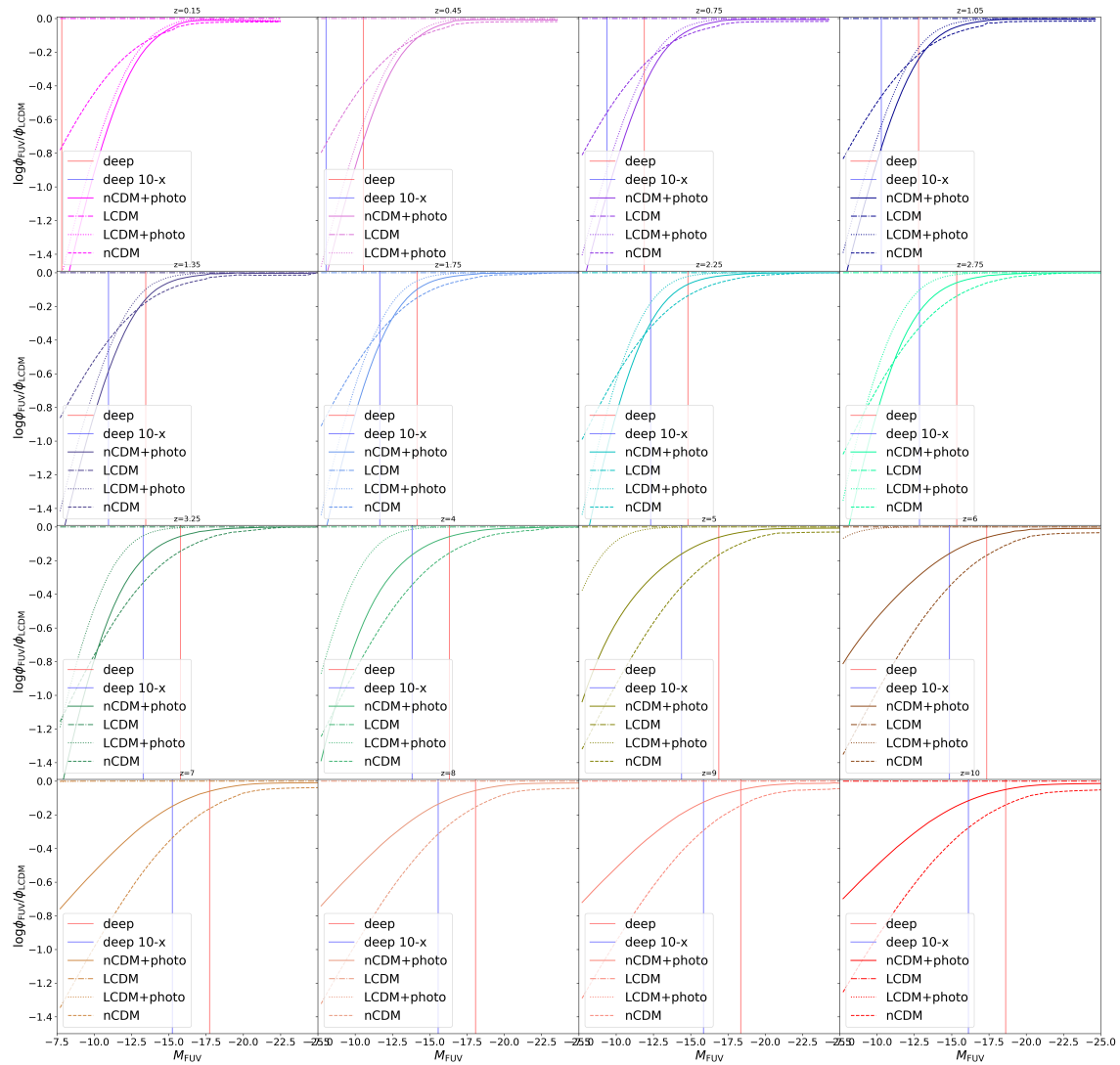


Fig. 3.9: Ratio of the different Luminous Function described on section ?? and the Luminous function of the LCDM model at different redshifts $z \in (0.15, 10)$

Galaxy Mass function ϕ_{GMF}

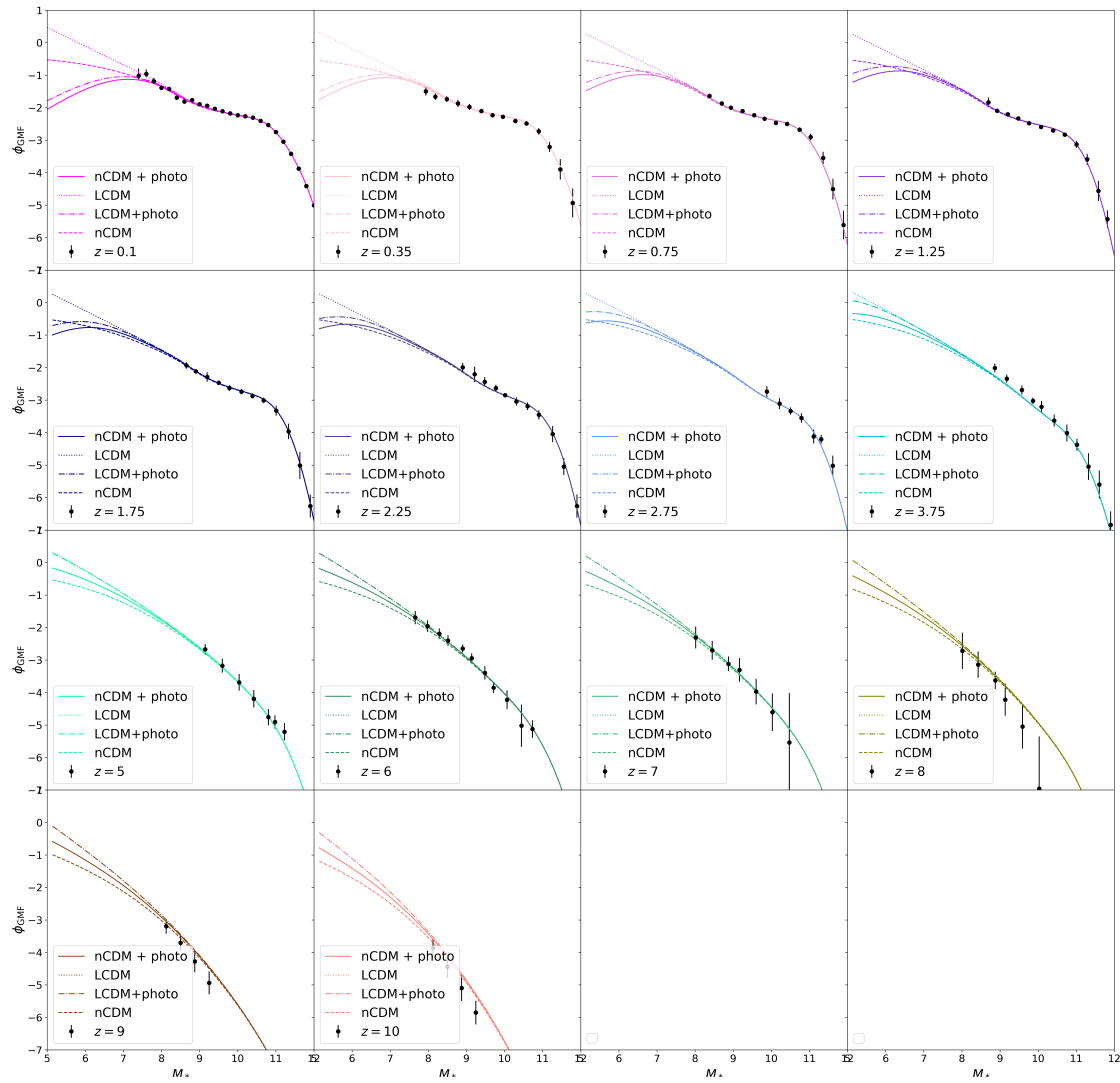


Fig. 3.10: Galaxy Stellar Mass Function (GSMF) at different redshifts $z \in (0.1, 10)$

Luminosity function quotient $\phi_{\text{GSMF}, i} / \phi_{\text{CDM}}$

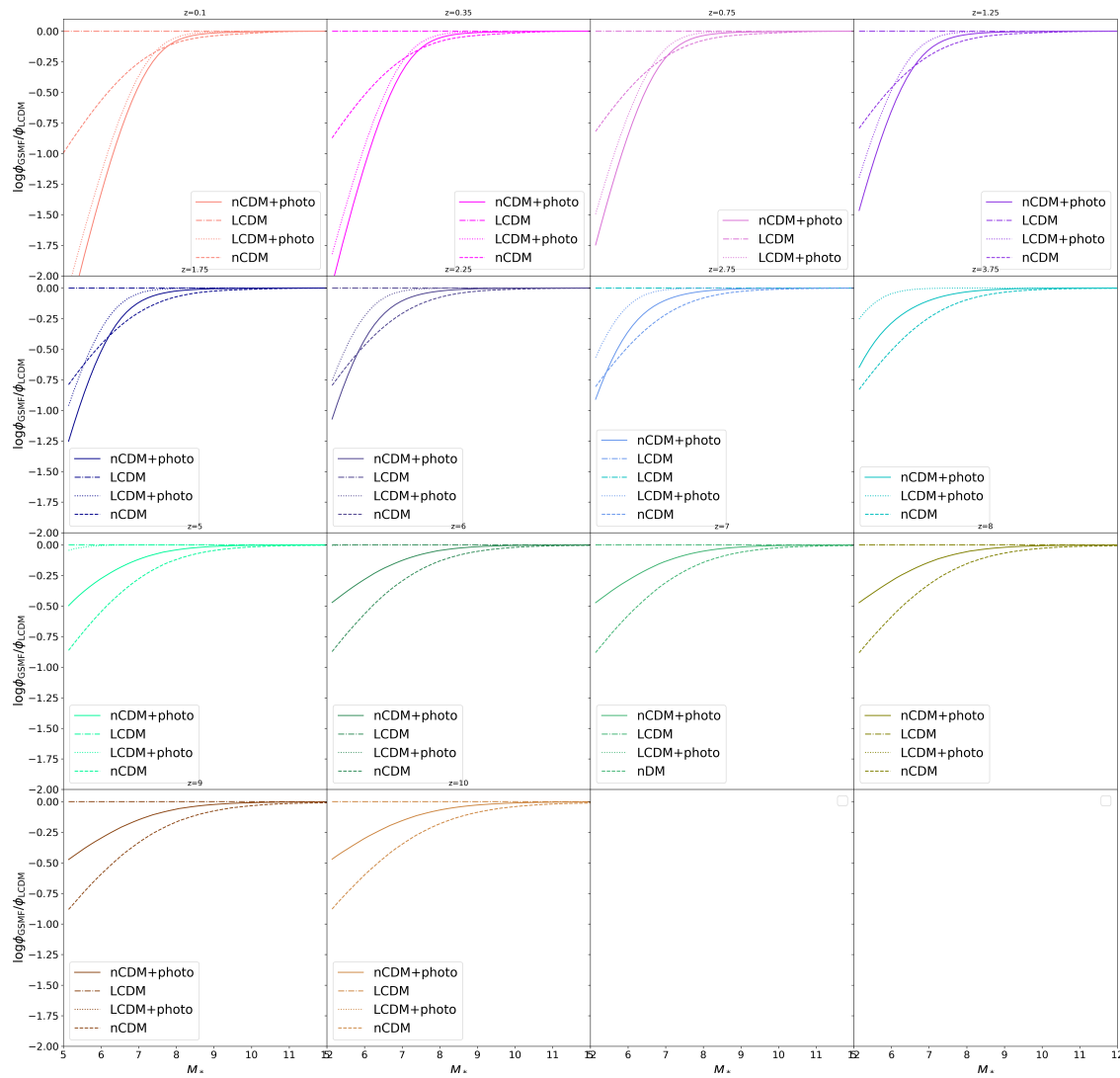


Fig. 3.11: Ratio of the different Galaxy Stellar Mass Function described on section ?? and the GSMF of the LCDM model at different redshifts $z \in (0.1, 10)$

3.3.5 Conclusions

In this work we explored two mechanisms of small-scale structure suppression in order to alleviate the so-called overabundance of satellite galaxies in the standard cosmological paradigm Λ CDM using the SHAM approach that connects galaxy's properties into halo properties. The main goal here was to alleviate the above tension, in addition to study the degeneracy between the suppression coming from the UV background and that expected from the cutoff to the power spectrum of a n CDM model. As we discussed above, this degeneracy is not completely resolved in our analysis, nevertheless we established a workable method that may be able to discern between a CDM model and a n CDM when we compare with the available astrophysical observations. The already launched James Webb Space Telescope will possess an unprecedented infrared sensitivity and spatial resolution required for detecting faint, distant galaxies that are extremely difficult or impossible to detect with any current facilities [158]. These observations will provide significant insights into the statistical properties of the galaxy population near low masses as can be noticed in Figures 3.8 and 3.9. If we can reach lower at the masses, we will be able to distinguish between the different models here proposed and possibly have knowledge of what is the most appropriate mechanism to suppress the overabundance of small-scale galactic structures.

The dark sector of the Universe.

Scalar Field Dark Energy

” *Contributing to know more about this two mysterious components of our Universe [Dark Energy and Dark Matter] is just astonishing*

— **Alma Xochitl Gonzalez Morales**
Co-chair of the Lyman-alpha working group at
DESI

4.1 Dark Energy

The standard cosmological model, Λ CDM, also has problems in the sector of the dark energy, such as the so-called *cosmological constant problem* [159] and the *coincidence problem* [160]. The observations suggest that a large fraction of the energy density of the universe, the dark energy, has negative pressure. One description of this component is to associate it with vacuum energy density; nevertheless, we have known for several decades that Λ , the cosmological constant, is certainly much smaller than typical contributions to the vacuum energy that can be estimated from the Standard Model of particle physics [161]. That is, the discrepancy of 123 orders of magnitude between the interpretation of the cosmological constant from a particle physics point of view as the vacuum energy density $\rho_p = 5.16 \times 10^{99} \text{ g m}^{-3}$ and the present value observed of the Hubble parameter squared that corresponds to a density of $\rho_\Lambda \sim 10^{-24} \text{ g m}^{-3}$. Then, the behavior of the dark energy can be described by other approaches, for example a scalar field and variety of scalar models have been studied in this direction. The simplest case is the so-called quintessence described by a classic scalar field minimally coupled to gravity that has a density and equation of state (EoS) that vary with time, $w = w(t)$, in contrast with the static cosmological constant. The ghost fields are the

optimal scalar fields for this component of the dark sector due to the property of having a negative kinetic term which leads to an EoS parameter $w \leq -1$. In this chapter we explore a quintessence–complex scalar field with attractive self interaction to describe the cosmic acceleration of the Universe [13] and a wormhole solution of the Einstein equations considering a family of massive, complex and self–interacting ghost scalar fields [14].

4.2 Complex Scalar Field Dark Energy

Introduction

The inclusion of the dark components of the Universe in Einstein equations gives a consistent description of the current observed dynamics at a large scale [162, 163, 36]. These components are known as dark energy and, at a galactic level [164, 165, 166, 167, 32], dark matter. The nature of such dark components remains unknown. Dark energy, although at first order is modelled as a repulsive gravitational term such as the Cosmological Constant Λ , certain observations have shown some tensions in the Hubble flow in the standard Λ CDM model [168], so it seems like it is not sufficient to describe the dark energy with a constant term; it is thus proposed to be modelled by different types of matter, such that the relation between the spatial components of the corresponding stress energy tensor to the temporal one, is consistent with the observed dynamics; that is, using an analogy with fluid dynamics, it can be defined an Equation-of-State (EoS) $T_i^i = -w c^2 T_0^0$ (i. e. $p = w \rho$ for the pressure and density of a fluid like description). The behaviour of the function w can be related to the observations, as described below, and its value at the present is close to minus one.

Regarding the modelling of the dark matter, several models have proposed that it should be considered as a weakly interactive particle. However, not strong evidence of such a particle has been detected in the current projects that have been created *ex professo* to obtain a detection either directly [37, 38, 39, 40] or indirectly [41, 42, 43]. It must be faced the possibility that dark matter had zero interaction with the baryonic matter.

Indeed, as mentioned above, the Theory of General Relativity allows to describe several kinds of matter/energy, in comparison to the Newtonian case. In this way, once there are models of one type of matter or another, consistent with the observations, the next

step is the determination of characteristic features generated on the baryonic matter by each kind of matter which could, in principle, be detected. Even supposing that there is no interaction of the baryonic matter with the dark components, other than gravitational, it can still be seen that the density distribution of the different types of matter/energy has a very distinctive feature which affects the distribution of baryonic matter, and that could tell at least what kind of matter better describes the observed density distribution, see e.g [111] for a discussion on the subject. As an example of the latter, in [169] was studied how the density perturbations evolve inside a dark matter halo considering that the matter was a collection of non-interactive particles, whose dynamics are described by the Vlasov equation. The main result in that work was that the final state has a very distinct distribution in the coordinate space, a double peaked Gaussian in the density and, in the phase space, a volcano-like form in the distribution function, features that could affect the baryonic density distribution, which is an observable quantity.

To define analogous strategies regarding the dark energy, there are several considerations that must be taken into account. It is a component associated mainly with the cosmic acceleration [170, 171, 172] which, as mentioned above, can be modelled with the simple inclusion of a properly tuned Λ in the Einstein's equations, although this constant rules out the usual Minkowski's solution, and the asymptotic limits of all the well established solutions to the Einstein's equations need to be modified. It is an exciting fact that there is a new constant of Nature, see [173] for an interesting discussion on the subject, but the implications in the equations themselves enhance the need to prove the veracity of such model, a fact which is done proposing more general models to describe the cosmic acceleration. In addition to its modeling with different kinds of matter, another way to proceed, is to propose alternative gravity models of matter that can describe the current observed dynamics [174, 175, 176].

Within the models proposed to describe the dark energy other than a constant term, in Einstein gravity, those considering a scalar field can be the simplest, well motivated choice from a particle physics point of view. Nevertheless, the great challenge is to determine the appropriate scalar potential $V(\Phi)$ that could explain current cosmological observations. An example of a description by a scalar field minimally coupled to gravity is the *quintessence* model. The main motivation for considering it is to reduce the so-called *fine-tuning* problem, issue that has been explored by the tracker quintessence solutions. However, the predicted values on these models for the EoS at the present epoch is not in good agreement with supernovae results [160, 177]. Another example is the exponential quintessence potential that focus on models and parameters which lead

to inflation, nevertheless nucleosynthesis constraints require that the energy density of the scalar field be $\Omega_\phi \leq 0.2$, i.e., it would never dominate the Universe [178]. Another dynamical potentials proposed in [179] and [180] avoid successfully the fine-tuning and cosmic coincidence problem, but the values of the potential parameters can not be unambiguously determined in order to match the observations constraints.

The above models are made up of real scalar fields. However, also complex scalar fields should be considered since such fields (unlike the real case) have been invoked in many different sectors of particle physics [181] (such as the Higgs mechanism) and interestingly in the scene of ultra cold gases [182]; they can be used to construct static distributions as Boson stars [183], and also configurations surrounding a black hole, the so-called wigs [184], and they can even define static configurations with an associated angular momentum number [185, 14]. Furthermore, a real quantized scalar field yields the same field equations as those obtained by using a classical complex scalar field [100]. These reasons motivated us to consider a dark energy model described by a massive quintessence-complex scalar field with attractive self interaction. Such field was formerly studied in [26] and, in the present work, we revisited the idea focusing in the so-called peculiar branch solution of the Einstein-Klein-Gordon equations in order to obtain parameter restrictions of the potential consistent with the current precision observations. Although we are aware of the latest results regarding the possible dynamical behavior of the EoS [168] and the impossibility for a single canonical field to evolve crossing over $w = -1$ because of the no-go theorem [186], it is interesting to explore in detail the properties of the previously mentioned branch and in computing best fit values of their parameters, in order to have a quantitative description of the model and a clearer picture of what the model needs in order to be consistent with such a dynamical behavior of the dark energy.

This section is organised as follows: in Sec. 4.2.1 we briefly describe the Friedman background considering a complex scalar field instead of the standard cosmological constant. In Sec. 4.2.2 we study the Einstein-Klein-Gordon equations to describe dark energy based in the fact that the scalar potential can be proposed as an effective *fluid*, with the caution of not solving the EoS, but solving Klein-Gordon first, and with the field and its derivative, compute the density and the scalar pressure, and subsequently compute the corresponding w . We consider the fast oscillation regime, where the pulsation ω of the scalar field is assumed to be faster than the Hubble expansion. An EoS is obtained for a peculiar branch in such fast oscillation regime. We denote the model presented in this manuscript as Complex Scalar Field Dark Energy (CSFDE). In Sec. 4.2.2 a generic EoS with a complex scalar field mimicking the dark energy term is

presented. A description of the current late-time observations are given in Sec. 4.2.3. These samplers will be employed to constrain the *only* free cosmological parameter that goes into the expression for the EoS of our CSFDE model. In Sec. 4.2.4 we describe the methodology to proceed with the precision analysis and discuss the cosmological constraints obtained. Finally, our conclusions are given in Sec. 4.2.5.

4.2.1 Complex Scalar Field in an homogeneous background

In this section we derive first the evolution equations for a homogeneous and flat universe filled with radiation, baryonic and dark matter components and an effective density which will mimic the dark energy component. In the second part, we introduce the complex scalar field to describe such effective density and obtain the corresponding Klein-Gordon equation.

Friedman equations

First, let us consider a homogeneous isotropic Universe, described by the Friedman-Lemaître-Robertson-Walker metric 3.26. From this point forward we consider spatial flatness. As it is standard, we can derive the Friedman equation and the energy conservation equation by introducing the above metric in the Einstein's equations. Before continue with this straightforward calculation, let us establish our pivot model: the paradigmatic cosmological model, Λ CDM, which considers a total density of the Universe $\rho_T = \rho_r + \rho_b + \rho_{\text{cdm}} + \rho_{\text{DE}}$, normalised by the critical density given by $\rho_{\text{crit}} = 3H_0^2/8\pi G$, where H_0 is the Hubble parameter at present time and G is the gravitational constant. According to this, we can derive the constraint equation from the Friedman evolution as

$$\left(\frac{H}{H_0}\right)^2 = \Omega_m + \Omega_\Lambda, \quad (4.1)$$

with

$$\Omega_m = \frac{\Omega_{r,0}}{a^4} + \frac{\Omega_{b,0}}{a^3} + \frac{\Omega_{\text{cdm},0}}{a^3}, \quad (4.2)$$

where $\Omega_i = \rho_i/\rho_{\text{crit}}$ ($i = \text{cdm}, b, r$), represents the density parameter and the symbols cdm, b, r correspond to cold dark matter (CDM), baryonic matter and radiation, respectively.

According to [1], the cosmological values for the densities described above are: $\Omega_{\text{cdm}}h^2 = 0.120 \pm 0.001$, $\Omega_b h^2 = 0.0224 \pm 0.0001$, $\Omega_\Lambda = 0.674 \pm 0.013$ and $\Omega_m =$

0.315 ± 0.007 . Currently, this model has proved to be consistent with several observations, however, it has problems in regards to the tension on the value of some parameters like those of σ_8 and H_0 [187].

As indicated in the Introduction, it is interesting to explore dynamic EoS since they alleviate tensions between certain cosmological parameters. Classical scalar fields are simple models for introducing time-dependent equations of state. The case of a scalar field minimally coupled to gravity, with a positive canonical kinetic term, called quintessence [188, 160]. Extensions to this model have been widely considered, for example some by including non-canonical scalar fields or negative signed kinetic terms. However in this work, we consider a simpler case, which considers a rapidly oscillating minimally coupled complex scalar field [181, 10, 26].

The Klein-Gordon equation

We use the evolution described as a starting point, and introduce a complex scalar field in order to model dark energy. Our proposal is based in the fact that the scalar potential $V(|\Phi|^2)$, has a quartic-form with a negative scattering length as

$$V(|\Phi|^2) = \frac{m^2 c^2}{2\hbar^2} |\Phi|^2 - \frac{2\pi A_s m}{\hbar^2} |\Phi|^4, \quad (4.3)$$

where m is the complex scalar field mass, A_s the absolute value of the scattering length and \hbar the reduced Planck constant. This scalar potential describes, for instance, a relativistic Bose-Einstein condensate at zero temperature with attractive self-interaction [189, 190], and it is also similar to the Higgs potential of particle physics but with an overall opposite sign.

The evolution of this complex scalar field in the cosmological scenario described above is given by the Klein-Gordon equation

$$\frac{1}{c^2} \frac{d^2 \Phi}{dt^2} + \frac{3H}{c^2} \frac{d\Phi}{dt} + 2 \frac{dV}{d|\Phi|^2} \Phi = 0, \quad (4.4)$$

from where we can express the complex scalar field as

$$\Phi = |\Phi| e^{i\theta}. \quad (4.5)$$

Solutions to the Einstein-Klein-Gordon equations would require in total six parameters related to initial conditions for the real and imaginary parts of Φ and their first time

derivative together with the scalar field values for m and A_s . A further simplification can be made within this model when, consistently with dark energy-like behavior, we assume that the field is oscillating rapidly, this leads to a three-parameter model.

In our proposal, we are going to follow the procedure given in [26], of which we summarize some key points. Using (4.5) in (4.60), the Klein-Gordon equation can be divided into a real and an imaginary part, from which the second leads to the equation:

$$Q = -\frac{1}{\hbar c^2} a^3 |\Phi|^2 \frac{d\theta}{dt}, \quad (4.6)$$

where Q is constant¹ and a the scale factor.

From the real part, and using the conserved charge Q explicitly in this equation, we obtain

$$\frac{1}{c^2} \left[\frac{d^2 |\Phi|}{dt^2} - \frac{Q^2 \hbar^2 c^4}{a^6 |\Phi|^3} \right] + \frac{3H}{c^2} \frac{d|\Phi|}{dt} + 2 \frac{dV}{d|\Phi|^2} |\Phi| = 0. \quad (4.7)$$

The term containing Q^2 is usually related to a centrifugal force when making the analogy of this equation with that of fictitious particle with radial coordinate $|\Phi|$, hence the name spintessence for that model [26, 10].

In the real case, with a quartic potential analogous to (4.3), we have $\theta = 0$, therefore the conserved quantity Q in (4.6) is equal to zero, implying among other things, that the solution must have a rapidly oscillating behavior with an equation of state also oscillating around $w = 0$ [28] and the solutions to the equation of motion must be obtained by numerical integration in an appropriate set of variables. The quartic potential is not the only possibility, for instance taking a massless scalar field ($\mu = 0$, $\lambda = 0$) the equation of state stays trivially at the value $w = 1$. Other (real) scalar fields, describing quintessence potentials, as the ones listed in the introduction, may have dynamical EoS some of which also oscillate in time. In this work we take the opposite approach, namely $Q \gg 0$, leading to an exact solution of the problem which is useful in the implementation of tests for the model with cosmological analyzes. To compute the energy density and pressure of the complex scalar field, we consider the following expressions:

¹After integration, the imaginary part of the Klein-Gordon equation leads to a conserved quantity, which corresponds to the conserved charge of a complex scalar field, given by $Q = \frac{1}{c^2 \hbar} \int dx^3 \sqrt{-g} \text{Im}(\Phi \partial_t \Phi^*)$.

$$\epsilon = \frac{1}{2c^2} \left| \frac{d\Phi}{dt} \right|^2 + V(|\Phi|^2), \quad (4.8)$$

$$P = \frac{1}{2c^2} \left| \frac{d\Phi}{dt} \right|^2 - V(|\Phi|^2). \quad (4.9)$$

Notice how we can connect these equations to the ones presented in Sec.4.2.1 where the quantity ϵ will replace the Λ CDM quantity $\rho_{\text{crit}}\Omega_\Lambda$ in the Friedman equation.

From the equations (4.60), (4.8) and (4.9) we can obtain a useful equation for the energy density that resembles the continuity equation for a perfect fluid

$$\frac{d\epsilon}{da} + \frac{3}{a}(\epsilon + P) = 0. \quad (4.10)$$

With these equations, now we are ready to study particular solutions of the Einstein-Klein-Gordon system evolving with a complex scalar field mimicking the dark energy component. As mentioned, this particular model in the fast oscillation regime and its homogeneous solution have already been presented previously by [26], and we extend the study in order to obtain analytical expressions for most of the quantities of the solution, including $w(z)$.

4.2.2 Dark Energy Solution in the fast oscillation regime

In [26] was found that in the fast-oscillation regime, i.e., when the oscillation frequency of the scalar field is much larger than the value of the Hubble function, the solution of the Einstein-Klein-Gordon equations for the case of a complex scalar field with an attractive self interaction potential (4.3) has two different solutions. One solution (called normal branch) resembles to a dark matter scalar field, while the other solution (called peculiar branch) corresponds to a quintessence model. This solution only exists in the fast oscillation regime, in which the scalar field suddenly emerges and behaves as dark energy at late times.

Following the same logic, in this paper we propose a deduction of an exact solution for the equation of state of the quintessence field. Once with this equation, we explore their possible constraints by using current observational data.

Peculiar branch solution in the fast oscillation approximation

To establish the fast oscillation regime mentioned above, we consider the following condition which needs to be satisfied during the evolution of the scalar field

$$\omega = \frac{d\theta}{dt} \gg H. \quad (4.11)$$

In addition to the latter condition, we will impose that the magnitude of the scalar field change slowly on time respect to the angular frequency of oscillation ω as:

$$\frac{1}{|\Phi|} \frac{d|\Phi|}{dt} \ll \omega. \quad (4.12)$$

Conditions (4.11)-(4.12) set the so-called fast oscillation regime of the Klein-Gordon equation (4.60). Following this prescription, (4.7) can be reduce to

$$\omega^2 = 2c^2 \frac{dV}{d|\Phi|^2}. \quad (4.13)$$

This allows us to write the fast oscillation condition in terms of the charge Q defined in (4.6), which becomes

$$\frac{Q^2 \hbar^2 c^4}{a^6 |\Phi|^4} = 2c^2 \frac{dV}{d|\Phi|^2}. \quad (4.14)$$

Using the expression for the scalar field potential (4.3), we can approximate (4.8) using the condition (4.13) as

$$\begin{aligned} \epsilon &= \frac{1}{2c^2} \left[\left(\frac{d|\Phi|}{dt} \right)^2 + \omega^2 |\Phi|^2 \right] + \frac{m^2 c^2}{2\hbar^2} |\Phi|^2 - \frac{2\pi A_s m}{\hbar^2} |\Phi|^4 \\ &\approx \frac{m^2 c^2}{\hbar^2} |\Phi|^2 - \frac{6\pi A_s m}{\hbar^2} |\Phi|^4, \end{aligned} \quad (4.15)$$

By a similar approach, the scalar pressure from (4.10) can take the approximate form

$$P \approx -\frac{2\pi A_s m}{\hbar^2} |\Phi|^4. \quad (4.16)$$

Solving (4.15) for $|\Phi|^2$, we obtain two possible branches that correspond to solutions of the Einstein-Klein-Gordon system in the fast oscillation approximation

$$|\Phi|^2 = \frac{c^2 m}{12\pi A_s} \left(1 \pm \sqrt{1 - \frac{24\pi A_s \hbar^2}{m^3 c^4} \epsilon} \right). \quad (4.17)$$

Notice that this is a different result in comparison to the repulsive self-interaction case [22], where there is an unique branch in the solution since only the (+) sign of the square root is possible. Furthermore, in [26] was shown that for the attractive self-interaction case (4.17) and when we take the negative sign, the scalar field undergoes a matter-like phase (and even an inflation epoch). While for the positive branch, the solution behaves as dark energy. From this point forward we will take the positive sign, to focus on that particular branch.

Therefore, by using (4.17) in (4.16) we obtain

$$P(\epsilon) = -\frac{m^3 c^4}{72\pi A_s \hbar^2} \left(1 + \sqrt{1 - \frac{24\pi A_s \hbar^2}{m^3 c^4} \epsilon} \right)^2. \quad (4.18)$$

Physical solutions of this latter equation correspond to those values of ϵ smaller than a certain ϵ_i :

$$\epsilon_i = \frac{m^3 c^4}{24\pi A_s \hbar^2}. \quad (4.19)$$

From the two latter expressions, notice that $P(\epsilon_i) = -\frac{m^3 c^4}{72\pi A_s \hbar^2}$, implies that $w_i = \frac{P(\epsilon_i)}{\epsilon_i} = -1/3$.

The scale factor for which the energy density takes the value ϵ_i can be calculated by inserting the value of $|\Phi|^2$ evaluated in ϵ_i , and taking the result on the fast oscillation condition (4.14):

$$a_i = \sqrt[3]{\frac{12\sqrt{3}\pi A_s \hbar^2 |Q|}{m^2 c^2}}. \quad (4.20)$$

For convenience, we re-define a dimensionless quantity in terms of the differential equation for the energy density as

$$\bar{\epsilon} = \frac{\epsilon}{\epsilon_i}, \quad (4.21)$$

therefore (4.10) can be written as

$$\frac{d\bar{\epsilon}}{da} = -\frac{3}{a} \left[\bar{\epsilon} - \frac{1}{3} \left(1 + \sqrt{1 - \bar{\epsilon}} \right)^2 \right]. \quad (4.22)$$

Evaluating in $\epsilon = \epsilon_i$, we can see that $d\bar{\epsilon}/da$, takes a negative value of $-\frac{2}{a_i}$, therefore for $a < a_i$ the solution is not valid. The value a_i indicates the scale factor at the time when the scalar field turns on. Furthermore, at $a \rightarrow \infty$, ϵ approaches to a constant value.

Now, taking the fast oscillation equation (4.14) and inserting $|\Phi|^2$ from (4.17) we obtain

$$\left(\frac{a_i}{a} \right)^6 = 3 \left(1 + \sqrt{1 - \bar{\epsilon}} \right)^2 - 2 \left(1 + \sqrt{1 - \bar{\epsilon}} \right)^3. \quad (4.23)$$

In order to find the asymptotic value of ϵ , when $a \rightarrow \infty$, we should consider the fast oscillation equation (4.14), which for potential (4.3) takes the form

$$\frac{Q\hbar c^2}{a^3} = \sqrt{2}c|\Phi|^2 \sqrt{\frac{m^2 c^2}{2\hbar^2} - \frac{4\pi A_s m}{\hbar^2} |\Phi|^2}. \quad (4.24)$$

Since ϵ decreases with a , then $|\Phi|^2$ increases as $a \rightarrow \infty$ as we can notice from (4.17), therefore the term inside the square root in (4.24) should vanish as $a \rightarrow \infty$, leading to an asymptotic value of

$$|\Phi_\Lambda|^2 = \frac{mc^2}{8\pi A_s}. \quad (4.25)$$

Using (4.15) and (4.18) we can obtain

$$\epsilon_\Lambda = \frac{m^3 c^4}{32\pi A_s \hbar^2} = \frac{3}{4} \epsilon_i, \quad (4.26)$$

$$P(\epsilon_\Lambda) = -\epsilon_\Lambda. \quad (4.27)$$

Notice how in the limit $a \rightarrow \infty$, the scalar field has an EoS with a value $w_\Lambda = -1$. Therefore the EoS interpolates between the values $-1/3$ and -1 . This is a result of both the rapidly oscillating behavior of the field and the chosen peculiar branch, although not a general property of a homogeneous complex cosmological scalar field nor a direct consequence of having a non-zero conserved quantity Q . This result is very different

from the one that would have been obtained for the other branch of the solution or even for the real case. In those cases we would not have a scalar field solution with $w < 0$ that turns on at a certain scale factor a_i and not before.

Exact solution for the dark energy term-like

To obtain an expression for ϵ in terms of the scale factor, we have to solve the Eq. 4.23. This can be obtained making the change of variable

$$\zeta = \sqrt{1 - \bar{\epsilon}} + \frac{1}{2}. \quad (4.28)$$

The latter leads to an expression in terms of a cubic equation

$$\zeta^3 - \frac{3}{4}\zeta + \frac{1}{2} \left(\frac{a_i^6}{a^6} - \frac{1}{2} \right) = 0, \quad (4.29)$$

which has three real solutions. However, it must satisfy the conditions $\zeta(a_i) = \frac{1}{2}$ and $\zeta(a \rightarrow \infty) = 1$. The only solution that satisfy these conditions is

$$\zeta(a) = \cos \left[\frac{1}{3} \arccos \left(1 - 2 \frac{a_i^6}{a^6} \right) \right], \quad (4.30)$$

in terms of this function $\zeta(a)$, the energy density and the EoS parameter are given by the following expressions

$$\epsilon(a) = \left[1 - \left(\zeta(a) - \frac{1}{2} \right)^2 \right] \epsilon_i, \quad (4.31)$$

$$w(a) = - \frac{\left(\zeta(a) + \frac{1}{2} \right)^2}{3 - 3 \left(\zeta(a) - \frac{1}{2} \right)^2}. \quad (4.32)$$

This is the so-called Complex Scalar Field Dark Energy (CSFDE) model. These solutions should be considered only in certain region $a_i < a < a_e$ of the evolution of the Universe, the upper limit a_e is defined as the scale factor when the fast oscillation regime ceases to be valid, which we will calculate below. This is evident from (4.14), since ω get suppressed by the term a^6 , while $|\Phi|$ goes to a constant value. From now on, a will

only be referred to this range. First, we must make sure that the solution at a_i satisfy the fast oscillation approximation described in the latter section.

Under these ideas, the fast oscillation condition $\omega \gg H$ is given by

$$\frac{Q^2 \hbar^2 c^4}{a^6 |\Phi|^4} \gg \frac{8\pi G}{3c^2} (\rho_m + \epsilon), \quad (4.33)$$

where $\rho_m = \Omega_m / \rho_{\text{crit}}$, see (4.2). By performing the substitution of $|\Phi|^2$ using (4.17), re-writing it in terms of $\bar{\epsilon}$ and, finally, taking $\epsilon \gg \rho_m$, we can obtain

$$\left(\frac{a_i}{a}\right)^2 \gg \frac{mG}{3c^2 A_s} \bar{\epsilon} (1 + \sqrt{1 - \bar{\epsilon}})^2. \quad (4.34)$$

This condition will be satisfied initially if

$$\frac{3c^2 A_s}{mG} \gg 1. \quad (4.35)$$

In order to compute the value $a_e > a_i$, where the solution is no longer valid, we will consider the end of the fast oscillation regime when $\omega = NH$ (with $N = 200$ analogous to [22]). If $a_e \gg 1$ and also $a_e \gg a_i$, in order to be able to make the approximations $\epsilon \gg \rho_m$ and $a_i/a_e \ll 1$ in (4.34), then the end value of the scale factor will be

$$a_e \approx \sqrt[6]{\frac{768 \pi^2 A_s^3 \hbar^4 Q^2}{N^2 G m^5 c^2}}. \quad (4.36)$$

In Fig. 4.1 we show an example for the evolution of the equation of state parameter w between the values for the scale factor a_i and a_e , determined by specific values of m , A_s and Q . In this example we take² a_i to be the value $a_{\text{min}} = 0.1 < 1/(1 + z_{\text{max}})$ where $z_{\text{max}} = 2.26$ corresponds to the maximum redshift used in the multiple data sets within the analysis described in the next section. In this way, we ensure that the scalar field is present throughout the a range of the analysis. We have restricted this example to the case where $a_e = 1$, thus ensuring that the limit of rapid oscillations and therefore the cosmological constant type behaviour continues to be valid today.

To give a qualitative description about what is happening in the complete cosmological model where dark energy is described by the scalar field solution described at Sec. 4.2.2,

²This particular choice of a_i and a_e in our example reduces the dimension of the free parameter space from 3 to 2, thus we can put Q and A_s in terms of m : $Q = \frac{4a_{\text{min}}^9 m c^4}{27\sqrt{3\pi N G h^4}}$, $A_s = \frac{9N^2 G \hbar^2 m}{16a_{\text{min}}^6 c^2}$.

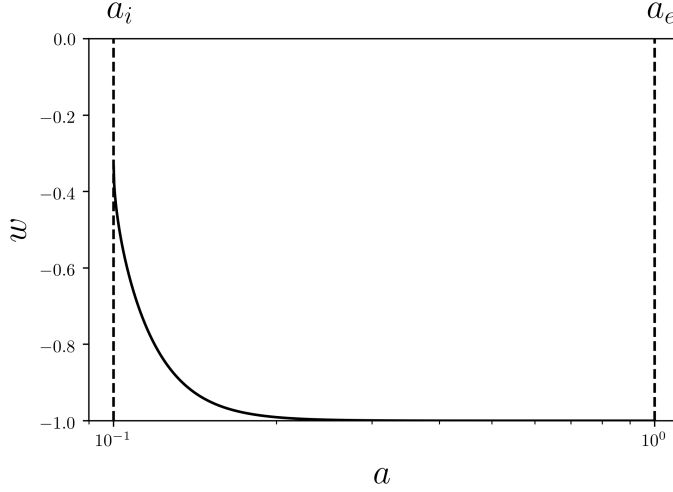


Fig. 4.1: Evolution of the w Eq. (4.32) as a function of the scale factor, a , in the quintessence model. The dashed vertical lines represent the valid interval of the solution; the left line is taken as the value $a_i = 0.1$ and the right limit a_e is defined as the scale factor when the fast oscillation regime ceases, Eq. (4.36).

we present in Fig. 4.2 the energy density fractions of the quintessence model with the same values a_i and a_e as in Fig. 4.1, additionally, for our example we have chosen the initial scalar field energy density to be $\epsilon_i \equiv \frac{4}{3}\epsilon_\Lambda = \frac{3}{4}\rho_{\text{crit}}\Omega_\Lambda$. In other words, we have chosen that the asymptotic value for the energy density of the scalar field coincides with the current energy density for Λ in the pivot model. Interestingly, it turns out that this condition on the example fixes the three free parameters of our model, leading to a mass $m \sim 10^{-22}\text{eV}/c^2$, frequently used in the ultralight models of dark matter [28, 49, 45]. The Fig. 4.2 is almost indistinguishable from the corresponding figure for the Λ CDM model, this is because the discontinuity for ϵ appears in an epoch where the contribution to the total energy density of the scalar field is relatively small and also because ϵ quickly tends to the ϵ_Λ value, as can be inferred from Fig. 4.1 and Eq. 4.31.

Parametric Equation of State in the late cosmic acceleration approximation

Let us write explicitly (4.32) as an effective dark energy EoS described by a complex scalar field with a Bose-Einstein condensate-like potential. By using the standard

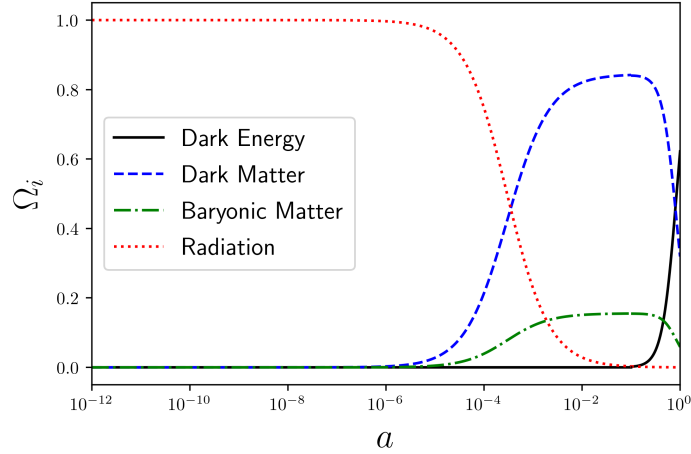


Fig. 4.2: Evolution of the fractions Ω_i of the energy density of each component of the Universe i as a function of the scale factor, a , in the quintessence model. Different components are represented with different line styles as labeled in the legend.

definition $a = 1/(1+z)$ and expand the function ζ in (4.30) with the assumption $a \gg a_i$ we obtain:

$$w(z) = w_0 + w_a(1+z)^6, \quad (4.37)$$

where $w_0 = -1$ and $w_a = \frac{16}{27}a_i^6$. Notice that this generic expression for the EoS impose directly on w_0 the cosmological constant value. We will refer to this particular parametrization of the scalar field model as *parametric form for the CSFDE model*.

The quantity a_i which completely determines w_a , is restricted to have values consistent with a scalar field present at any time in the past. Therefore we should take the range $0 < a_i < 1$ which, translated to w_a , corresponds to the range

$$w_a \in \left(0, \frac{16}{27}\right). \quad (4.38)$$

Actually the validity of the parametric equation of state (4.37) requires pushing the value a_i further back in time. We could take, for instance $a_i = 0.3$, which satisfies the above conditions. In this case, the parametric equation of state (4.37) has a maximum absolute error with respect to the exact case (4.32) of 8×10^{-2} .

We should remark that (4.37) is not obtained as in the traditional derivation of the solution of the conservation equation, where an effective dark energy fluid needs to be consider and certain fixed values of w denote the different matter in the universe.

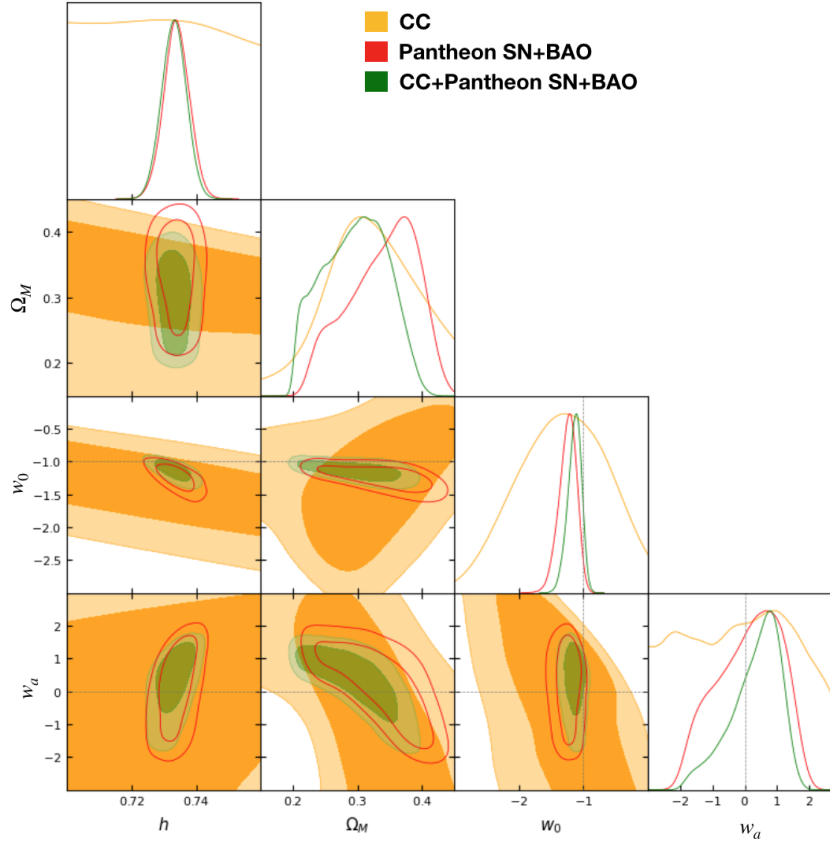


Fig. 4.3: The 68% confidence level (C.L.), 95% CL. and 99.7% regions inferring from the parametric CSFDE (4.37) using CC (yellow C.L), Pantheon supernovae + BAO (red C.L) and the full sample (CC+SN+BAO) (green C.L).

4.2.3 Observational constraints

To perform the statistical analyses for the parametric CSFDE (4.37) and to find current constraints of the model, we are going to consider in this paper late-time data sets as SNeIa (Pantheon), Observational Hubble data (OHD) and Baryon Acoustic Oscillations (BAO).

Each observational data has the following features:

- Pantheon SNeIa compilation: This sample is one of the latest Type Ia Supernovae (SN) compilations [191] and it contains 1048 SNeIa at redshift $0.01 < z < 2.26$. The constraining power of this kind of supernovae is due that this observation

can be used as standardizable candles. This can be implemented through the use of the distance modulus

$$\mathcal{F}(z, \Theta)_{\text{theo}} = 5 \log_{10} [D_L(z, \Theta)] + \mu_0, \quad (4.39)$$

where D_L is the luminosity distance given by

$$D_L(\Theta) = (1 + z) \int_0^z \frac{c dz'}{H_0 E(z', \Theta)}, \quad (4.40)$$

and $\Theta = \{w_0, w_a\}$ is the vector with the free cosmological parameters to be fitted. We notice that the factor c/H_0 can be absorbed in μ_0 . Furthermore, we can write $\Delta\mathcal{F}(\Theta) = \mathcal{F}_{\text{theo}} - \mathcal{F}_{\text{obs}}$, using for this purpose the distance modulus \mathcal{F}_{obs} associated with the observed magnitude. At this point it may be thought that a possible χ_{SN}^2 is given by

$$\chi_{SN}^2(\Theta) = (\Delta\mathcal{F}(\Theta))^T \cdot C_{SN}^{-1} \cdot \Delta\mathcal{F}(\Theta), \quad (4.41)$$

where C_{SN} is the total covariance matrix. This equation can be used to contain the nuisance parameter μ_0 , which in turn is a function of the Hubble constant, the speed of light c and the SNeIa absolute magnitude. To circumvent this issue, χ_{SN}^2 is marginalized analytically with respect to μ_0 and we can obtain a new χ_{SN} estimator

$$\chi_{SN}^2(\Theta) = (\Delta\mathcal{F}(\Theta))^T \cdot C_{SN}^{-1} \cdot \Delta\mathcal{F}(\Theta) + \ln \frac{S}{2\pi} - \frac{k^2(\Theta)}{S}, \quad (4.42)$$

where S is the sum of all entries of C_{SN}^{-1} . This equation gives an estimation of the precision of these data independently of Θ , and k is $\Delta\mathcal{F}(\Omega_m, \Omega_r, \Omega_\Lambda)$ but weighed by a covariance matrix as follows:

$$k(\Theta) = (\Delta\mathcal{F}(\Theta))^T \cdot C_{SN}^{-1}. \quad (4.43)$$

Also, for this sampler we are taking the nuisance parameter M inside the sample, for this we choose the respective values of M from a statistical analysis of the Λ CDM model with a fixing H_0 from the Late Universe measurements (SH0ES + H0LiCOW) as $H_0 = 73.8 \pm 1.1 \text{ km/s/Mpc}$ with $M = -32.79$.

- BAO measurements: we consider the sampler of 15 transversal measurements obtained in a quasi model-independent approach. This can be done by computing the 2-point angular correlation function tracers via $D_A(z; r_{\text{drag}})$ [192]. The sampler is given in a redshift range $[0.11, 2.225]$. These kind of observations contribute with important features by comparing the data of the sound horizon today to the sound horizon at the time of recombination (extracted from the CMB anisotropy data). The BAO distances are given by $d_z \equiv \frac{r_s(z_d)}{D_V(z)}$, with $r_s(z_d) = \frac{c}{H_0} \int_{z_d}^{\infty} \frac{c_s(z)}{E(z)} dz$ being the comoving sound horizon at the baryon dragging epoch, c the light velocity, z_d is the drag epoch redshift and $c_s^2 = c^2/3[1 + (3\Omega_{b0}/4\Omega_{\gamma0})(1+z)^{-1}]$ the sound speed with Ω_{b0} and $\Omega_{\gamma0}$ the present values of baryon and photon density parameters, respectively. The dilation scale is given by

$$D_V(z, \Omega_m; \Theta) = \left[\frac{c z (1+z)^2 D_A^2}{H(z, \Omega_m; \Theta)} \right]^{1/3}, \quad (4.44)$$

where D_A is the angular diameter distance

$$D_A(z, \Omega_m; \Theta) = \frac{1}{1+z} \int_0^z \frac{c d\tilde{z}}{H(\tilde{z}, \Omega_m; \Theta)}, \quad (4.45)$$

where $\Theta = \{w_0, w_a\}$. Through the comoving sound horizon, the distance ratio d_z is related to the expansion parameter h (defined such that $H \doteq 100h$) and the physical densities Ω_m and Ω_b . To connect the BAO data with SNeIa (Pantheon) to CMB data (PL18), we consider the Alcock-Paczynski distortion parameter:

$$F(z, \Theta) = (1+z) \frac{D_A(z, \Theta) H(z, \Theta)}{c}. \quad (4.46)$$

Notice that this possible by calibrating the D_A from BAO with the d_L from supernovae in a cosmology-independent way and we define:

$$\chi_{BAO}^2 = (\Delta \mathcal{F}_{BAO})^T \cdot C_{BAO}^{-1} \cdot \Delta \mathcal{F}_{BAO}, \quad (4.47)$$

where $\Delta \mathcal{F}_{BAO}$ is the difference between the observational data and the resulting value for Θ , and C_{BAO}^{-1} is the inverse of the covariance matrix reported in the reference mentioned above.

- Observational Hubble data (CC): we consider a sample of 51 measurements in the redshift range $0.07 < z < 2.0$ [193]. A calibration of this sample was presented in [194]. Moreover, we should be careful since this sample contains data from BAO that can overlapping the sampler. This sample gives a measurement of

Parameters	CC	Pantheon+BAO	CC+Pantheon+BAO
h	0.714 ± 0.071	0.734 ± 0.0040	0.733 ± 0.0038
w_0	-1.30 ± 0.72	-1.24 ± 0.15	-1.14 ± 0.12
w_a	-0.8 ± 2.4	0.13 ± 1.3	0.33 ± 0.93
Ω_m	0.325 ± 0.094	0.337 ± 0.072	0.296 ± 0.047

Tab. 4.1: Background best fits values for Eq. (4.37). For CC, Pantheon+BAO and CC+Pantheon+BAO.

the expansion rate without relying on the nature of the metric between the chronometer and us as observers. The normalised parameter $h(z)$ can be computed by considering the values of SH0ES and H0LiCOW given above. In this sample are content 31 data points from passive galaxies and 20 data points are estimated from BAO data under a Λ CDM prior. However, BAO OHD data points can be computed by using the r_s at the drag epoch from PL18.

To perform the fit of the free parameters of our theoretical setting through the construction of a χ_H^2 as

$$\chi_H^2 = \sum_{i=1}^{51} \frac{[H(z_i, \mathbf{x}) - H_{obs}(z_i)]^2}{\sigma_H^2(z_i)}, \quad (4.48)$$

where $H_{obs}(z_i)$ is the observed value at z_i , $\sigma_H(z_i)$ are the observational errors, and $H(z_i, \mathbf{x})$ is the value of a theoretical H for the same z_i with the specific parameter vector \mathbf{x} .

4.2.4 Methodology

To proceed with the cosmological precision test of the parametric CSFDE model (4.37), we compute the χ^2 -statistic using each of the observational samplers described. Then we find the values of the parameters which minimize each of those individual contributions up to $2\text{-}\sigma$. We repeat the procedure using the total sample, i.e., $\chi_{\text{Total}}^2 = \chi_{\text{SN}}^2 + \chi_{\text{BAO}}^2 + \chi_{\text{OHD}}^2$. In Table 4.1 we report the mean and best fits for the cosmological parameters and the model parameters, w_0 and w_a , for the join samplers CC+BAO+Pantheon SN.

In Fig. 4.3 we provide the confidence regions, which inform us from a Bayesian point of view on the degree of correlations among the cosmological parameters and the statistical tension between the observables. For the full data set combination we draw

the contours by choosing two shades of a single colour, and we let the dark and light hues represent the 1σ and 2σ regions, respectively.

In the analyzes performed, the posterior distribution of the parameter w_a in the EoS remains unconstrained in the range allowed by the model (see Eq. 4.38). Results in Fig. 4.3 and Table 4.1 indicate that the value of w_a spans the entire validity domain in a 1σ contour. Nevertheless, the more general parametric model (4.37), can be in fact constrained. We emphasize that the analysis has been done using the parametric equation 4.37 without necessarily being associated with the model for which we have an exact solution. For this parametric model, the result of the statistical analysis indicates that, the parameters w_0 and w_a are constrained. However, it is in relation to the proposed theoretical model that the parameters are not constrained.

4.2.5 Conclusions

Complex scalar field theory has been used from a Bose-Einstein condensate point of view to describe the cosmic acceleration observed. This makes possible to construct quintessence–complex scalar field scenarios, which can mimic dark energy effects. In this particular backstage, we proposed a study of the peculiar branch solution of the Einstein-Klein-Gordon equations in the fast oscillation regime, where the complex scalar field is modelled as an effective dark fluid. As it is standard, from these field equations it is possible to derive an effective equation of state (4.37), which is a more general model, here called parametric CSFDE. In this panorama, the cosmological parameters related with the model can be constrained using current observational surveys in order to study epochs where the dark energy (at $z = 0$) and dark matter ($z \approx 9$) domination occurs.

Using the join samplers as CC+BAO+Pantheon, the parametric CSFDE model (4.37) was constrained, taking the values, within $1-\sigma$, of $w_a = 0.33 \pm 0.93$ and $w_0 = -1.14 \pm 0.12$. Moreover, within the considered w_a range, it is not possible to constrain the model, which best fit parameters are not consistent with the theoretical scalar field model (Eq. 4.38). The quantity w_0 , which is a free parameter in the parametric model, is well constrained in all our analyzes within values consistent with the late cosmic acceleration as well as with the theoretical model, given that it is consistent with the constant value $w_0 = -1$ within $2-\sigma$.

We remark that the CSFDE model has a theoretical restriction for the w_a parameter that is not suitable for a statistical analysis with early-time data, e.g., CMB. However, this

limitation could be addressed if, for instance, one considers two scalar fields instead of one. Furthermore, some of the conditions applied, as for example the narrow fast oscillation regime, could be relaxed giving enough freedom, so that both using or not using the CMB data, the best fit parameters could be determined.

Finally, we can see that the CSFDE model cannot reproduce an oscillating behaviour of the EoS associated with a dynamical dark energy.

This result points out the necessity of more than one canonical scalar field to reproduce viable cosmological scenarios. Further investigation could require combinations of scalar fields like quintom scenarios or changes in the kinetic term. Also exact solutions for other scalar potentials in the fast oscillation regime could lead to models favored by Bayesian analyzes. This will be reported elsewhere.

4.3 Wormholes

A wormhole is a solution to the Einstein's equations that connects two distant points in spacetime and there are plenty approaches in this topic available in the literature; just to mention a few, there is a wormhole approach in the context of $f(R, T)$ gravity (e.g. [195, 196]), in teleparallel gravity (e.g. [197, 198]), also in the Finslerian framework (see e.g. [199]) and in the axion approach of particle physics and cosmology (e.g. [200, 201]). Here we are interested in such that are made of ghost scalar fields that constitute exotic matter described by the addition of an angular momentum parameter that can be used to describe the observed accelerated expansion of the Universe.

Introduction

The essential property of General Relativity, namely, that matter determines the geometry of the spacetime, acquires a new light when the matter is such that it violates the energy conditions [202, 203, 204, 205, 206]. In particular, the violation of the null energy condition opens the possibility for the existence of globally hyperbolic, asymptotically flat spacetimes with non-trivial topological structures [207]. Such matter, usually referred to as exotic in the literature, generates peculiar responses in the properties of the spacetime curvature with important consequences on the effective gravitational potential, producing potential "bumps" instead of the usual potential wells. To provide an explicit example, in Fig. 4.4, we present the gravitational effective

potentials for a massive, radially infalling test particle for two cases: the first one is due to the presence of a point mass which generates the usual gravitational well, whereas the second one is generated by a distribution of exotic matter (as the one discussed later in this work) in which case the potential exhibits a different type of convexity corresponding to a gravitational potential bump.

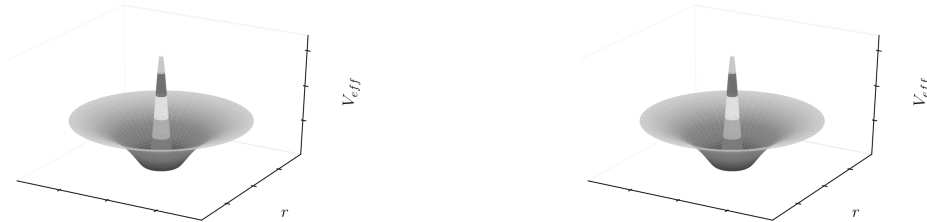


Fig. 4.4: Gravitational potential produced by a point mass $\sim -1/r$ (left panel) and by the exotic distribution presented in this work (right panel), see section 4.3.4. In both cases a test particle with vanishing angular momentum is considered.

Moreover, under specific circumstances, the *bump* could be such that it connects two separated regions of spacetime. The resulting configuration is dubbed *wormhole*, and it offers challenges and opportunities to better understand the relation between matter and geometry, aside from the fact that, being bona fide solutions to Einstein’s equations, it could potentially describe an astrophysical scenario if exotic matter turns out to actually being present in our Universe.

In cosmology, matter with negative pressure can be used to describe the observed accelerated expansion of the Universe [208, 209, 210, 188] and seems to be favored by several observational constraints [211, 212, 213]. Additionally, modeling the dark energy with an equation of state of the form $p = \omega\rho$, the observations suggest a value of ω close to -1 or even smaller, in which case the existence of astrophysical or cosmological wormholes becomes plausible.

The studies of traversable wormholes have their origin with Ellis’ work [214], where the author presented a black hole like solution to Einstein’s equations, and in order to remove the singularity, used a scalar field and *drain* the hole. Actually, the same solution, based on a different approach was obtained almost at the same time by Bronnikov [215]. It turned out that the solution represented a bridge between two regions of the spacetime [216]. Over the years, the idea was further developed, and the best known example of a traversable wormhole appeared in 1988, in the work

of Morris and Thorne [217]. Since then, a plethora of literature has arisen and the complexity of the models has increased, see for example [218, 219] and references therein.

In order to obtain a wormhole solution to the Einstein equations, some works use generation procedures, such as the Newman-Janis algorithm, which allows to obtain a Kerr black hole solution starting from a Schwarzschild one; in this way, a rotating (although not asymptotically flat) solution was obtained starting from one of the original Ellis models [220]. There is also a technique which uses the thin shell approach, which assumes that the matter is concentrated in a three-dimensional submanifold. However, a common practice is to analyze the geometry describing a putative wormhole without mentioning the possible matter that could generate it, artificially producing general forms of such wormholes which might even include rotation [221]; in the words of Morris and Thorne: fixed the geometry.. “and let the builders of a wormhole synthesize, or search throughout the universe for, materials or fields with whatever stress-energy tensor might be required” [217].

In the present work, we prefer to avoid this “reversed engineering approach” and assume the specification of a suitable matter model which allows for a large class of static, spherically symmetric and traversable wormhole solutions. In particular, following the recent approach in [185] to construct a generalized class of static and spherically symmetric boson stars, we consider a family of massive, complex and self-interacting ghost scalar fields similar to the one considered in Dzhunushaliev *et al.* [222, 223], but which includes an extra parameter ℓ mimicking the effects of the angular momentum. In this way, new spherical and traversable wormhole solutions can be constructed which generalize those of Refs. [222, 223] to $\ell > 0$. Accordingly, and following the terminology of the ℓ -boson stars, we dub these solutions ℓ -wormholes.

While Ellis’ original solutions use a massless, time-independent real scalar field without self-interaction, in this work we consider massive, complex and self-interacting scalar fields with a harmonic time-dependency *à la* Dzhunushaliev *et al.* [222, 223], but instead of considering just a single field we consider a family of fields with angular momentum number ℓm with ℓ fixed and $m = -\ell, \dots, \ell$. Assuming like in [185] that each of these fields has exactly the same radial dependency, we obtain static, spherically symmetric wormhole solutions. When $\ell = 0$, the mass of the scalar field, its self-interaction and the time-frequency vanish one recovers Ellis’ wormhole solutions.

The new wormholes have several interesting characteristics, such as curvature scalars and effective potentials which smooth out the features of the corresponding 0-wormholes.

The geodesic motion helps us to understand the role played by the ℓ -parameter in the spacetime configuration. Finally, the presence of a new parameter gives rise to the possibility that this wormhole might be stable, a feature that will be discussed in a followup work.

The paper is organized as follows. In Section 4.3.1, we specify our metric ansatz describing static, spherical symmetric and traversable wormhole spacetimes and introduce the matter model. In Section 4.3.2, we derive the static field equations in spherical symmetry, discuss some qualitative properties of the wormhole solutions and then construct numerical solutions to the field equations whose main properties are discussed next in Section 4.3.3. In Section 4.3.4, we discuss the embedding diagrams visualizing the spatial geometry of the solutions, derive the geodesic equations for massive or massless test particles propagating in the wormhole metric and analyze the motion under several conditions determined by the wormhole parameters. Finally, we discuss and summarize our results in Section 4.3.5.

4.3.1 Foundations

The determination of the stress-energy-momentum tensor that supports a wormhole geometry is of the utmost importance to understand its physical properties and structure. As already mentioned in the introduction, an asymptotically flat wormhole geometry in general relativity requires the matter to be *exotic*, that is, matter that does not fulfill the regular properties of the usual matter we deal with everyday.³ More specifically, the matter must violate the null energy condition, $T_{\mu\nu}k^\mu k^\nu \geq 0$, where $T_{\mu\nu}$ is the stress-energy-momentum tensor and k^μ any null vector [217, 219, 226]. Incidentally, this is also the fundamental ingredient of the so-called ghost energy, a model not excluded by observations to be a candidate for dark energy. For instance, constraints from the Supernovae Ia Hubble diagram [227] favor the existence of an equation of state for such dark fluid, $p = \omega\rho$ with $\omega < -1$, a model consistent with ghost energy [205].

In practice, violation of the null energy condition is accomplished by changing the global sign in the stress-energy-momentum tensor in Einstein's equations. Ellis called this the other polarity of the equations [214]. This change in sign in the equations is attributed to the type of matter, and has multiple implications which might lead to misunderstandings. A global change in sign to the stress-energy-momentum tensor

³However, it should be mentioned that there are examples of traversable wormholes without exotic matter in modified theories of gravity [224] or in general relativity when the asymptotic flatness condition is replaced by adS-asymptotics [225].

implies that the usual definition of density also has the opposite sign and is thus negative.

In this work we interpret the physical properties of the wormhole directly in terms of the theory of General Relativity and Einstein's field equations, so that the exotic matter produces a different reaction in the curvature of the spacetime, particularly in the effective potential in which the test particles move, generating bumps instead of wells, so that a particle has to spend potential energy in order to get closer to the source, while it gains kinetic energy and accelerates when getting away from it; like when climbing a mountain to reach the summit and then going down.

In particular, we stress that when talking about test particles we assume the validity of the weak equivalence principle, which assumes that the inertial and gravitational masses are equal to each other. Therefore, free-falling test particles or photons always follow causal geodesics of the underlying spacetime, regardless of the sign of their mass.⁴ The "bump interpretation" mentioned so far will become evident when analyzing the geodesic motion of test particles in Section 4.3.4.

Metric ansatz

We will consider a static spherically symmetric spacetime with a line element of the form:

$$ds^2 = -a(r) c^2 dt^2 + a(r)^{-1} dr^2 + R^2(r) d\Omega^2, \quad (4.49)$$

where R and a are positive functions only of the radial coordinate r , and $d\Omega^2 = d\theta^2 + \sin^2 \theta d\varphi^2$. Notice that for $R^2 = r^2 + b^2$, with b a positive constant, and $a = 1$, the reflection-symmetric Ellis wormhole metric is recovered [214] and, from it, with a suitable redefinition of the radial coordinate, one obtains the usual form of the Morris–Thorne like wormhole [217]. Also note that the coordinate r our work is based on extends from $-\infty$ to $+\infty$, and we will demand that R be regular at the throat $r = 0$, which corresponds to a minimum of the area $4\pi R^2$ of the invariant two-spheres.

Matter content of the wormhole

In the present chapter, we consider a set of several massive scalar fields with a self-interaction term. Our configurations are constructed in such a way that the sum of

⁴However, see [228] for bizarre implications in systems involving hypothetical point particles with positive and negative masses.

the fields preserves the spherical symmetry of the stress-energy-momentum tensor and includes an extra parameter associated with the angular momentum number ℓ . This approach was introduced in [229] in the context of critical collapse, and recently used in [185] to construct ℓ -boson stars.

We start with the Lagrangian density for N complex massive scalar fields

$$\mathcal{L}_\Phi = -\frac{1}{2\kappa} \left[\sum_{i=1}^N \eta \nabla_\mu \Phi_i \nabla^\mu \Phi_i^* + V(|\Phi|^2) \right], \quad (4.50)$$

with a quartic potential

$$V(|\Phi|^2) = \sum_{i=1}^N V^{(i)} = \sum_{i=1}^N \left(\eta_\mu \frac{m_\Phi^2 c^2}{\hbar^2} |\Phi_i|^2 + \eta_\lambda \frac{\lambda}{2\hbar^2} |\Phi_i|^2 \sum_{j=1}^N |\Phi_j|^2 \right), \quad (4.51)$$

where $\kappa = 8\pi G/c^4$, \hbar is the reduced Planck constant, m_Φ is the mass of the scalar field particle and λ is the parameter measuring the strength of the quartic interaction term. The values $\eta = \eta_\mu = \eta_\lambda = 1$ represent the canonical scalar fields while $\eta = \eta_\mu = -\eta_\lambda = -1$ describe the type of ghost fields in which we will be interested in, and from now on we fix the latter choice. In the following, for convenience, we will work with the rescaled quantities $\mu = m_\Phi c/\hbar$ and $\Lambda = \lambda/2\hbar^2$ instead of m_Φ and λ .

The stress-energy-momentum tensor associated with the scalar field Φ_i is thus given by

$$T_{\mu\nu}^{(i)} = \frac{c^4}{16\pi G} \left[-(\nabla_\nu \Phi_i \nabla_\mu \Phi_i^* + \nabla_\nu \Phi_i^* \nabla_\mu \Phi_i) - g_{\mu\nu} \left(-\nabla_\alpha \Phi_i \nabla^\alpha \Phi_i^* + V^{(i)} \right) \right], \quad (4.52)$$

while the total stress-energy-momentum tensor that we plug into Einstein's field equations is

$$T_{\mu\nu} = \sum_{i=1}^N T_{\mu\nu}^{(i)}. \quad (4.53)$$

In [229], for the case of real scalar fields, and in the appendix of [185], for complex ones, it was shown that for an appropriate superposition, a stress-energy-momentum tensor of the form (4.53) with $\Lambda = 0$ may be spherically symmetric, even though the individual fields Φ_i have non-vanishing angular momentum. Here, we generalize this result further to include the self-interaction of the field. The procedure is as follows.

Each scalar field Φ_i has the form

$$\Phi_i(t, r, \theta, \varphi) = \phi_\ell(t, r) Y^{\ell m}(\theta, \varphi), \quad i = \ell + 1 + m, \quad (4.54)$$

where m varies over $-\ell, -\ell + 1, \dots, \ell$ (such that i varies from 1 to $N = 2\ell + 1$) and $Y^{\ell m}(\theta, \varphi)$ denote the standard spherical harmonics. Here, the parameter ℓ is kept fixed and the amplitudes $\phi_\ell(t, r)$ are equal to each other for all m . Using the addition theorem for the spherical harmonics [230], one can show that the resulting stress-energy-momentum tensor in Eq. (4.53) for the $N = 2\ell + 1$ fields is spherically symmetric.

Next, one considers a stationary state with harmonic time dependence for the scalar field

$$\phi_\ell(t, r) = e^{i\omega t} \chi_\ell(r), \quad (4.55)$$

where χ_ℓ is function of r and ω is a real constant. Once such procedure is carried out, the following non-trivial components of the stress-energy-momentum tensor are obtained:

$$T^t_t = \frac{c^4}{8\pi G} \frac{2\ell+1}{8\pi} \left\{ a \left(\frac{d\chi_\ell}{dr} \right)^2 + \left[\frac{\ell(\ell+1)}{R^2} + \mu^2 - \frac{2\ell+1}{4\pi} \Lambda \chi_\ell^2 + \frac{\omega^2}{a} \right] \chi_\ell^2 \right\}, \quad (4.56)$$

$$T^r_r = \frac{c^4}{8\pi G} \frac{2\ell+1}{8\pi} \left\{ -a \left(\frac{d\chi_\ell}{dr} \right)^2 + \left[\frac{\ell(\ell+1)}{R^2} + \mu^2 - \frac{2\ell+1}{4\pi} \Lambda \chi_\ell^2 - \frac{\omega^2}{a} \right] \chi_\ell^2 \right\}, \quad (4.57)$$

$$T^\theta_\theta = T^\varphi_\varphi = \frac{c^4}{8\pi G} \frac{2\ell+1}{8\pi} \left\{ a \left(\frac{d\chi_\ell}{dr} \right)^2 + \left[\mu^2 - \frac{2\ell+1}{4\pi} \Lambda \chi_\ell^2 - \frac{\omega^2}{a} \right] \chi_\ell^2 \right\}. \quad (4.58)$$

Notice how the procedure of adding individual stress-energy-momentum tensors maintains the spherical symmetry and yields a result that depends on the angular momentum number ℓ through the centrifugal-like terms $\ell(\ell + 1)/R^2$. As expected and shown below, this dependency plays a nontrivial role in the solutions of Einstein's equations. The mixed components T^t_r , T^t_θ and T^t_φ vanish; indicating that there are no fluxes of matter in this case, which is compatible with the assumption of staticity of the metric.

Notice also that the stress-energy-momentum tensor (4.56–4.58) violates the null energy condition everywhere; for instance, the null vector field $k = a^{-1/2}c^{-1}\partial_t + a^{1/2}\partial_r$ gives

$$T_{\mu\nu}k^\mu k^\nu = -T^t_t + T^r_r = -\frac{c^4}{8\pi G} \frac{2\ell+1}{4\pi} \left[a \left(\frac{d\chi_\ell}{dr} \right)^2 + \frac{\omega^2}{a} \chi_\ell^2 \right], \quad (4.59)$$

which is negative unless the scalar field vanishes.

Now, one can compute the equation of motion for each individual field, i. e. the Klein-Gordon equation, using the fact that the divergence of the total stress-energy-momentum tensor is zero. Each amplitude obeys the identical equation:

$$\frac{d}{dr} \left[a R^2 \frac{d\chi_\ell}{dr} \right] + R^2 \left(\frac{\omega^2}{a} - \frac{\ell(\ell+1)}{R^2} - \mu^2 + \frac{2\ell+1}{2\pi} \Lambda \chi_\ell^2 \right) \chi_\ell = 0, \quad (4.60)$$

where we have used the fact that spherical harmonics are eigenfunctions of the Laplace-Beltrami operator

$$\Delta_{S^2} Y^{\ell m} = \left(\frac{\partial^2}{\partial \theta^2} + \cot \theta \frac{\partial}{\partial \theta} + \frac{1}{\sin^2 \theta} \frac{\partial^2}{\partial \varphi^2} \right) Y^{\ell m} = -\ell(\ell+1) Y^{\ell m}. \quad (4.61)$$

As an example of the construction of the ℓ -wormhole by the contribution of individual non-spherical scalar fields, in Fig. 4.5 we show the distribution of the density at the throat for the fields $(\phi_1 Y^{1-1}, \phi_1 Y^{10}, \phi_1 Y^{11})$. The values are given by Eq. (4.53) for the $T^t_t \propto \rho$ component. This is the case for $\ell = 1$ wormhole, so that there are three values for m . The first sphere represents the sum of the $m = -1$ and $m = 1$ contributions, the second one represents the $m = 0$ field, and the combination is given in such a way that the total density (the third sphere) is spherically symmetric.

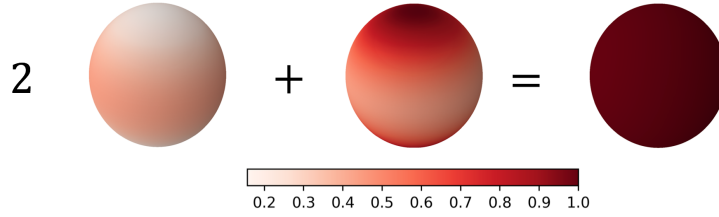


Fig. 4.5: Normalized density at the throat for a $\ell = 1$ wormhole. The first sphere represents the $m = \pm 1$ contribution while the center sphere corresponds to the $m = 0$ contribution.

4.3.2 Stationary Wormhole equations

In order to obtain the remaining field equations, it is helpful to notice that with the stress-energy-momentum tensor components given by Eqs. (4.56, 4.57, 4.58) the following equation is satisfied

$$\frac{T^t_t - T^r_r}{2} - T^\theta_\theta = -\frac{c^4}{8\pi G} \frac{2\ell+1}{8\pi} \left(\mu^2 - \frac{2\ell+1}{4\pi} \Lambda \chi_\ell^2 - \frac{2}{a} \omega^2 \right) \chi_\ell^2. \quad (4.62)$$

On the other hand, from the line element Eq. (4.49), we obtain the Bianchi-Einstein tensor, $G^\mu{}_\nu$, and the same linear combination of the components gives:

$$\frac{G^t{}_t - G^r{}_r}{2} - G^\theta{}_\theta = -\frac{1}{2R^2} \frac{d}{dr} \left[R^2 \frac{da}{dr} \right]. \quad (4.63)$$

Thus, with the aid of Einstein's equations:

$$G^\mu{}_\nu = \frac{8\pi G}{c^4} T^\mu{}_\nu, \quad (4.64)$$

we obtain our next field equation:

$$\frac{1}{2R^2} \frac{d}{dr} \left[R^2 \frac{da}{dr} \right] = \frac{2\ell+1}{8\pi} \left(\mu^2 - \frac{2\ell+1}{4\pi} \Lambda \chi_\ell^2 - \frac{2}{a} \omega^2 \right) \chi_\ell^2. \quad (4.65)$$

Notice that when a static, massless scalar field (regular or exotic) without interaction is considered, then a particular solution is obtained in which the metric function a is constant.

A further field equation comes from the combination of the $G^t{}_t$ component plus the $G^r{}_r$ one, and the corresponding $T^\mu{}_\nu$ components:

$$\frac{dR^2}{dr} \frac{da}{dr} + a \frac{d^2 R^2}{dr^2} - 2 = \frac{2\ell+1}{4\pi} \left[R^2 \left(\mu^2 - \frac{2\ell+1}{4\pi} \Lambda \chi_\ell^2 \right) + \ell(\ell+1) \right] \chi_\ell^2. \quad (4.66)$$

As mentioned above, for the first independent field equation, we consider the Klein-Gordon equation, Eq. (4.60). In this way we obtain a system of equations in which each function $\chi_\ell(r)$, $a(r)$ and $R^2(r)$ appears as the only second derivative:

$$\chi_\ell'' = - \left(\frac{R^{2'}}{R^2} + \frac{a'}{a} \right) \chi_\ell + \frac{1}{a} \left[\mu^2 - \frac{\omega^2}{a} + \frac{\ell(\ell+1)}{R^2} - \frac{2\ell+1}{2\pi} \Lambda \chi_\ell^2 \right] \chi_\ell, \quad (4.67)$$

$$a'' = -\frac{R^{2'}}{R^2} a' + \frac{2\ell+1}{4\pi} \left(\mu^2 - \frac{2}{a} \omega^2 - \frac{2\ell+1}{4\pi} \Lambda \chi_\ell^2 \right) \chi_\ell^2, \quad (4.68)$$

$$a R^{2''} = -a' R^{2'} + 2 + \frac{2\ell+1}{4\pi} \left[\left(\mu^2 - \frac{2\ell+1}{4\pi} \Lambda \chi_\ell^2 \right) R^2 + \ell(\ell+1) \right] \chi_\ell^2, \quad (4.69)$$

where a prime denotes derivative with respect to r . The remaining field equation is the rr -component of Eq. (4.64) which yields

$$\frac{R^{2'}}{2R^2} \left(a' + \frac{a R^{2'}}{2R^2} \right) - \frac{1}{R^2} = \frac{2\ell+1}{8\pi} \left[-a \chi_\ell^{2'} + \left(\mu^2 - \frac{2\ell+1}{4\pi} \Lambda \chi_\ell^2 - \frac{\omega^2}{a} + \frac{\ell(\ell+1)}{R^2} \right) \chi_\ell^2 \right], \quad (4.70)$$

which can be interpreted as a constraint since it only involves zeroth and first-order derivatives of the fields. Provided the second-order field equations (4.67, 4.68, 4.69) are satisfied, the twice contracted Bianchi identity $\nabla_\mu G^\mu_r = 0$ and $\nabla_\mu T^\mu_r = 0$ imply that

$$\frac{d}{dr} \left[aR^4 \left(G^r_r - \frac{8\pi G}{c^4} T^r_r \right) \right] = 0, \quad (4.71)$$

such that it is sufficient to solve Eq. (4.70) at one point (the throat, say).

A particular simple solution arises when a static, spherical, massless scalar field (regular or exotic) without interaction is considered. In this case, the parameters ω , μ , and Λ vanish and considering $\ell = 0$, the field equations (4.67–4.70) can be integrated explicitly [214, 215], see also [231]. The simplest (but not unique) solution is obtained assuming that the metric function a is constant. This yields the solution

$$a = 1, \quad R^2 = b^2 + r^2, \quad \chi_{\text{Ellis}}(r) = \sqrt{8\pi} \arctan\left(\frac{r}{b}\right), \quad (4.72)$$

which has the property that the metric functions a , R^2 and the gradient of χ_{Ellis} are reflection symmetric about the throat $r = 0$. In Fig. 4.6, we present the plot of Ellis' ghost field and the corresponding energy density. Although the scalar field itself does not decay to zero simultaneously at both asymptotic ends $r \rightarrow \pm\infty$, its gradient does. Since in the massless case the stress-energy-momentum tensor and equations of motion only depend on the gradient of the scalar field, the configuration is localized from a physical point of view. Furthermore, we observe that the density is negative everywhere. The curvature and Kretschmann scalars are given by $R_{s,\text{Ellis}} = -\frac{2b^2}{(r^2+b^2)^2}$ and $K_{\text{Ellis}} = R_{s,\text{Ellis}}^2$ (see Fig. 4.7), respectively, and like the density, they have a fixed sign.

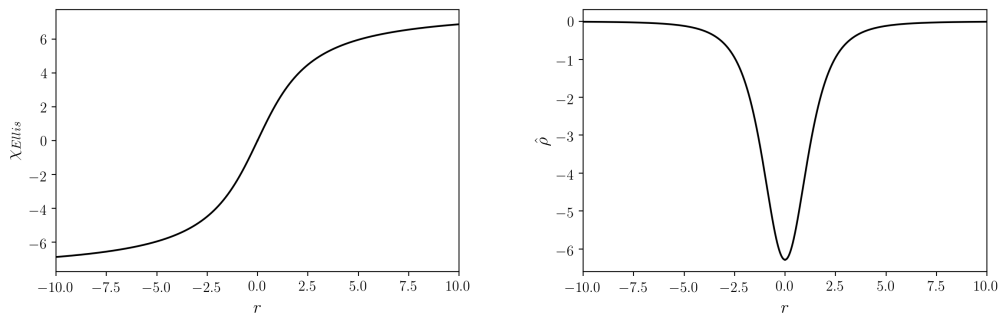


Fig. 4.6: Ghost field and the corresponding density for the original Ellis wormhole.

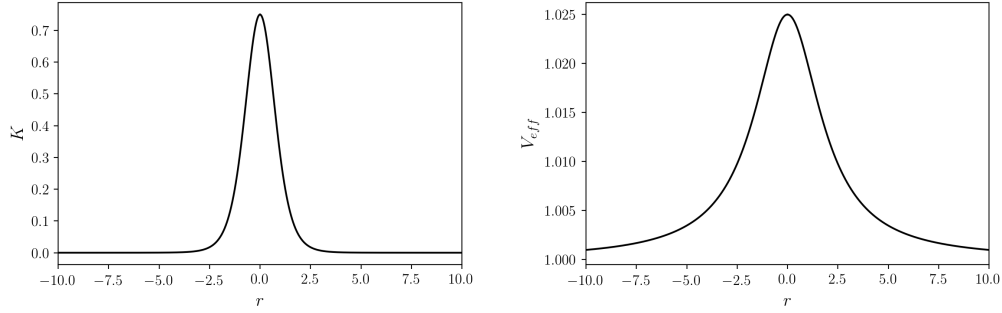


Fig. 4.7: Kretschmann scalar and effective potential, $V_{eff} = L^2/R^2 + \kappa$ for a massive particle propagating on the reflection-symmetric Ellis wormhole.

In the following, we consider much more general wormhole solutions in which the parameters ω , ℓ , μ and Λ do not necessarily vanish. These solutions are obtained by numerically integrating the field equations (4.67, 4.68, 4.69) and taking into account the constraint (4.70). For simplicity, in this article, we restrict ourselves to the reflection-symmetric case (although more general wormhole solutions which are asymmetric about the throat could also be considered). These solutions satisfy the following boundary conditions at the throat, $r = 0$:

$$\chi'_\ell(0) = 0, \quad (4.73)$$

$$a'(0) = 0, \quad (4.74)$$

$$R^{2'}(0) = 0. \quad (4.75)$$

Denoting by $b := R(0)$ the areal radius of the throat, the constraint (4.70) yields the following condition at $r = 0$:

$$\left[1 + \frac{(2\ell + 1)\ell(\ell + 1)}{8\pi} \chi_\ell(0)^2\right] b^{-2} = \frac{2\ell + 1}{8\pi} \left(\frac{\omega^2}{a(0)} - \mu^2 + \frac{2\ell + 1}{4\pi} \Lambda \chi_\ell(0)^2\right) \chi_\ell(0)^2, \quad (4.76)$$

which fixes the radius b of the throat and requires $a(0)$ and $\chi_\ell(0) \neq 0$ to be chosen such that

$$\frac{\omega^2}{a(0)} + \frac{2\ell + 1}{4\pi} \Lambda \chi_\ell(0)^2 > \mu^2. \quad (4.77)$$

Note that this inequality and Eq. (4.68) also imply that a has a local maximum at the throat. Next, Einstein's equation (4.69) together with the conditions (4.73, 4.74, 4.75), implies the relation

$$\frac{1}{2} a(0) (R^2)''(0) = \frac{2\ell + 1}{8\pi} \left[b^2 \left(\mu^2 - \frac{2\ell + 1}{4\pi} \Lambda \chi_\ell(0)^2 \right) + \ell(\ell + 1) \right] \chi_\ell^2(0) + 1. \quad (4.78)$$

Using Eq. (4.76) this can be simplified considerably,

$$\frac{1}{2}a(0)(R^2)''(0) = \frac{2\ell + 1}{8\pi} \frac{b^2\omega^2}{a(0)} \chi_\ell(0)^2, \quad (4.79)$$

which shows that the throat is indeed a local minimum⁵ of R^2 . For $\ell = 0$ the Eqs. (4.76, 4.79) reduce to the corresponding equations in Ref. [222] (see their equation (18) and the unnumbered equation below it.) Due to Eq. (4.76), one has two free parameters at the throat, given by $\chi_\ell(0) \neq 0$ and $a(0)$, say. As can be checked, the field equations (4.67, 4.68, 4.69, 4.70) as well as the conditions (4.76, 4.79) are invariant with respect to the transformations

$$(\omega, t, r, a, R^2, \chi_\ell) \mapsto \left(\frac{\omega}{\sqrt{B}}, \sqrt{B}t, \frac{r}{\sqrt{B}}, \frac{a}{B}, R^2, \pm\chi_\ell \right), \quad (4.80)$$

with $B > 0$ a real parameter. Therefore, one can fix the value of $a(0)$ to one, say, and adjust the value of B such that $a(r) \rightarrow 1$ for $r \rightarrow \infty$. In this way, one is left with just one shooting parameter ($\chi_\ell(0) > 0$, say) at the throat $r = 0$.

At $r \rightarrow \pm\infty$, we require asymptotic flatness,

$$\chi_\ell(r) \rightarrow 0, \quad (4.81)$$

$$a(r) \rightarrow 1, \quad (4.82)$$

$$\frac{R(r)}{r} \rightarrow 1. \quad (4.83)$$

Under these assumptions, the field equation (4.67) for the scalar field reduces to

$$\chi_\ell''(r) \approx (\mu^2 - \omega^2)\chi_\ell(r), \quad (4.84)$$

which shows that⁶

$$\omega^2 < \mu^2, \quad (4.85)$$

is required to have the exponentially decaying solution $\chi_\ell(r) \approx e^{-\sqrt{\mu^2 - \omega^2}r}$. Approximating the (exponentially decaying) right-hand sides of Eqs. (4.65, 4.66) to zero, one obtains the following behavior of the metric coefficients in the asymptotic region:

$$a \approx e^{-\frac{c_0}{r+c_1}}, \quad R^2 \approx (r + c_1)^2 e^{\frac{c_0}{r+c_1}}, \quad r \rightarrow \infty, \quad (4.86)$$

⁵For $\omega \neq 0$ the right-hand side of Eq. (4.79) is positive since χ_ℓ and χ_ℓ' cannot both vanish at $r = 0$; otherwise it would follow from Eq. (4.67) that χ_ℓ vanishes identically. For the special case $\omega = 0$ see the proof of Theorem 2 below.

⁶The limiting value $\omega^2 = \mu^2$ is discussed in Ref. [222].

for some constants c_0 and c_1 .

Qualitative analysis of the solutions

Before numerically constructing the wormhole solutions, we make a few general remarks regarding the restrictions on the parameters ω , μ and Λ and the initial condition $\chi_\ell(0)$ and regarding the qualitative properties of the solutions. We assume in the following that $(\chi_\ell(r), a(r), R^2(r))$ is a smooth solution of Eqs. (4.60, 4.65, 4.66) (or, equivalently, of Eqs. (4.67, 4.68, 4.69)) on the interval $[0, \infty)$ which satisfies $a > 0$, $R^2 > 0$, the boundary conditions (4.73, 4.74, 4.75) at $r = 0$ and (4.81, 4.82, 4.83) at $r \rightarrow \infty$, and is subject to the conditions (4.76, 4.79) at the throat. We had already observed that an exponentially decaying solution at infinity requires $\omega^2 \leq \mu^2$. Furthermore, at the throat, the inequality (4.77) needs to be satisfied. A first immediate consequence of this last inequality is that the parameters ω and Λ cannot be both zero. In fact, one has the following stronger result which shows that the self-interaction term is needed.

Theorem 1 *There are no reflection-symmetric solutions with the above properties if $\Lambda = 0$ ⁷.*

Proof. We prove the theorem by contradiction. If $\Lambda = 0$, the inequality (4.77) implies that

$$\mu^2 < \frac{\omega^2}{a(0)} \leq \frac{\mu^2}{a(0)}, \quad (4.87)$$

which requires $a(0) < 1$ and $\omega^2 > 0$. However, Eq. (4.68) with $\Lambda = 0$ implies that at any point $r = r_c$ where the derivative of a vanishes, the equality

$$a''(r_c) = \frac{2\ell + 1}{4\pi} \left(\mu^2 - \frac{2\omega^2}{a(r_c)} \right) \chi_\ell(r_c)^2 \quad (4.88)$$

holds. Since $\mu^2 - 2\omega^2/a(0) < 0$, a has a local maximum at the throat, as already remarked above, such that $a(r)$ decreases for $r > 0$ small enough. Since $a(r) \rightarrow 1$ as $r \rightarrow \infty$ there must be a point $r = r_c$ for which a ceases to decrease, corresponding

⁷The theorems stated here were established by Dr. Olivier Sarbach in the original work [185].

to a (local) minimum of a . At this point, we must have $a(r_c) < a(0)$, $a'(r_c) = 0$ and $a''(r_c) \geq 0$. On the other hand, since

$$\mu^2 - \frac{2\omega^2}{a(r_c)} < \mu^2 - \frac{2\omega^2}{a(0)} < 0, \quad (4.89)$$

Eq. (4.88) implies $a''(r_c) < 0$, provided that $\chi_\ell(r_c) \neq 0$, which leads to a contradiction. If $\chi_\ell(r_c) = 0$, we do not obtain an immediate contradiction since in this case it follows that $a''(r_c) = 0$. However, in this case, we must have $\chi'_\ell(r_c) \neq 0$ since otherwise χ_ℓ (as a solution of the second-order equation (4.67)) would be identically zero. By differentiating Eq. (4.68) twice with respect to r and evaluating at $r = r_c$ one obtains $a'''(r_c) = 0$ and

$$a''''(r_c) = \frac{2\ell + 1}{2\pi} \left(\mu^2 - \frac{2\omega^2}{a(r_c)} \right) \chi'_\ell(r_c)^2 < 0, \quad (4.90)$$

which shows that $r = r_c$ is a local maximum of a and yields again a contradiction. This concludes the proof of the theorem. \square

The next result implies that there cannot be more than one throat.

Theorem 2 *Under the assumptions stated at the beginning of this subsection, the function $R^2(r)$ is strictly monotonously increasing and strictly convex on the interval $[0, \infty)$.*

Proof. By combining Eqs. (4.69,4.70) one obtains the simple equation

$$\frac{(R^2)''}{R^2} = \frac{1}{2} \left[\frac{(R^2)'}{R^2} \right]^2 + \frac{2\ell + 1}{4\pi} \left(\chi_\ell'^2 + \frac{\omega^2}{a^2} \chi_\ell^2 \right) \quad (4.91)$$

for R^2 , which shows that $(R^2)'' \geq 0$ and hence that R^2 is convex. We show further that the right-hand side of Eq. (4.91) cannot vanish at any point. This is clearly the case if $\omega \neq 0$ since χ_ℓ' and χ_ℓ cannot vanish at the same point (otherwise it would follow from Eq. (4.67) that χ_ℓ is identically zero). Next, we rule out the exceptional case in which $\omega = 0$ and there existed a point $r_0 \geq 0$ where $(R^2)'(r_0) = \chi_\ell'(r_0) = 0$. If this case occurred, successive differentiation of Eq. (4.91) would yield

$$(R^2)'''(r_0) = 0, \quad \frac{(R^2)''''(r_0)}{R^2(r_0)} = \frac{2\ell + 1}{2\pi} [\chi_\ell''(r_0)]^2. \quad (4.92)$$

Further, evaluating Eq. (4.70) at $r = r_0$ one would obtain

$$-\frac{1}{R^2(r_0)} = \frac{2\ell + 1}{8\pi} \left(\mu^2 - \frac{2\ell + 1}{4\pi} \Lambda \chi_\ell(r_0)^2 + \frac{\ell(\ell + 1)}{R^2(r_0)} \chi_\ell(r_0)^2 \right), \quad (4.93)$$

implying that $\chi_\ell(r_0) \neq 0$ and that the expression inside the parenthesis on the right-hand side must be negative. Eq. (4.67) would then imply that

$$a(r_0) \frac{\chi_\ell''(r_0)}{\chi_\ell(r_0)} < -\frac{2\ell+1}{4\pi} \Lambda \chi_\ell(r_0)^2 < 0, \quad (4.94)$$

and hence $\chi_\ell''(r_0) \neq 0$ and $(R^2)''''(r_0) > 0$. It follows that any critical point of R^2 must be a strict minimum of R^2 . However, since R^2 is convex there can be only one such critical point which is the one at the throat. Therefore, it follows from Eq. (4.91) that $(R^2)''(r) > 0$ for all $r > 0$ and the theorem is proven. \square

Numerical shooting algorithm

Next, we describe a shooting algorithm which allows us to find asymptotically flat wormhole solutions from a given set of initial conditions at the throat by numerically integrating the equations outwards. As discussed above, there is only one free parameter to start the shooting procedure. Such parameter is the value of the scalar field at the throat, $\chi_\ell(0)$.

Since the shooting method is such that solves a boundary value problem by reducing to an initial value problem and we are looking for the desired solutions in the same spirit as the boson stars (see for instance [96]), in which the solutions are parametrized by the value of the scalar field at the center of the configuration so that for each solution a set of discrete values for the frequency is found to satisfy the asymptotic flatness conditions, each with different number of nodes for the scalar field profile, this algorithm is ideal. Qualitatively, the same happens with the ℓ -wormhole solutions discussed here. All the solutions reported in this article are those corresponding to the ground state, in which the scalar field χ_ℓ has no nodes.

So for given values of $a(0)$, Λ , ℓ , ω , only one particular value of $\chi_\ell(0)$ picks the $\chi_\ell \rightarrow 0$ solution at infinity. We can see this in the approximation of the Klein-Gordon equation for large r . If we assume that $a(r)$ tends to unity and $R(r)$ to the coordinate r fast enough, then Eq. (4.84) is satisfied, which is consistent with exponential decay of χ_ℓ for large r as long as $\mu^2 - \omega^2 > 0$. In a similar way we see that if χ_ℓ is exponentially decaying at both infinities then, from (4.68) we obtain $\frac{d^2 a}{dr^2} + \frac{2}{r} \frac{da}{dr} \approx 0$, which has solutions:

$$a \approx B + \frac{A}{r}, \quad (4.95)$$

$\omega = 0$	$\ell = 0$			$\ell = 1$			$\ell = 2$		
	$\chi_\ell(0)$	$R(0)$	$a(0)$	$\chi_\ell(0)$	$R(0)$	$a(0)$	$\chi_\ell(0)$	$R(0)$	$a(0)$
$\Lambda = 0.5$	6.26	1.07	1.40	3.94	1.72	7.43	3.08	2.71	20.21
$\Lambda = 0.7$	4.91	1.75	0.80	3.21	1.97	2.59	2.58	2.81	7.04
$\Lambda = 1.0$	3.90	2.79	0.58	2.48	2.70	1.03	2.08	3.14	2.51
$\Lambda = 4.0$	1.81	13.21	0.41	1.05	13.14	0.42	0.82	13.00	0.44

Tab. 4.2: Central values of the field χ_ℓ and metric functions R and a for several values of $\Lambda = 0.5, 0.7, 1.0, 4.0$ and $\ell = 0, 1, 2$ with $\omega = 0$.

where A and B are constants. This is a particular simplification over Eq. (4.86) that is useful in the numerical procedure. In particular B will enter as a normalization factor, since we will ask for $B = 1$, as required by the asymptotic condition (4.82).

As mentioned previously, $\chi_\ell(0)$ is used as the shooting parameter so the requirements needed to find a solution are those described in the previous paragraphs. Using the LSODA FORTRAN solver for initial value problems of ordinary differential equations, we perform the integration of the system (4.67–4.69) starting at the value $r = 0$ using steps of $\Delta r = 1 \times 10^{-6}$ until a final value is reached. This finite value of the asymptotic boundary needs to be sufficiently large for the functions to reach their asymptotic behavior. Once the desired behavior of χ_ℓ is obtained up to a precision of order Δr , the asymptotic values of R and a are adjusted by means of the transformation (4.80) which leaves the system of equations invariant, where the parameter B is chosen equal to the corresponding coefficient in Eq. (4.95).

Examples are shown in Tables 4.2 and 4.3. Their physical implications are shown in section 4.3.3. The 0-wormhole recovers the wormhole studied by Dzhunushaliev *et al.* in [222] for complex, massive and self-interacting ghost scalar fields. Our results match those of them as can be seen in the $\Lambda = 4.0$ row in Table 4.2 when the following change of variables is performed:

$$r \mapsto \int_0^r \frac{dr}{\sqrt{a(r)}}, \quad \Lambda \mapsto \frac{\Lambda}{4}, \quad \chi_\ell \mapsto \sqrt{\frac{8\pi}{2\ell+1}} \chi_\ell, \quad (4.96)$$

which takes into account the differences in the definitions, nondimensionalization and the coordinate election. These authors also studied the case for a real scalar field in a previous work [223], which in fact corresponds to the $\omega = 0$ results in this paper.

$\Lambda = 0.7$	$\ell = 0$			$\ell = 1$			$\ell = 2$				
	$\chi_\ell(0)$	$R(0)$	$a(0)$	$\chi_\ell(0)$	$R(0)$	$a(0)$	$\chi_\ell(0)$	$R(0)$	$a(0)$		
$\omega = 0.1$	4.88	1.77	0.83	$\omega = 0.3$	3.18	2.01	2.60	$\omega = 0.8$	2.56	2.85	7.03
$\omega = 0.2$	4.64	2.01	1.07	$\omega = 0.5$	2.95	2.34	2.82	$\omega = 1.0$	2.36	3.28	7.13
$\omega = 0.3$	4.06	3.01	2.25	$\omega = 0.8$	2.45	3.67	4.49	$\omega = 1.6$	1.94	5.01	9.77

Tab. 4.3: Central values of the field χ_ℓ and metric functions R and a for several values of ω and $\ell = 0, 1, 2$ with $\Lambda = 0.7$.

Energy density, mass and curvature scalars

In order to help interpreting the solutions presented in the next section, we discuss several scalar quantities, like the energy density ρ of the ghost field measured by static observers, the Misner-Sharp mass function and the scalars related with the curvature of the spacetime, such as the Ricci scalar R_s and the Kretschmann scalar K . These quantities will turn out to be helpful for understanding the features of the ghost field and its action on the geometry.

Explicitly, the function ρ , associated with the density of the ghost field, is given by

$$\rho = -\frac{T^t_t}{c^2} = \left(\frac{c^2}{8\pi G} \right) \hat{\rho}, \quad (4.97)$$

where $\hat{\rho}$ is defined by

$$\hat{\rho} = -(2\ell + 1) \left[a \chi_\ell'^2 + \left(\frac{\ell(\ell + 1)}{R^2} + \mu^2 - \frac{2\ell + 1}{4\pi} \Lambda \chi_\ell^2 + \frac{\omega^2}{a} \right) \chi_\ell^2 \right]. \quad (4.98)$$

A striking feature of the wormhole solutions is that despite the presence of the exotic matter which violates the null energy condition everywhere, the density may still be positive at the throat,⁸ as will be shown in the numerical examples discussed in the next section. In fact, using Eq. (4.70) one can obtain the following simple expression for $\hat{\rho}$ at the throat:

$$\hat{\rho}(0) = \frac{8\pi}{b^2} - 2(2\ell + 1) \frac{\omega^2}{a(0)} \chi_\ell(0)^2, \quad (4.99)$$

which shows explicitly that for those solutions with $\omega = 0$ the energy density is indeed positive near the throat. The plots in the next section show that this behavior also holds for other solutions with small enough values of ω^2 .

⁸Note that the violation of the null energy condition implies the violation of the weak energy condition, which means that there exists at least one observer which measures negative energy density. Our example shows that this observer does not necessarily need to be a static one.

$\omega = 0, \Lambda = 1$	$M_\infty (m_{\text{pl}}^2/m_\Phi)$
$\ell = 0$	0.677
$\ell = 1$	0.224
$\ell = 2$	-1.25
$\ell = 3$	-4.69

Tab. 4.4: Total mass values for ℓ -wormholes with $\Lambda = 1$, $\omega = 0$ and $\ell = 0, 1, 2, 3$.

The total (ADM) mass of the wormhole configurations can be computed from the asymptotic limit $M_\infty = \lim_{r \rightarrow \infty} M(r)$ of the Misner-Sharp mass function [232] $M(r)$, defined by

$$\frac{2GM}{c^2} = R [1 - g^{\mu\nu} (\nabla_\mu R)(\nabla_\nu R)] = R (1 - aR'^2). \quad (4.100)$$

From Eqs. (4.86, 4.95) one obtains $GM_\infty/c^2 = c_0/2 = -A/2$. Alternatively, using Eqs. (4.69, 4.70) one also obtains $M' = 4\pi\rho R^2 R'$ which can be integrated to

$$M(r) = \frac{c^2}{2G} \left(b + \int_0^r \hat{\rho}(\bar{r}) R^2(\bar{r}) R'(\bar{r}) d\bar{r} \right), \quad (4.101)$$

with $b = R(0)$ the throat's areal radius (see Fig. 4.16 to visualize a particular value of $b = 5$). As long as $\hat{\rho}$ is positive near the throat, the mass function increases as one moves away from the throat. However, M decreases as soon as $\hat{\rho}$ becomes negative, so that solutions which have either sign of the total mass are possible. This is shown in Table 4.4, where values of the total mass M_∞ for our wormhole were computed taking several values of ℓ and fixing the values of all other parameters.

The Ricci scalar, $R_s = R^\mu{}_\mu$, associated with the geometry given by Eq. (4.49) has the form

$$R_s = -a'' - 2a \frac{R^{2''}}{R^2} + a \left(\frac{R^{2'}}{R^2} \right)^2 + \frac{2}{R^2} (1 - a' R^{2'}). \quad (4.102)$$

A further commonly used curvature measure is the Kretschmann scalar, defined by $K = R^{\mu\nu\sigma\tau} R_{\mu\nu\sigma\tau}$. For the metric under consideration, Eq. (4.49), the Kretschmann scalar has the following explicit form:

$$K = a'' + 2 \left(\frac{a R^{2''}}{R^2} \right)^2 + 2a \frac{R^{2''} R^{2'}}{R^4} \left(a' - \frac{a R^{2'}}{R^2} \right) + \frac{4}{R^4} + \left[\frac{3}{4} \left(\frac{a R^{2'}}{R^2} \right)^2 - \frac{a^{2'} R^{2'}}{2R^2} + a'^2 - 2 \frac{a}{R^2} \right] \left(\frac{R^{2'}}{R^2} \right)^2. \quad (4.103)$$

All these quantities will turn out to be helpful when understanding the role played by the several parameters of the solution in the geometry and in the dynamics of the bodies moving on it.

From Einstein's equations, Eq. (4.64), we have that $R_s = -\frac{8\pi G}{c^4} T$ with T the trace of the stress-energy-momentum tensor. Numerical experiments show that the behavior of the stress-energy-momentum tensor components in the throat region are similar to each other, and thus $R_s \approx \frac{8\pi G}{c^2} \rho$, as seen in the actual solutions. That is, the Ricci scalar goes as the density, irrespective of its character, exotic or usual matter. We will discuss this fact in more detail in the explicit cases that we present below.

4.3.3 Numerical wormhole solutions

Following the procedure described above, we are able to obtain several solutions to the Einstein-Klein-Gordon system, given the four parameters, namely μ, ω, Λ , and ℓ . We will present the solutions first for trivial values of the angular momentum parameter, $\ell = 0$, and vary the self-interaction parameter Λ , while keeping the oscillation frequency ω fixed and then we explore the properties of the solution for some values of ω maintaining Λ fixed, as was done in [222, 223]. Next, we repeat the study for different values of ℓ . In all our solutions presented in this work, we keep the mass of the scalar field μ fixed. These experiment allow us to have a better understanding on the role that each parameter plays in determining the geometry of the solutions.

All the solutions presented are asymptotically flat, and are generated by looking for a solution of the ghost scalar field, once the parameters ℓ, Λ and ω are chosen. We fix the value of mass parameter μ to one, and the distance scale of the solution is given by the dimensionless parameter $\hat{r} = \mu r$. Also, from Eq. (4.76) we see that the size of the wormhole throat $R(0)$ is given by

$$R(0) = \left(\frac{\ell(\ell + 1) + \frac{8\pi}{(2\ell+1)\chi_\ell^2(0)}}{\frac{2\ell+1}{4\pi}\Lambda\chi_\ell^2(0) + \frac{\omega^2}{a(0)} - \mu^2} \right)^{1/2}. \quad (4.104)$$

In Fig. 4.8, we present this localized solution, for the case $\ell = 0, \omega = 0$, for several values of Λ . All the other solutions with $\ell > 0$ are localized as well. Notice how the amplitude of the pulse decreases as the value of the self-interaction parameter Λ increases.

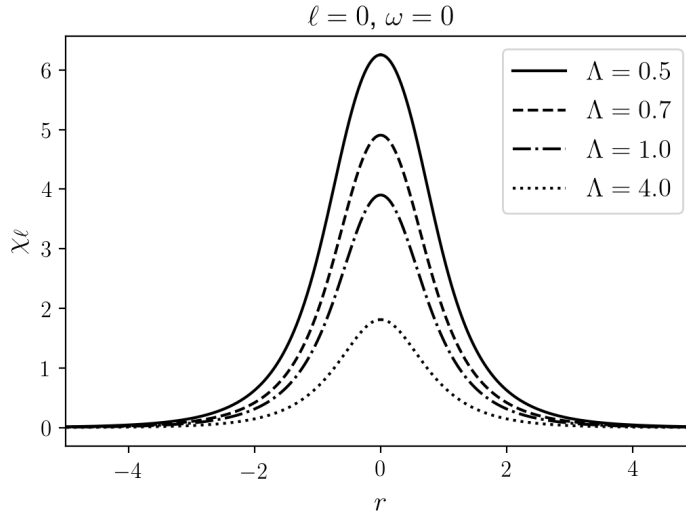


Fig. 4.8: Solitonic profile for the 0-wormhole, for $\Lambda \in [0.5, 4.0]$, and $\omega = 0$.

In our experiments, we see that the ghost density, in order to form a wormhole, is distributed in such a way that it has a positive value in the region of the throat, and then it starts to have larger concentrations of negative ghost density on both sides of the throat, as shown in Fig. 4.9. From the geometric perspective, as suggested above, the profile of the Ricci scalar follows the density one and has a convex region at the throat, surrounded by concave zones, see Fig. 4.11.

Also we will show that, in general, as can be seen in Fig. 4.9, the action of the self-interaction parameter, Λ , smooths out this behavior of the exotic density and spacetime interaction. Indeed, the scalar field, at least the massive ghost field, possess a radial pressure that creates the throat and then the spacetime strongly reacts generating regions of negative density; it is the role of the self-interaction term to smooth down such reaction and allows to keep the wormhole throat open with smaller amount of ghost density. Conversely, as the self-interaction parameter Λ becomes smaller, the metric coefficient a , the curvature scalars and density at the throat become more and more localized, an observation which is compatible with the result in Theorem 1 where we have shown that the solutions cease to exist for $\Lambda = 0$.

0-wormhole

We start our discussion for the case with vanishing angular momentum, *i. e.* $\ell = 0$ that is, an Ellis-type wormhole solution (see Sec. 4.3.2). Setting also ω equal to zero for

the moment, we start by sweeping a range of values for the self-interaction parameter, Λ . The corresponding results for the scalar field and the density profile are shown in Figs. 4.8 and 4.9, respectively. As mentioned above, the ghost density has regions of positive magnitude near the throat, and regions with negative density which tend to zero from below in the asymptotic region.

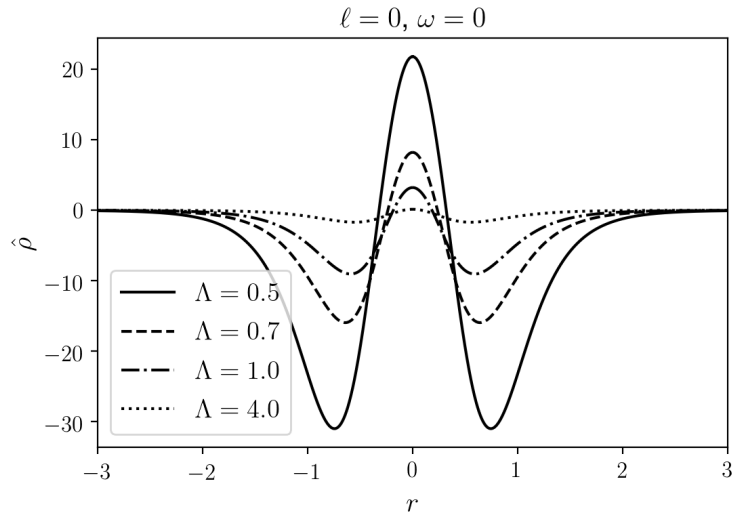


Fig. 4.9: Density profile for the 0-wormhole, for $\Lambda \in [0.5, 4.0]$ and $\omega = 0$.

The corresponding metric coefficients, $a(r)$ and $R(r)$ are shown in Fig. 4.10. Notice how the metric coefficient $a(r)$ shows concave regions which will determine a similar behavior in the effective potential of the spacetime, which in turn will imply the existence of particles moving on bound trajectories. Again, the effect of the self-interaction parameter is to smooth out the concavity of the metric functions.

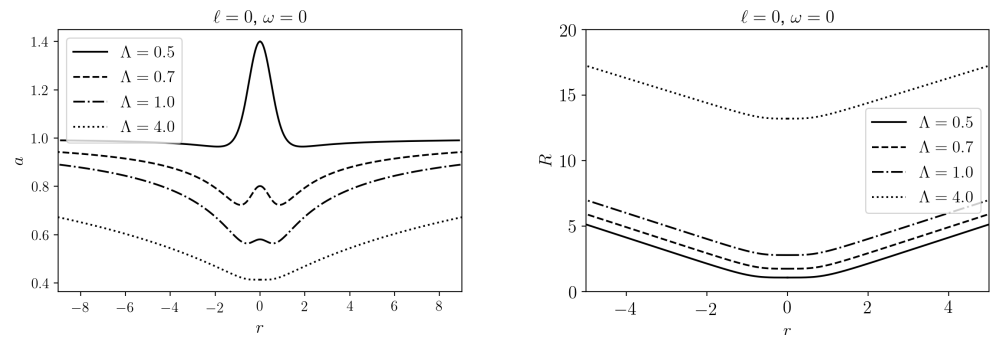


Fig. 4.10: Metric coefficients for $\Lambda \in [0.5, 4.0]$ and $\omega = 0$.

Regarding the curvature scalars, as expected, the Ricci scalar R_s has a behavior which follows the one of the density, with regions of positive values and then valleys with negative values of the curvature as we can see in Fig. 4.11. The Kretschmann scalar, however, is very different and shows two peaks of positive values and they decrease as the self-interaction parameter grows, and the central one is negative in the region of the throat, surrounded by bumps.

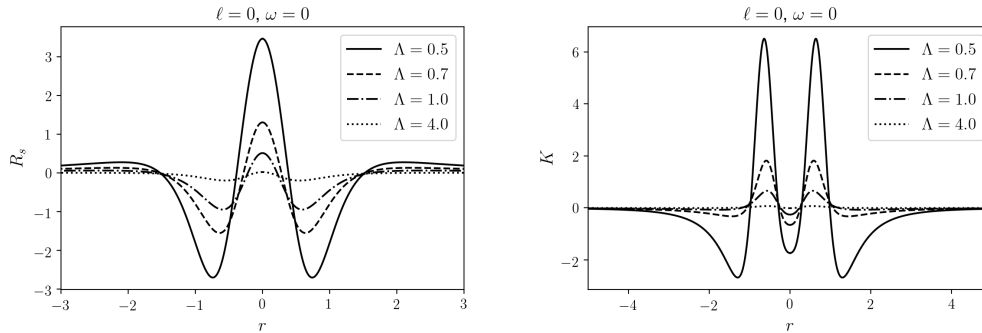


Fig. 4.11: Ricci and Kretschmann scalars for $\Lambda \in [0.5, 4.0]$ and $\omega = 0$.

The next step is to increase the parameter ω keeping $\ell = 0$ and the self-interaction parameter $\Lambda = 0.7$ fixed. We show in Fig. 4.12 the corresponding density and Kretschmann scalar for three non-zero values, $\omega = 0.1, 0.3, 0.5$, of the frequency. Notice the difference between the behavior of the Kretschmann scalar, in which a larger value of ω gives the effect of increasing the central value, acting in the same way as the parameter Λ discussed above.

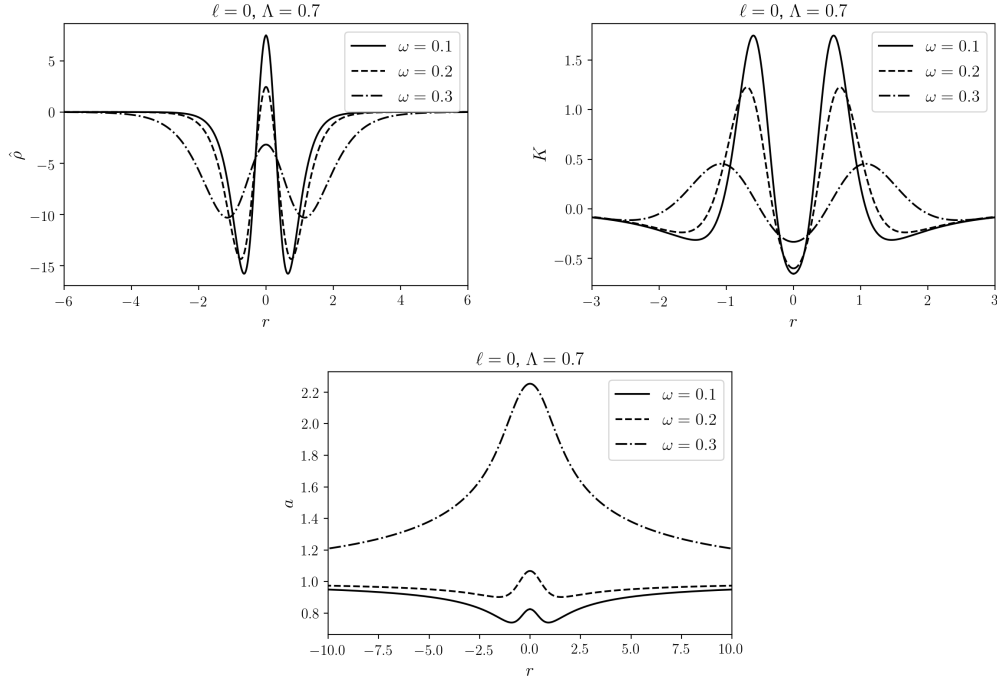


Fig. 4.12: Density profile, curvature scalar and metric function a for the 0-wormhole, $\Lambda = 0.7$ and $\omega = 0.1, 0.2, 0.3$.

ℓ -wormhole

In this section we present the behavior of the ℓ parameter and the effect on the metric functions and the curvature scalars. For the latest we can see in Fig. 4.13 that an increment on the ℓ parameter increases the central peak for the Ricci scalar and decreases the central bump for the Kretschmann scalar. The case for $a(r)$ is quite different: while for $\ell = 1$ the two minima are still present, for larger values of the ℓ parameter the central peak is increased and the minima disappear. The presence of a minimum (or two in this case) also corresponds to positive total masses as can be verified in Table 4.4 and Fig. 4.14, consequently, its absence corresponds to negative masses. This is a general property of all solutions given the asymptotic behavior of a (see Eq. 4.95).

On the other hand, as is shown in Fig. 4.15, the increment of the ω parameter plays a role quite similar to the one made by the ℓ parameter: an increase on the former elevates the central peak on the metric function $a(r)$.

Moreover, as can be seen from a comparison of Figs. 4.10 and 4.13, the effect of the Λ parameter on the metric coefficient a is opposite to the one generated by the

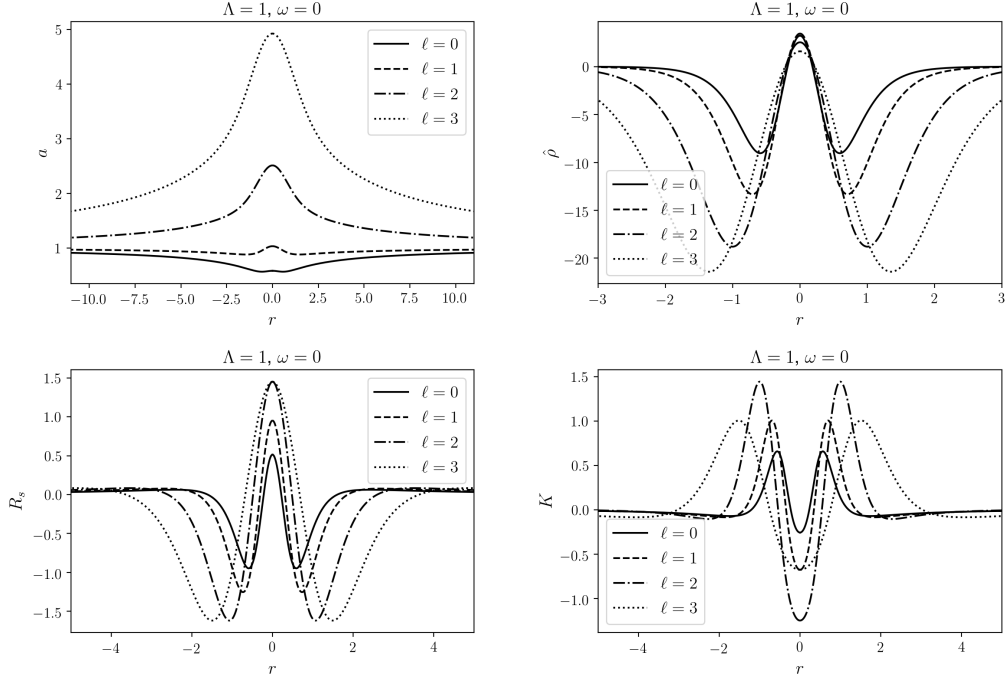


Fig. 4.13: Metric function $a(r)$, density profile $\hat{\rho}$ and R_s , K scalars for $\ell \geq 0$, $\Lambda = 1.0$ and $\omega = 0$.

ℓ parameter on that metric coefficient. Indeed, for small values of Λ , the metric coefficient a has a global maximum at the throat, while for large values of this Λ , the metric coefficient a only has a local maximum. Thus, for small values of Λ , the ℓ parameter is not able to change the qualitative behavior of the metric coefficient, while for larger values of Λ , the appearance of the local maximum is recovered or enhanced with the parameter ℓ . This fact will have consequences on the effective potential and the geodesic motion of particles, as discussed below.

4.3.4 Embedding diagrams and geodesic motion

In order to gain a better understanding of the configurations described by the scalar field and the geometry in the vicinity of the throat, in this section we discuss the embedding procedure and geodesic motion. Because the metric (4.49) is static and spherically symmetric, it is sufficient to analyze the induced geometry on a $t = \text{constant}$ and $\theta = \pi/2$ slice, described by the two-metric

$$d\Sigma^2 = a^{-1}dr^2 + R^2d\varphi^2. \quad (4.105)$$

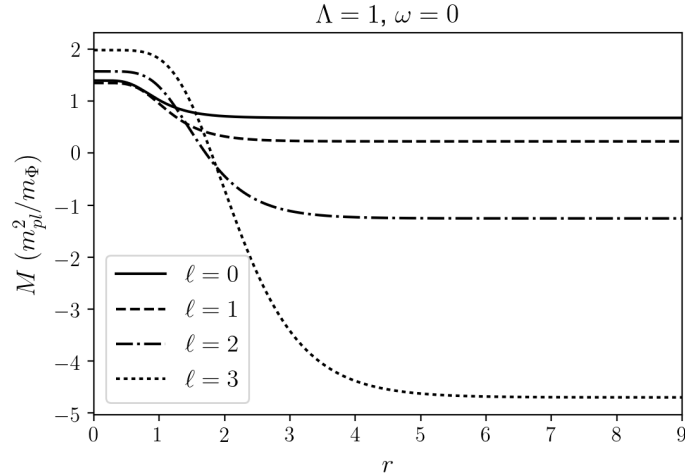


Fig. 4.14: Mass function $M(r)$ for the parameters $\ell \geq 0$, $\Lambda = 1$ and $\omega = 0$.

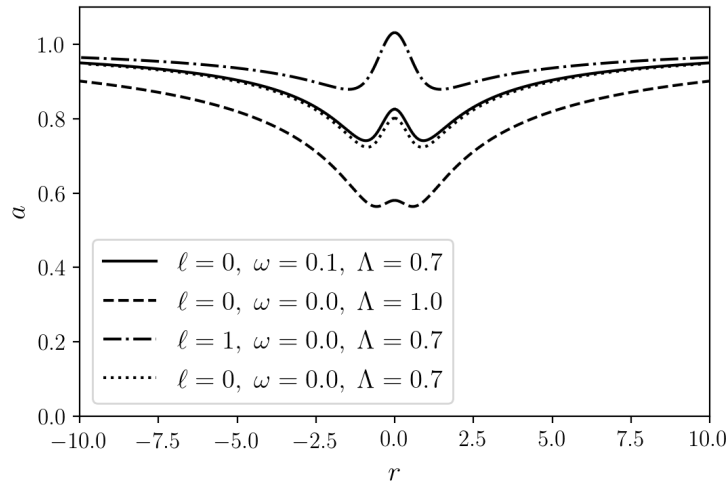


Fig. 4.15: Metric function a for different values of the parameters ℓ , ω and Λ .

In order to visualize this geometry as a two-dimensional surface embedded in three-dimensional flat space we shall employ cylindrical coordinates (ρ, φ, z) . The metric for a flat space in these coordinates is

$$dS^2 = d\rho^2 + \rho^2 d\varphi^2 + dz^2 . \quad (4.106)$$

We seek for the functions $\rho(r)$ and $z(r)$, specifying a surface with the same geometry as the one described by the metric (4.105).

The line element for the embedding surface will be

$$d\Sigma^2 = \left[\left(\frac{dz}{dr} \right)^2 + \left(\frac{d\rho}{dr} \right)^2 \right] dr^2 + \rho^2 d\varphi^2, \quad (4.107)$$

if the following conditions are satisfied:

$$\rho = R, \quad (4.108)$$

and

$$\left(\frac{dz}{dr} \right)^2 + \left(\frac{d\rho}{dr} \right)^2 = \frac{1}{a}. \quad (4.109)$$

Using the expression (4.108) to calculate $\frac{d\rho}{dr}$, Eq. (4.109) gives the following differential equation for $z(r)$:

$$\frac{dz}{dr} = \left[\frac{1}{a} - \frac{1}{4} \frac{(R^{2'})^2}{R^2} \right]^{1/2}. \quad (4.110)$$

Integrating this equation gives the function $z = z(r)$; in order to plot it in an Euclidean space, we need to find r as a function of ρ . However, it is not possible to express this function $r = r(\rho)$ in closed form because R was found numerically. Nevertheless, one can obtain $r = r(\rho)$ numerically from (4.108) and finally get $z = z(\rho)$.

In Fig. 4.16 we show the visualization of this embedding. It is seen that as ℓ increases from 0 to 2, the profile of the embedding representing the wormhole's geometry becomes more and more curved (which is analogous to the increase of $|R_s|$ and $|K|$ shown in Fig. 10), with a slight decrease in the throat's radius.

Geodesic motion

In order to describe the motion of the particles in the spacetimes described above, we start from the Lagrangian for the metric (4.49),

$$\mathcal{L} = g_{\mu\nu} u^\mu u^\nu + \kappa c^2 = -ac^2 (u^0)^2 + a^{-1} (u^r)^2 + R^2 [(u^\theta)^2 + \sin^2 \theta (u^\varphi)^2] + \kappa c^2, \quad (4.111)$$

where $u^\mu = \dot{x}^\mu$ is the four velocity and the parameter κ assumes the values 1 or 0, depending on whether the particle is massive or massless. respectively. The line element is spherically symmetric and static, so that the energy, $E = -\frac{\partial \mathcal{L}}{\partial u^0}$, the azimuthal

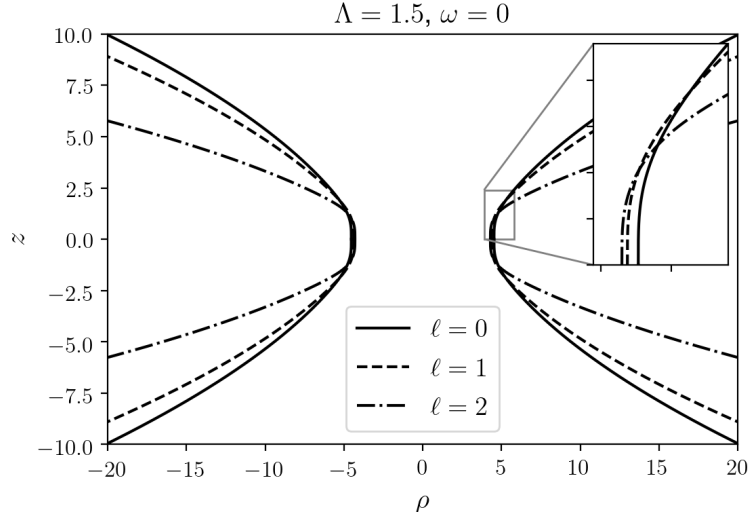


Fig. 4.16: Embedding of the different ℓ -wormholes, for $\Lambda = 1.5, \omega = 0$. The complete embedding diagram is obtained by rotating this figure about the z axis. In the enlarged picture we underline the change of the value of the throat radius for the given values of ℓ .

momentum, $L_\varphi = \frac{\partial \mathcal{L}}{\partial u^\varphi}$, and the total angular momentum, $L^2 = \left(\frac{\partial \mathcal{L}}{\partial u^\theta}\right)^2 + \frac{L_\varphi^2}{\sin^2 \theta}$, are conserved quantities. Explicitly, they have the form:

$$E = -\frac{\partial \mathcal{L}}{\partial u^0} = ac^2 u^0, \quad (4.112)$$

$$L_\varphi = \frac{\partial \mathcal{L}}{\partial u^\varphi} = R^2 \sin^2 \theta u^\varphi. \quad (4.113)$$

Since we are only interested in the motion of a single particle (as opposed to a swarm of particles) we can choose the angles such that the orbital plane coincides with the equatorial plane $\theta = \pi/2$, in which case $L_\varphi = L$. In this way, we can express the components of the four-velocity in terms of the conserved quantities L and E , and the normalization condition $g_{\mu\nu} u^\mu u^\nu = -\kappa c^2$ yields the radial equation of motion:

$$(u^r)^2 + V_{\text{eff}} = \frac{E^2}{c^2}, \quad (4.114)$$

with the effective potential

$$V_{\text{eff}} = \frac{a L^2}{R^2} + a \kappa c^2. \quad (4.115)$$

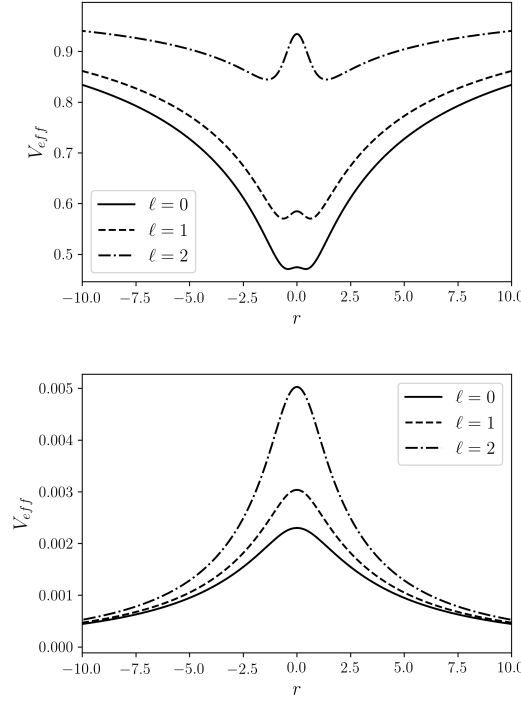


Fig. 4.17: Effective potential for time-like (left panel) and null geodesics (right panel) for $L = \sqrt{\frac{1}{10}}$.

In Fig. 4.17 we plot V_{eff} for the parameter choices $L = \sqrt{\frac{1}{10}}$, $\omega = 0$ and $\Lambda = 1.5$ for time-like and a null geodesics. As expected, the term involving L generates an angular momentum barrier, corresponding to a local maximum of the effective potential located at the throat $r = 0$. (Recall from Section 4.3.2 that $a(r)$ has a local maximum while $R^2(r)$ has a local minimum at $r = 0$.) This maximum corresponds to an unstable equilibrium point giving rise to circular unstable particle orbits. For the $\ell = 0$ case, and for this value of L and with $\kappa = 1$, the effective potential also has a minimum at $r \approx \pm 1.34$, which means that bound orbits also exist for this value of L .

In Fig. 4.18 we plot different geodesics for massive particle with $L = \sqrt{1/10}$ and $\Lambda = 1.5$ in the $\ell = 0, 1, 2$ wormholes. Here we picked the same initial conditions in terms of the initial radial velocity $u^r(0) = 0$ and initial position $r(0) = 0.65$, $\varphi(0) = \pi$ ending up with particles with different energies and qualitatively different motion. As stated above, one can assume without loss of generality that the motion is confined to the equatorial plane $\theta = \frac{\pi}{2}$, so that it can be plotted in the embedding surface. As can be noticed from the plots, the motion is quite interesting and can be understood based on the behavior of the effective potential and the energy level of the test particle.

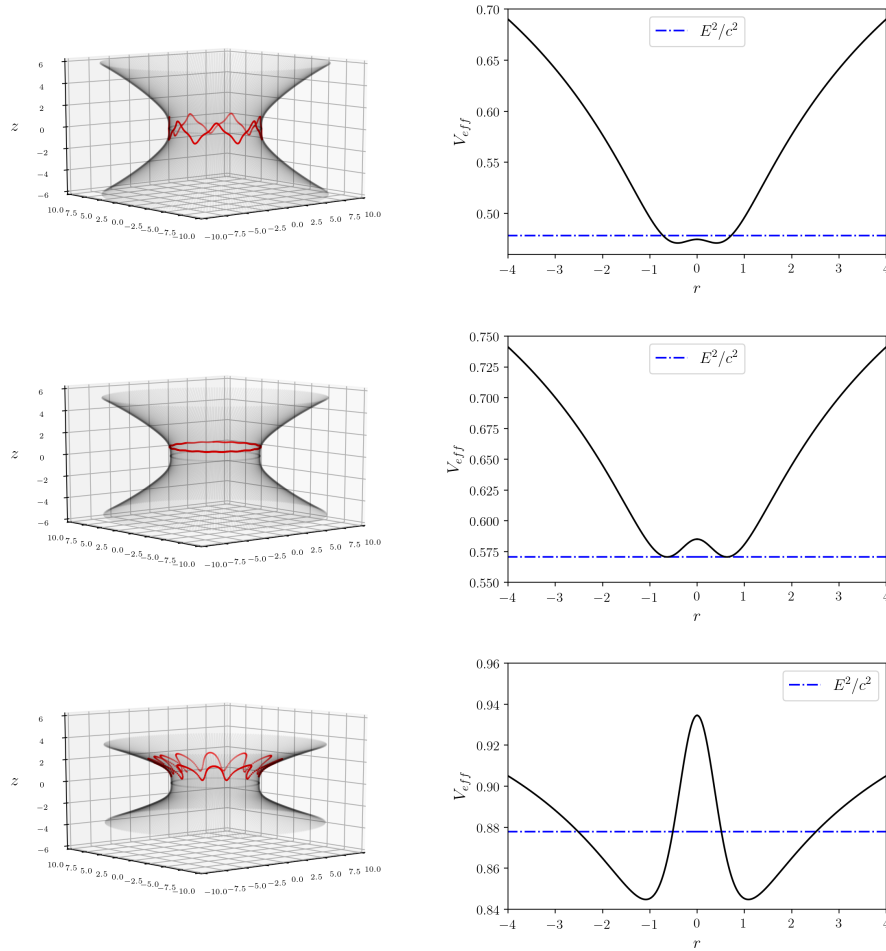
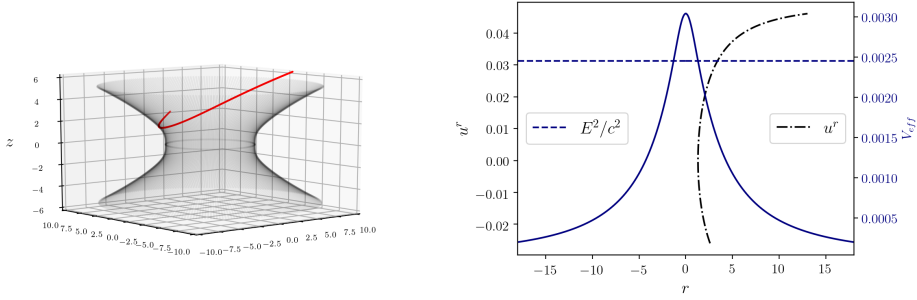
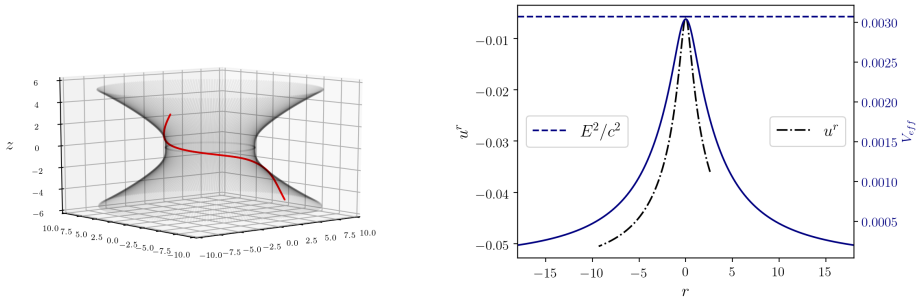


Fig. 4.18: Different $\ell = 0$ (top), $\ell = 1$ (middle) and $\ell = 2$ (bottom) geodesics for $\kappa = 1$, $\omega = 0$, $\Lambda = 1.5$, $L = \sqrt{1/10}$. On the left we plot the motion of the particle in the embedding surface of the wormhole and on the right the value of E and V_{eff} .

In order to further clarify the behavior of the geodesics, in Fig. 4.19 we plot the trajectory in the embedding diagram and the radial velocity u^r for two different null geodesics with angular momentum $L = \sqrt{1/10}$ propagating in the $\ell = 1$ wormhole. In the first case, shown in Fig. 4.19a, the particle does not have sufficient energy to traverse the throat so it starts approaching the throat with a decrement of the velocity, reaches a zero radial velocity and resumes its motion going away from the throat. On the other hand, the second example in Fig. 4.19b shows that, for a particle that has enough energy to pass through the throat, the absolute value of its velocity decreases as it moves towards the throat (from right to left) until it traverses the throat, after which the absolute value of the velocity increases again as the particle moves away from the throat on the other side of the wormhole.



(a) A particle having insufficient energy to pass through the wormhole. The motion starts at $r = 2.6$, the velocity decreases until the particle arrives near the throat after which it returns, moving away with increasing speed. In this case the particle stays on the same side of the wormhole and does not cross the throat.



(b) A particle starts its motion at $r = 2.6$, traverses the throat, and continues its motion with a growing absolute value of the velocity.

Fig. 4.19: Two different $\ell = 1$ geodesics for $\kappa = 0$, $L = \sqrt{1/10}$, $\omega = 0$, $\Lambda = 1.5$. We plot the motion with their corresponding E (right y-axis) and u^r (left y-axis) values.

4.3.5 Discussion and concluding remarks

We have described how to construct new families of traversable wormhole solutions which are parametrized by a parameter ℓ , related to the angular momentum of the ghost fields supporting the throat, and discussed its effects on the shape of the geometric functions characterizing the solution, and on the geodesic motion of the corresponding spacetime. These families generalize previous wormhole spacetimes discussed in the literature [222, 223] which are recovered from our models by setting $\ell = 0$.

Indeed, we have obtained *bona fide* solutions to the Einstein-Klein-Gordon system and performed a detailed analysis of such solutions, which allowed us to gain a better understanding on the effects of the new parameter ℓ . We have been able to establish

that its role on the geometric function a (determining the redshift factor), on the curvature scalars and on the density is quite similar to the role played by the frequency ω characterizing the time-dependency of the field, while its effect on these quantities is opposite to the one generated by the parameter of self-interaction Λ . Moreover, as can be clearly seen in the plot of the effective potential for time-like geodesics shown in Fig. 4.17, as the value of ℓ grows, the positions of the local minima move farther away from the throat, which is similar to the effect of increasing the angular momentum L of the test particles. In this sense, from the point of view of the test particle, the parameter ℓ plays a similar role than its conserved total angular momentum L .

It is interesting to point out that the energy density of some of our solutions – despite of the fact that the stress-energy-momentum violates the null energy condition – is actually positive close to the throat (but changes its sign as one moves away from it and then converges to zero which is consistent with our asymptotic flatness assumptions). In fact, the construction of a wormhole does not necessarily require measurements of a negative energy density made by static observers, as already indicated in [204]. However, the fact that the null energy condition is violated at the throat implies that such observers also measure a “superluminal” energy flux. In general, the wormhole solutions discussed in this article possess a much richer structure than the simple, reflection-symmetric Bronnikov-Ellis wormholes, whose energy density is everywhere negative. In particular, the spacetimes discussed here exhibit a rich profile of bumps and wells in their curvature scalars whose precise shape depends on the values of ℓ as much as it does on the other parameters.

Indeed, we presented a detailed analysis of the role played by the several parameters in our wormhole solutions, namely the self-interaction term Λ , the oscillating frequency, ω , and the angular momentum parameter, ℓ of the scalar fields. Moreover, we have proved that there are no solutions for which the metric and scalar fields are reflection-symmetric about the throat if $\Lambda = 0$ (see Theorem 1). In this sense, the self-interaction term needs to be included in the action in order to extend the solution space. Actually, we have seen that it plays a smoothing role in the geometric reaction to the ghost matter. Also, we have seen that the effects on the geometry of the self-interaction parameter is opposite to the effects due to the frequency ω . As mentioned previously, the role of the ℓ parameter on the geometry is similar to the one generated by the frequency. This fact can be used to obtain real scalar field wormholes, with a new degree of freedom analogous to the case in which the solution space is extended by permitting the scalar field to be complex and harmonic in time. As shown in Theorem 2,

all our wormhole solutions are characterized by a single throat whose areal radius is fixed by the parameters and the value of the scalar field at the throat, see Eq. (4.104).

We also provided a study of the effects of the parameters on the embedding diagrams visualizing the spatial geometry of the solutions, including the shape of the throat for several relevant cases. Finally, we presented a detailed analysis of the effective potential describing the motion of free-falling test particles as a function of the parameters, and we showed how the potential may present a local maximum at the throat which is surrounded by regions with local minima. Accordingly, we obtained several interesting types of trajectories. Depending on the values of the parameters and on those of the constants of motion (namely, the energy and angular momentum of the particle), we displayed trajectories approaching the throat until they reach a turning point and go back, other trajectories which describe bound motion on either side of the throat, and then we even obtained orbits that are bound but cross the throat repeatedly and keep passing from one side of the Universe to the other; a nice property for a space station!

In the plots of Fig. 4.19 we have shown the behavior of the geodesics passing through the throat, we presented the absolute value of the particle's radial velocity and showed that it decreases as the particle approaches the throat until it crosses it after which it increases again as the particle gets further away from the throat. Such behavior is consistent with the interpretation that the reaction of the geometry to the ghost matter is to create bumps in the effective potential, instead of the wells generated by the usual matter. As mentioned at the beginning of Section 4.3.1, there is no need to invoke negative masses to explain such behavior; it is simpler to imagine that the reaction of the geometry to the ghost matter is to create bumps that the particle have to surmount, consistent with the fact that the absolute value of the velocity decreases as it approaches the throat, and then, goes down the hill.

The new configurations we have found and discussed in this article considerably extend the parameter space describing wormhole solutions of the Einstein-scalar field equations, and they provide a large arena that offers the possibility to further study the intriguing properties of wormhole spacetimes, including the relation between the properties of exotic matter and their geometry. While it has been shown that the solutions with $\ell = 0$ are linearly unstable [231, 233, 222], there is hope that such a large arena may contain a set of parameter values with $\ell > 0$ describing stable wormholes or unstable wormholes with a very large timescale associated to their instability, a question that will be discussed in a future work.

Conclusions

In this work are presented several analysis to incorporate complex scalar fields motivated by models coming from particle physics (as Bose–Einstein condensate and also as beyond the Standard Model of particle physics) in the cosmological evolution in the context of the dark sector of the Universe. We denote these fields as *classical* in the sense that a single scalar field does not interact in any way, except the gravitational interaction, with the rest of the matter components of the Universe.

It was developed a quintessence and complex scalar field model to describe the cosmic acceleration observed in the study of the peculiar branch solution of the KGE system of equations in the fast oscillation regime (Chapter 4.2). It was possible to derive an effective equation of state that we called parametric Complex Scalar Field Dark Energy whose parameters can be constrained using current observational surveys as CC+BAO+Pantheon. Nevertheless, it was not possible to constraint the parameter w_a within the allowed theoretical values due to the fact that the fitted value $w_a = 0.33 \pm 0.93$ is inconsistent with the Eq. 4.38, $w_a \in \left(0, \frac{16}{27}\right)$. It is remarkable that we derived from first principles an equation of state whose parameters were fitted via a scalar field analysis with topical cosmological observations; this derivation is not usual in the literature, since the equations of state are proposed generally so that the component in question behaves in the appropriate way. On the other hand, it was not applicable a statistical analysis with CMD data but this limitation could be resolved if two scalar fields are considered instead of a single one in order to reproduce viable cosmological scenarios that includes, for instance, an oscillating behavior of the EoS.

In this sense, it was presented, in Chapter 3.2, an analysis to combine some scalar fields coming from physics beyond the Standard Model of particle physics (BSM) with a classical scalar field where both of the fields would constitute the dark matter component of the Universe. Then, we explore via constrains from the effective number of neutrino species, N_{eff} , the proportions of each field in two cases: a classical field and a Higgs–like field that we call Model I, and the Model II constituted by a Higgs–like and an axion–like fields. In the Model I analysis, it was found that the Higgs–like field can compose up to 58% of the dark matter density today and the remaining 42% be a classical scalar field and produce, even so, a cosmological model consistent with

the observations. In the Model II, made fully of two BSM fields, it was not possible to find allowed values consistent with the N_{eff} constraint. This results could open the possibility to take into account the direct and indirect searches for more than one candidate to dark matter, which may contribute to the relic density in different proportions, and thus modify the expected fluxes in the experimental analysis.

We also explore, through a SHAM approach of dark matter, the degeneracy between two mechanisms of the suppression of small structures coming from the Λ CDM cosmology and that expected from the cutoff of the power spectrum of several non-CDM models, within which lies the scalar field dark matter known as fuzzy DM. Although this degeneracy was not resolved in the work, a method was established that, with the advent of new and deeper observations with the JWST, can discern between a CDM and an nCDM model when fitted through astrophysical observations.

The scalar field studies allowed us to also describe how to construct new families of traversable wormhole solutions supported by ghost scalar fields parametrized by a parameter related to the angular momentum, ℓ . Despite being purely theoretical objects, it was presented a detailed analysis of the role played by the parameters of the field: the self-interaction term, the oscillating frequency and the ℓ parameter. This analysis, along with the displayed geodesics of a particle with energy and angular momentum given, provide the possibility of further studies regarding wormhole spacetimes, including the relation between the properties of exotic matter and their geometry and the future exploration of the stability of such ℓ -wormholes. The understanding of these exotic objects can provide new possibilities on the behavior of the ghost scalar fields and, in consequence, the possible description of the dark energy of the Universe.

The work presented here in addition, represents a bridge that links some of the results on theoretical Physics with those of the Astronomy, as well as contextualize them in the field of Astrophysics. We hope that this effort will contribute to making the scalar field a more visible, analyzable and considerable possibility for the adequate description of the dark sector of the Universe.

References

- [1]Planck Collaboration et al. “Planck 2018 results. VI. Cosmological parameters.” In: arXiv e-prints, arXiv:1807.06209 (July 2018), arXiv:1807.06209. arXiv: 1807.06209 [astro-ph.CO].
- [2]Matts Roos. “Astrophysical and cosmological probes of dark matter.” In: J. Mod. Phys. 3 (2012), p. 1152. DOI: 10.4236/jmp.2012.329150. arXiv: 1208.3662 [astro-ph.CO].
- [3]Matthew R. Buckley and Annika H. G. Peter. “Gravitational probes of dark matter physics.” In: Phys. Rept. 761 (2018), pp. 1–60. DOI: 10.1016/j.physrep.2018.07.003. arXiv: 1712.06615 [astro-ph.CO].
- [4]Gianfranco Bertone et al. “Gravitational wave probes of dark matter: challenges and opportunities.” In: SciPost Phys. Core 3 (2020), p. 007. DOI: 10.21468/SciPostPhysCore.3.2.007. arXiv: 1907.10610 [astro-ph.CO].
- [5]V. A. Rubakov. “Cosmology and Dark Matter.” In: 2019 European School of High-Energy Physics. Dec. 2019. arXiv: 1912.04727 [hep-ph].
- [6]Jens Stücker et al. “Simulating the complexity of the dark matter sheet - II. Halo and sub-halo mass functions for non-cold dark matter models.” In: 509.2 (Jan. 2022), pp. 1703–1719. DOI: 10.1093/mnras/stab3078. arXiv: 2109.09760 [astro-ph.CO].
- [7]Bharat Ratra and P. J. E. Peebles. “Cosmological consequences of a rolling homogeneous scalar field.” In: Phys. Rev. D 37 (12 June 1988), pp. 3406–3427. DOI: 10.1103/PhysRevD.37.3406. URL: <https://link.aps.org/doi/10.1103/PhysRevD.37.3406>.
- [8]P. J. E. Peebles and Bharat Ratra. “Cosmology with a Time Variable Cosmological Constant.” In: Astrophys. J. Lett. 325 (1988), p. L17. DOI: 10.1086/185100.
- [9]C. Wetterich. “Cosmology and the Fate of Dilatation Symmetry.” In: Nucl. Phys. B 302 (1988), pp. 668–696. DOI: 10.1016/0550-3213(88)90193-9. arXiv: 1711.03844 [hep-th].
- [10]Latham A. Boyle, Robert R. Caldwell, and Marc Kamionkowski. “Spintessence! New models for dark matter and dark energy.” In: Phys. Lett. B 545 (2002), pp. 17–22. DOI: 10.1016/S0370-2693(02)02590-X. arXiv: astro-ph/0105318.
- [11]Pedro Miguel, Gregório Carrilho, and Marika Haderer. “A Scalar Field Theory for Dark Matter Dark Energy Interaction.” In: 2012.

- [12]Eréndira Gutiérrez-Luna et al. “Scalar field dark matter with two components: Combined approach from particle physics and cosmology.” In: 105.8, 083533 (Apr. 2022), p. 083533. DOI: 10.1103/PhysRevD.105.083533. arXiv: 2110.10258 [astro-ph.CO].
- [13]Belen Carvente et al. “Observational constraints on complex quintessence with attractive self-interaction.” In: *Mon. Not. Roy. Astron. Soc.* 503.3 (2021), pp. 4008–4015. DOI: 10.1093/mnras/stab650. arXiv: 2008.11211 [gr-qc].
- [14]Belen Carvente et al. “Traversable ℓ -wormholes supported by ghost scalar fields.” In: *Class. Quant. Grav.* 36.23 (2019), p. 235005. DOI: 10.1088/1361-6382/ab4dfb. arXiv: 1906.08295 [gr-qc].
- [15]Abraão Jessé Capistrano de Souza. “Introductory Chapter: The Physics of Dark Sector.” In: *Essentials on Dark Matter*. Ed. by Abraão Jessé Capistrano de Souza. Rijeka: IntechOpen, 2018. Chap. 1. DOI: 10.5772/intechopen.80234. URL: <https://doi.org/10.5772/intechopen.80234>.
- [16]L. Arturo Ureña-López. “Brief Review on Scalar Field Dark Matter Models.” In: *Front. Astron. Space Sci.* 6 (2019), p. 47. DOI: 10.3389/fspas.2019.00047.
- [17]Tonatiuh Matos and L. Arturo Ureña-López. “Further analysis of a cosmological model with quintessence and scalar dark matter.” In: *Phys. Rev. D* 63 (6 Feb. 2001), p. 063506. DOI: 10.1103/PhysRevD.63.063506. URL: <https://link.aps.org/doi/10.1103/PhysRevD.63.063506>.
- [18]C. Wetterich. “Cosmology and the fate of dilatation symmetry.” In: *Nuclear Physics B* 302.4 (1988), pp. 668–696. ISSN: 0550-3213. DOI: [https://doi.org/10.1016/0550-3213\(88\)90193-9](https://doi.org/10.1016/0550-3213(88)90193-9). URL: <https://www.sciencedirect.com/science/article/pii/0550321388901939>.
- [19]Michael S. Turner. “Coherent scalar-field oscillations in an expanding universe.” In: 28.6 (Sept. 1983), pp. 1243–1247. DOI: 10.1103/PhysRevD.28.1243.
- [20]Sang-Jin Sin. “Late-time phase transition and the galactic halo as a Bose liquid.” In: 50.6 (Sept. 1994), pp. 3650–3654. DOI: 10.1103/PhysRevD.50.3650. arXiv: hep-ph/9205208 [hep-ph].
- [21]Luca Amendola and Riccardo Barbieri. “Dark matter from an ultra-light pseudo-Goldstone-boson.” In: *Physics Letters B* 642.3 (Nov. 2006), pp. 192–196. DOI: 10.1016/j.physletb.2006.08.069. arXiv: hep-ph/0509257 [hep-ph].
- [22]Bohua Li, Tanja Rindler-Daller, and Paul R. Shapiro. “Cosmological Constraints on Bose-Einstein-Condensed Scalar Field Dark Matter.” In: *Phys. Rev. D* 89.8 (2014), p. 083536. DOI: 10.1103/PhysRevD.89.083536. arXiv: 1310.6061 [astro-ph.CO].
- [23]Abril Suárez and Pierre-Henri Chavanis. “Hydrodynamic representation of the Klein-Gordon-Einstein equations in the weak field limit: General formalism and perturbations analysis.” In: 92.2, 023510 (July 2015), p. 023510. DOI: 10.1103/PhysRevD.92.023510. arXiv: 1503.07437 [gr-qc].

- [24]F. Siddhartha Guzmán. “Accretion disk onto boson stars: A way to supplant black hole candidates.” In: *Phys. Rev. D* 73 (2 Jan. 2006), p. 021501. DOI: 10.1103/PhysRevD.73.021501. URL: <https://link.aps.org/doi/10.1103/PhysRevD.73.021501>.
- [25]Pierre-Henri Chavanis and Tiberiu Harko. “Bose-Einstein condensate general relativistic stars.” In: *Phys. Rev. D* 86 (6 Sept. 2012), p. 064011. DOI: 10.1103/PhysRevD.86.064011. URL: <https://link.aps.org/doi/10.1103/PhysRevD.86.064011>.
- [26]Abril Suárez and Pierre-Henri Chavanis. “Cosmological evolution of a complex scalar field with repulsive or attractive self-interaction.” In: *Phys. Rev. D* 95.6 (2017), p. 063515. DOI: 10.1103/PhysRevD.95.063515. arXiv: 1608.08624 [gr-qc].
- [27]T. Barreiro, E. J. Copeland, and N. J. Nunes. “Quintessence arising from exponential potentials.” In: *Phys. Rev. D* 61 (12 May 2000), p. 127301. DOI: 10.1103/PhysRevD.61.127301. URL: <https://link.aps.org/doi/10.1103/PhysRevD.61.127301>.
- [28]Juan Magana and Tonatiuh Matos. “A brief Review of the Scalar Field Dark Matter model.” In: *J. Phys. Conf. Ser.* 378 (2012). Ed. by Juan Barranco et al., p. 012012. DOI: 10.1088/1742-6596/378/1/012012. arXiv: 1201.6107 [astro-ph.CO].
- [29]Tonatiuh Matos, Alberto Vázquez-González, and Juan Magaña. “2 as dark matter.” In: *Monthly Notices of the Royal Astronomical Society* 393.4 (Feb. 2009), pp. 1359–1369. ISSN: 0035-8711. DOI: 10.1111/j.1365-2966.2008.13957.x. eprint: <https://academic.oup.com/mnras/article-pdf/393/4/1359/3249700/mnras0393-1359.pdf>. URL: <https://doi.org/10.1111/j.1365-2966.2008.13957.x>.
- [30]Sander M. Vermeulen et al. “Direct limits for scalar field dark matter from a gravitational-wave detector.” In: 600.7889 (Dec. 2021), pp. 424–428. DOI: 10.1038/s41586-021-04031-y. arXiv: 2103.03783 [gr-qc].
- [31]Hector Olivares et al. “How to tell an accreting boson star from a black hole.” In: 497.1 (Sept. 2020), pp. 521–535. DOI: 10.1093/mnras/staa1878. arXiv: 1809.08682 [gr-qc].
- [32]Gianfranco Bertone and Dan Hooper. “History of dark matter.” In: *Reviews of Modern Physics* 90.4, 045002 (Oct. 2018), p. 045002. DOI: 10.1103/RevModPhys.90.045002. arXiv: 1605.04909 [astro-ph.CO].
- [33]Andrey V. Kravtsov, Oleg Y. Gnedin, and Anatoly A. Klypin. “The Tumultuous Lives of Galactic Dwarfs and the Missing Satellites Problem.” In: 609.2 (July 2004), pp. 482–497. DOI: 10.1086/421322. arXiv: astro-ph/0401088 [astro-ph].
- [34]Charlie Conroy, Risa H. Wechsler, and Andrey V. Kravtsov. “Modeling Luminosity-dependent Galaxy Clustering through Cosmic Time.” In: *The Astrophysical Journal* 647.1 (Aug. 2006), pp. 201–214. DOI: 10.1086/503602. URL: <https://doi.org/10.1086/503602>.
- [35]N. Aghanim et al. “Planck 2018 results. VI. Cosmological parameters.” In: *Astron. Astrophys.* 641 (2020). [Erratum: *Astron. Astrophys.* 652, C4 (2021)], A6. DOI: 10.1051/0004-6361/201833910. arXiv: 1807.06209 [astro-ph.CO].

- [36] Scott Dodelson. *Modern Cosmology*. Amsterdam: Academic Press, 2003. ISBN: 978-0-12-219141-1.
- [37] R. Bernabei et al. “Final model independent result of DAMA/LIBRA-phase1.” In: *Eur. Phys. J. C* 73 (2013), p. 2648. DOI: 10.1140/epjc/s10052-013-2648-7. arXiv: 1308.5109 [astro-ph.GA].
- [38] Thibault BoissiereDede Boissiere. “Low mass WIMP search with EDELWEISS-III: First Results.” In: *arXiv e-prints*, arXiv:1504.00820 (Apr. 2015), arXiv:1504.00820. arXiv: 1504.00820 [astro-ph.CO].
- [39] G. Angloher et al. “Results on light dark matter particles with a low-threshold CRESST-II detector.” In: *Eur. Phys. J. C* 76.1 (2016), p. 25. DOI: 10.1140/epjc/s10052-016-3877-3. arXiv: 1509.01515 [astro-ph.CO].
- [40] Xiangyi Cui et al. “Dark Matter Results From 54-Ton-Day Exposure of PandaX-II Experiment.” In: *Phys. Rev. Lett.* 119.18 (2017), p. 181302. DOI: 10.1103/PhysRevLett.119.181302. arXiv: 1708.06917 [astro-ph.CO].
- [41] Matthias Danninger. “Searches for Dark Matter Annihilations in the Sun with IceCube and DeepCore in the 79-string configuration.” In: *International Cosmic Ray Conference*. Vol. 5. International Cosmic Ray Conference. Jan. 2011, p. 141. DOI: 10.7529/ICRC2011/V05/0292.
- [42] M. Ackermann et al. “Limits on Dark Matter Annihilation Signals from the Fermi LAT 4-year Measurement of the Isotropic Gamma-Ray Background.” In: *JCAP* 09 (2015), p. 008. DOI: 10.1088/1475-7516/2015/09/008. arXiv: 1501.05464 [astro-ph.CO].
- [43] Q. Yan et al. “Measurements of nuclear interaction cross sections with the Alpha Magnetic Spectrometer on the International Space Station.” In: *Nuclear Physics A* 996 (2020), p. 121712. ISSN: 0375-9474. DOI: <https://doi.org/10.1016/j.nuclphysa.2020.121712>. URL: <http://www.sciencedirect.com/science/article/pii/S0375947420300221>.
- [44] Tonatiuh Matos and Francisco Siddhartha Guzman. “Scalar fields as dark matter in spiral galaxies.” In: *Class. Quant. Grav.* 17 (2000), pp. L9–L16. DOI: 10.1088/0264-9381/17/1/102. arXiv: gr-qc/9810028.
- [45] Lam Hui et al. “Ultralight scalars as cosmological dark matter.” In: *Phys. Rev. D* 95.4 (2017), p. 043541. DOI: 10.1103/PhysRevD.95.043541. arXiv: 1610.08297 [astro-ph.CO].
- [46] Abril Suárez, Victor H. Robles, and Tonatiuh Matos. “A Review on the Scalar Field/Bose-Einstein Condensate Dark Matter Model.” In: *Astrophys. Space Sci. Proc.* 38 (2014). Ed. by Claudia Moreno González, José Edgar Madriz Aguilar, and Luz Marina Reyes Barrera, pp. 107–142. DOI: 10.1007/978-3-319-02063-1_9. arXiv: 1302.0903 [astro-ph.CO].
- [47] Wayne Hu, Rennan Barkana, and Andrei Gruzinov. “Fuzzy Cold Dark Matter: The Wave Properties of Ultralight Particles.” In: 85.6 (Aug. 2000), pp. 1158–1161. DOI: 10.1103/PhysRevLett.85.1158. arXiv: astro-ph/0003365 [astro-ph].

- [48]R. Murgia et al. “Non-cold dark matter at small scales: a general approach.” In: Journal of Cosmology and Astroparticle Physics 2017.11 (Nov. 2017), pp. 046–046. DOI: 10.1088/1475-7516/2017/11/046. URL: <https://doi.org/10.1088/1475-7516/2017/11/046>.
- [49]Hsi-Yu Schive, Tzihong Chiueh, and Tom Broadhurst. “Cosmic Structure as the Quantum Interference of a Coherent Dark Wave.” In: Nature Phys. 10 (2014), pp. 496–499. DOI: 10.1038/nphys2996. arXiv: 1406.6586 [astro-ph.GA].
- [50]Philip Mocz et al. “Galaxy formation with BECDM II. Cosmic filaments and first galaxies.” In: Mon. Not. Roy. Astron. Soc. 494.2 (2020), pp. 2027–2044. DOI: 10.1093/mnras/staa738. arXiv: 1911.05746 [astro-ph.CO].
- [51]J. A. R. Cembranos, A. L. Maroto, and S. J. Núñez Jareño. “Cosmological perturbations in coherent oscillating scalar field models.” In: JHEP 03 (2016), p. 013. DOI: 10.1007/JHEP03(2016)013. arXiv: 1509.08819 [astro-ph.CO].
- [52]Luca Amendola. “Perturbations in a coupled scalar field cosmology.” In: Mon. Not. Roy. Astron. Soc. 312 (2000), p. 521. DOI: 10.1046/j.1365-8711.2000.03165.x. arXiv: astro-ph/9906073.
- [53]Argelia Bernal, Tonatiuh Matos, and Daro Nunez. “Flat central density profiles from scalar field dark matter halo.” In: Rev. Mex. A. A. 44 (2008), p. 149. arXiv: 0303455 [astro-ph].
- [54]José M. Torres et al. “Cosmological nonlinear structure formation in full general relativity.” In: Phys. Rev. D 90.12 (2014), p. 123002. DOI: 10.1103/PhysRevD.90.123002. arXiv: 1409.7953 [gr-qc].
- [55]Miguel Alcubierre et al. “Numerical studies of Φ^2 oscillatons.” In: Class. Quant. Grav. 20 (2003), pp. 2883–2904. DOI: 10.1088/0264-9381/20/13/332. arXiv: gr-qc/0301105.
- [56]P. A. Zyla et al. “Review of Particle Physics.” In: PTEP 2020.8 (2020), p. 083C01. DOI: 10.1093/ptep/ptaa104.
- [57]C. Espinoza et al. “The S_3 Symmetric Model with a Dark Scalar.” In: Phys. Lett. B 788 (2019), pp. 185–191. DOI: 10.1016/j.physletb.2018.11.028. arXiv: 1804.01879 [hep-ph].
- [58]R. Ballou et al. “New exclusion limits on scalar and pseudoscalar axionlike particles from light shining through a wall.” In: Phys. Rev. D 92.9 (2015), p. 092002. DOI: 10.1103/PhysRevD.92.092002. arXiv: 1506.08082 [hep-ex].
- [59]Klaus Ehret et al. “New ALPS Results on Hidden-Sector Lightweights.” In: Phys. Lett. B 689 (2010), pp. 149–155. DOI: 10.1016/j.physletb.2010.04.066. arXiv: 1004.1313 [hep-ex].
- [60]Peter Athron et al. “Global analyses of Higgs portal singlet dark matter models using GAMBIT.” In: Eur. Phys. J. C 79.1 (2019), p. 38. DOI: 10.1140/epjc/s10052-018-6513-6. arXiv: 1808.10465 [hep-ph].

- [61]Tomohiro Abe et al. “LHC Dark Matter Working Group: Next-generation spin-0 dark matter models.” In: Phys. Dark Univ. 27 (2020), p. 100351. DOI: 10.1016/j.dark.2019.100351. arXiv: 1810.09420 [hep-ex].
- [62]Peter W. Graham and Surjeet Rajendran. “New Observables for Direct Detection of Axion Dark Matter.” In: Phys. Rev. D 88 (2013), p. 035023. DOI: 10.1103/PhysRevD.88.035023. arXiv: 1306.6088 [hep-ph].
- [63]Cecile Robilliard et al. “No light shining through a wall.” In: Phys. Rev. Lett. 99 (2007), p. 190403. DOI: 10.1103/PhysRevLett.99.190403. arXiv: 0707.1296 [hep-ex].
- [64]R. Cameron et al. “Search for nearly massless, weakly coupled particles by optical techniques.” In: Phys. Rev. D 47 (1993), pp. 3707–3725. DOI: 10.1103/PhysRevD.47.3707.
- [65]Aaron S. Chou et al. “Search for axion-like particles using a variable baseline photon regeneration technique.” In: Phys. Rev. Lett. 100 (2008), p. 080402. DOI: 10.1103/PhysRevLett.100.080402. arXiv: 0710.3783 [hep-ex].
- [66]Pierre Pugnât et al. “First results from the OSQAR photon regeneration experiment: No light shining through a wall.” In: Phys. Rev. D 78 (2008), p. 092003. DOI: 10.1103/PhysRevD.78.092003. arXiv: 0712.3362 [hep-ex].
- [67]E. Zavattini et al. “New PVLAS results and limits on magnetically induced optical rotation and ellipticity in vacuum.” In: Phys. Rev. D 77 (2008), p. 032006. DOI: 10.1103/PhysRevD.77.032006. arXiv: 0706.3419 [hep-ex].
- [68]David J. E. Marsh. “Axion Cosmology.” In: Phys. Rept. 643 (2016), pp. 1–79. DOI: 10.1016/j.physrep.2016.06.005. arXiv: 1510.07633 [astro-ph.CO].
- [69]Eleonora Di Valentino et al. “Snowmass2021 - Letter of interest cosmology intertwined II: The hubble constant tension.” In: Astropart. Phys. 131 (2021), p. 102605. DOI: 10.1016/j.astropartphys.2021.102605. arXiv: 2008.11284 [astro-ph.CO].
- [70]Y. Akrami et al. “Planck 2018 results. VII. Isotropy and Statistics of the CMB.” In: Astron. Astrophys. 641 (2020), A7. DOI: 10.1051/0004-6361/201935201. arXiv: 1906.02552 [astro-ph.CO].
- [71]N. Aghanim et al. “Planck 2018 results. VIII. Gravitational lensing.” In: Astron. Astrophys. 641 (2020), A8. DOI: 10.1051/0004-6361/201833886. arXiv: 1807.06210 [astro-ph.CO].
- [72]Laura Lopez Honorez et al. “The Inert Doublet Model: An Archetype for Dark Matter.” In: JCAP 02 (2007), p. 028. DOI: 10.1088/1475-7516/2007/02/028. arXiv: hep-ph/0612275.
- [73]Qing-Hong Cao, Ernest Ma, and G. Rajasekaran. “Observing the Dark Scalar Doublet and its Impact on the Standard-Model Higgs Boson at Colliders.” In: Phys. Rev. D 76 (2007), p. 095011. DOI: 10.1103/PhysRevD.76.095011. arXiv: 0708.2939 [hep-ph].

- [74]Debasish Majumdar and Ambar Ghosal. “Dark Matter candidate in a Heavy Higgs Model - Direct Detection Rates.” In: Mod. Phys. Lett. A 23 (2008), pp. 2011–2022. DOI: 10.1142/S0217732308025954. arXiv: hep-ph/0607067.
- [75]Francesca Chadha-Day, John Ellis, and David J. E. Marsh. Axion Dark Matter: What is it and Why Now? 2021. arXiv: 2105.01406 [hep-ph].
- [76]R. D. Peccei and Helen R. Quinn. “CP Conservation in the Presence of Instantons.” In: Phys. Rev. Lett. 38 (1977), pp. 1440–1443. DOI: 10.1103/PhysRevLett.38.1440.
- [77]Steven Weinberg. “A New Light Boson?” In: Phys. Rev. Lett. 40 (1978), pp. 223–226. DOI: 10.1103/PhysRevLett.40.223.
- [78]Frank Wilczek. “Problem of Strong P and T Invariance in the Presence of Instantons.” In: Phys. Rev. Lett. 40 (1978), pp. 279–282. DOI: 10.1103/PhysRevLett.40.279.
- [79]Paul Langacker. The standard model and beyond. 2010. ISBN: 978-1-4200-7906-7.
- [80]P. Sikivie. “Of Axions, Domain Walls and the Early Universe.” In: Phys. Rev. Lett. 48 (1982), pp. 1156–1159. DOI: 10.1103/PhysRevLett.48.1156.
- [81]Pierre Sikivie. “Axion Cosmology.” In: Lect. Notes Phys. 741 (2008). Ed. by Markus Kuster, Georg Raffelt, and Berta Beltran, pp. 19–50. DOI: 10.1007/978-3-540-73518-2_2. arXiv: astro-ph/0610440.
- [82]P. Sikivie. “Experimental Tests of the Invisible Axion.” In: Phys. Rev. Lett. 51 (1983). Ed. by M. A. Srednicki. [Erratum: Phys.Rev.Lett. 52, 695 (1984)], pp. 1415–1417. DOI: 10.1103/PhysRevLett.51.1415.
- [83]Mathilde Fouche et al. “Search for photon oscillations into massive particles.” In: Phys. Rev. D 78 (2008), p. 032013. DOI: 10.1103/PhysRevD.78.032013. arXiv: 0808.2800 [hep-ex].
- [84]A. Afanasev et al. “New Experimental limit on Optical Photon Coupling to Neutral, Scalar Bosons.” In: Phys. Rev. Lett. 101 (2008), p. 120401. DOI: 10.1103/PhysRevLett.101.120401. arXiv: 0806.2631 [hep-ex].
- [85]Maurizio Giannotti et al. “Cool WISPs for stellar cooling excesses.” In: JCAP 05 (2016), p. 057. DOI: 10.1088/1475-7516/2016/05/057. arXiv: 1512.08108 [astro-ph.HE].
- [86]Maurizio Giannotti. “ALP hints from cooling anomalies.” In: 2015, pp. 26–30. DOI: 10.3204/DESY-PROC-2015-02/giannotti_maurizio. arXiv: 1508.07576 [astro-ph.HE].
- [87]Maurizio Giannotti et al. “Stellar Recipes for Axion Hunters.” In: JCAP 10 (2017), p. 010. DOI: 10.1088/1475-7516/2017/10/010. arXiv: 1708.02111 [hep-ph].
- [88]Alessandro De Angelis, Marco Roncadelli, and Oriana Mansutti. “Evidence for a new light spin-zero boson from cosmological gamma-ray propagation?” In: Phys. Rev. D 76 (2007), p. 121301. DOI: 10.1103/PhysRevD.76.121301. arXiv: 0707.4312 [astro-ph].

- [89]D. Horns and M. Meyer. “Indications for a pair-production anomaly from the propagation of VHE gamma-rays.” In: JCAP 02 (2012), p. 033. DOI: 10.1088/1475-7516/2012/02/033. arXiv: 1201.4711 [astro-ph.CO].
- [90]Stephen F. King and Christoph Luhn. “Neutrino Mass and Mixing with Discrete Symmetry.” In: Rept. Prog. Phys. 76 (2013), p. 056201. DOI: 10.1088/0034-4885/76/5/056201. arXiv: 1301.1340 [hep-ph].
- [91]G. C. Branco et al. “Theory and phenomenology of two-Higgs-doublet models.” In: Phys. Rept. 516 (2012), pp. 1–102. DOI: 10.1016/j.physrep.2012.02.002. arXiv: 1106.0034 [hep-ph].
- [92]Igor P. Ivanov. “Building and testing models with extended Higgs sectors.” In: Prog. Part. Nucl. Phys. 95 (2017), pp. 160–208. DOI: 10.1016/j.pnpnp.2017.03.001. arXiv: 1702.03776 [hep-ph].
- [93]Giorgio Arcadi. “2HDM portal for Singlet-Doublet Dark Matter.” In: Eur. Phys. J. C 78.10 (2018), p. 864. DOI: 10.1140/epjc/s10052-018-6327-6. arXiv: 1804.04930 [hep-ph].
- [94]J. Iliopoulos, C. Itzykson, and Andre Martin. “Functional Methods and Perturbation Theory.” In: Rev. Mod. Phys. 47 (1975), p. 165. DOI: 10.1103/RevModPhys.47.165.
- [95]R. Jackiw. “Functional evaluation of the effective potential.” In: Phys. Rev. D 9 (1974), p. 1686. DOI: 10.1103/PhysRevD.9.1686.
- [96]Steven L. Liebling and Carlos Palenzuela. “Dynamical Boson Stars.” In: Living Rev. Rel. 15 (2012). [Living Rev. Rel.20,no.1,5(2017)], p. 6. DOI: 10.12942/lrr-2012-6, 10.1007/s41114-017-0007-y. arXiv: 1202.5809 [gr-qc].
- [97]E. Seidel and W. M. Suen. “Oscillating soliton stars.” In: Phys. Rev. Lett. 66 (1991), pp. 1659–1662. DOI: 10.1103/PhysRevLett.66.1659.
- [98]Hong Zhang. “Axion Stars.” In: Symmetry 12.1 (2019), p. 25. DOI: 10.3390/sym12010025. arXiv: 1810.11473 [hep-ph].
- [99]Francisco X. Linares Cedeño, Alma X. González-Morales, and L. Arturo Ureña-López. “Ultralight DM bosons with an axion-like potential: scale-dependent constraints revisited.” In: JCAP 01 (2021), p. 051. DOI: 10.1088/1475-7516/2021/01/051. arXiv: 2006.05037 [astro-ph.CO].
- [100]J. Barranco and A. Bernal. “Self-gravitating system made of axions.” In: Phys. Rev. D 83 (2011), p. 043525. DOI: 10.1103/PhysRevD.83.043525. arXiv: 1001.1769 [astro-ph.CO].
- [101]Abbas I. Abdel Karim. “The Stability of the Fourth Order Runge-Kutta Method for the Solution of Systems of Differential Equations.” In: Commun. ACM 9.2 (Feb. 1966), pp. 113–116. ISSN: 0001-0782. DOI: 10.1145/365170.365213. URL: <https://doi.org/10.1145/365170.365213>.

- [102]Celia Escamilla-Rivera, Jackson Levi Said, and Jurgen Mifsud. “Performance of non-parametric reconstruction techniques in the late-time universe.” In: 2021.10, 016 (Oct. 2021), p. 016. DOI: 10.1088/1475-7516/2021/10/016. arXiv: 2105.14332 [astro-ph.CO].
- [103]Adam G. Riess et al. “Large Magellanic Cloud Cepheid Standards Provide a 1% Foundation for the Determination of the Hubble Constant and Stronger Evidence for Physics beyond Λ CDM.” In: *Astrophys. J.* 876.1 (2019), p. 85. DOI: 10.3847/1538-4357/ab1422. arXiv: 1903.07603 [astro-ph.CO].
- [104]Gianpiero Mangano et al. “Relic neutrino decoupling including flavor oscillations.” In: *Nucl. Phys. B* 729 (2005), pp. 221–234. DOI: 10.1016/j.nuclphysb.2005.09.041. arXiv: hep-ph/0506164.
- [105]Max Pettini and Ryan Cooke. “A new, precise measurement of the primordial abundance of Deuterium.” In: *Mon. Not. Roy. Astron. Soc.* 425 (2012), pp. 2477–2486. DOI: 10.1111/j.1365-2966.2012.21665.x. arXiv: 1205.3785 [astro-ph.CO].
- [106]Y. I. Izotov, G. Stasinska, and N. G. Guseva. “Primordial ^4He abundance: a determination based on the largest sample of HII regions with a methodology tested on model HII regions.” In: *Astron. Astrophys.* 558 (2013), A57. DOI: 10.1051/0004-6361/201220782. arXiv: 1308.2100 [astro-ph.CO].
- [107]Gary Steigman. “Neutrinos And Big Bang Nucleosynthesis.” In: *Adv. High Energy Phys.* 2012 (2012), p. 268321. DOI: 10.1155/2012/268321. arXiv: 1208.0032 [hep-ph].
- [108]Kenneth M. Nollett and Gary Steigman. “BBN And The CMB Constrain Neutrino Coupled Light WIMPs.” In: *Phys. Rev. D* 91.8 (2015), p. 083505. DOI: 10.1103/PhysRevD.91.083505. arXiv: 1411.6005 [astro-ph.CO].
- [109]Bohua Li, Paul R. Shapiro, and Tanja Rindler-Daller. “Bose-Einstein-condensed scalar field dark matter and the gravitational wave background from inflation: new cosmological constraints and its detectability by LIGO.” In: *Phys. Rev. D* 96.6 (2017), p. 063505. DOI: 10.1103/PhysRevD.96.063505. arXiv: 1611.07961 [astro-ph.CO].
- [110]Juan Barranco et al. “Schwarzschild black holes can wear scalar wigs.” In: *Phys. Rev. Lett.* 109 (2012), p. 081102. DOI: 10.1103/PhysRevLett.109.081102. arXiv: 1207.2153 [gr-qc].
- [111]Darío Núñez. “Discussion on dark matter nature.” In: *AIP Conf. Proc.* 1577.1 (2014), p. 208. DOI: 10.1063/1.4861956. arXiv: 1703.03286 [gr-qc].
- [112]Anatoly Klypin et al. “Where Are the Missing Galactic Satellites?” In: 522.1 (Sept. 1999), pp. 82–92. DOI: 10.1086/307643. arXiv: astro-ph/9901240 [astro-ph].
- [113]W. J. G. de Blok et al. “Mass Density Profiles of Low Surface Brightness Galaxies.” In: *The Astrophysical Journal* 552.1 (May 2001), pp. L23–L26. DOI: 10.1086/320262. URL: <https://doi.org/10.1086/320262>.

- [114]Michael Boylan-Kolchin, James S. Bullock, and Manoj Kaplinghat. “Too big to fail? The puzzling darkness of massive Milky Way subhaloes.” In: 415.1 (July 2011), pp. L40–L44. DOI: 10.1111/j.1745-3933.2011.01074.x. arXiv: 1103.0007 [astro-ph.CO].
- [115]Neil G. Ibata et al. “Velocity anti-correlation of diametrically opposed galaxy satellites in the low-redshift Universe.” In: 511.7511 (July 2014), pp. 563–566. DOI: 10.1038/nature13481. arXiv: 1407.8178 [astro-ph.GA].
- [116]Marcel S. Pawlowski et al. “Co-orbiting satellite galaxy structures are still in conflict with the distribution of primordial dwarf galaxies.” In: 442.3 (Aug. 2014), pp. 2362–2380. DOI: 10.1093/mnras/stu1005. arXiv: 1406.1799 [astro-ph.GA].
- [117]Takashi Okamoto, Liang Gao, and Tom Theuns. “Mass loss of galaxies due to an ultraviolet background.” In: 390.3 (Nov. 2008), pp. 920–928. DOI: 10.1111/j.1365-2966.2008.13830.x. arXiv: 0806.0378 [astro-ph].
- [118]A. J. Benson et al. “The effects of photoionization on galaxy formation - II. Satellite galaxies in the Local Group.” In: 333.1 (June 2002), pp. 177–190. DOI: 10.1046/j.1365-8711.2002.05388.x. arXiv: astro-ph/0108218 [astro-ph].
- [119]A. J. Benson et al. “The effects of photoionization on galaxy formation - I. Model and results at $z=0$.” In: 333.1 (June 2002), pp. 156–176. DOI: 10.1046/j.1365-8711.2002.05387.x. arXiv: astro-ph/0108217 [astro-ph].
- [120]Till Sawala et al. “The APOSTLE simulations: solutions to the Local Group’s cosmic puzzles.” In: 457.2 (Apr. 2016), pp. 1931–1943. DOI: 10.1093/mnras/stw145. arXiv: 1511.01098 [astro-ph.GA].
- [121]Kyle A. Oman et al. “Non-circular motions and the diversity of dwarf galaxy rotation curves.” In: 482.1 (Jan. 2019), pp. 821–847. DOI: 10.1093/mnras/sty2687. arXiv: 1706.07478 [astro-ph.GA].
- [122]Charlie Conroy, Risa H. Wechsler, and Andrey V. Kravtsov. “Modeling Luminosity-dependent Galaxy Clustering through Cosmic Time.” In: 647.1 (Aug. 2006), pp. 201–214. DOI: 10.1086/503602. arXiv: astro-ph/0512234 [astro-ph].
- [123]Peter S. Behroozi, Charlie Conroy, and Risa H. Wechsler. “A Comprehensive Analysis of Uncertainties Affecting the Stellar Mass-Halo Mass Relation for $0 < z < 4$.” In: 717.1 (July 2010), pp. 379–403. DOI: 10.1088/0004-637X/717/1/379. arXiv: 1001.0015 [astro-ph.CO].
- [124]Peter S. Behroozi, Risa H. Wechsler, and Charlie Conroy. “The Average Star Formation Histories of Galaxies in Dark Matter Halos from $z = 0-8$.” In: 770.1, 57 (June 2013), p. 57. DOI: 10.1088/0004-637X/770/1/57. arXiv: 1207.6105 [astro-ph.CO].
- [125]Aldo Rodriguez-Puebla et al. “Constraining the galaxy-halo connection over the last 13.3 Gyr: star formation histories, galaxy mergers and structural properties.” In: 470.1 (Sept. 2017), pp. 651–687. DOI: 10.1093/mnras/stx1172. arXiv: 1703.04542 [astro-ph.GA].

- [126]Risa H. Wechsler and Jeremy L. Tinker. “The Connection Between Galaxies and Their Dark Matter Halos.” In: 56 (Sept. 2018), pp. 435–487. DOI: 10.1146/annurev-astro-081817-051756. arXiv: 1804.03097 [astro-ph.GA].
- [127]Till Sawala et al. “The APOSTLE simulations: solutions to the Local Group’s cosmic puzzles.” In: Monthly Notices of the Royal Astronomical Society 457.2 (Feb. 2016), pp. 1931–1943. ISSN: 0035-8711. DOI: 10.1093/mnras/stw145. eprint: <https://academic.oup.com/mnras/article-pdf/457/2/1931/2930798/stw145.pdf>. URL: <https://doi.org/10.1093/mnras/stw145>.
- [128]Houjun Mo, Frank C. van den Bosch, and Simon White. Galaxy Formation and Evolution. 2010.
- [129]Till Sawala et al. “Bent by baryons: the low-mass galaxy-halo relation.” In: 448.3 (Apr. 2015), pp. 2941–2947. DOI: 10.1093/mnras/stu2753. arXiv: 1404.3724 [astro-ph.GA].
- [130]Ismael Ferrero et al. “The dark matter haloes of dwarf galaxies: a challenge for the Λ cold dark matter paradigm?” In: 425.4 (Oct. 2012), pp. 2817–2823. DOI: 10.1111/j.1365-2966.2012.21623.x. arXiv: 1111.6609 [astro-ph.CO].
- [131]Till Sawala et al. “The abundance of (not just) dark matter haloes.” In: Monthly Notices of the Royal Astronomical Society 431.2 (Mar. 2013), pp. 1366–1382. ISSN: 0035-8711. DOI: 10.1093/mnras/stt259. eprint: <https://academic.oup.com/mnras/article-pdf/431/2/1366/4258466/stt259.pdf>. URL: <https://doi.org/10.1093/mnras/stt259>.
- [132]Elcio Abdalla et al. “Cosmology intertwined: A review of the particle physics, astrophysics, and cosmology associated with the cosmological tensions and anomalies.” In: JHEAp 34 (2022), pp. 49–211. DOI: 10.1016/j.jheap.2022.04.002. arXiv: 2203.06142 [astro-ph.CO].
- [133]Matthias Hoelt et al. “Dwarf galaxies in voids: suppressing star formation with photoheating.” In: 371.1 (Sept. 2006), pp. 401–414. DOI: 10.1111/j.1365-2966.2006.10678.x. arXiv: astro-ph/0501304 [astro-ph].
- [134]Konstantinos Tassis et al. “Numerical Simulations of High-Redshift Star Formation in Dwarf Galaxies.” In: 587.1 (Apr. 2003), pp. 13–24. DOI: 10.1086/368148. arXiv: astro-ph/0212457 [astro-ph].
- [135]Nickolay Y. Gnedin. “Effect of Reionization on Structure Formation in the Universe.” In: 542.2 (Oct. 2000), pp. 535–541. DOI: 10.1086/317042. arXiv: astro-ph/0002151 [astro-ph].
- [136]Greg L. Bryan and Michael L. Norman. “Statistical Properties of X-Ray Clusters: Analytic and Numerical Comparisons.” In: 495.1 (Mar. 1998), pp. 80–99. DOI: 10.1086/305262. arXiv: astro-ph/9710107 [astro-ph].

- [137]I. K. Baldry et al. “Galaxy And Mass Assembly (GAMA): the galaxy stellar mass function at $z < 0.06$.” In: *Monthly Notices of the Royal Astronomical Society* 421.1 (2012), pp. 621–634. DOI: 10.1111/j.1365-2966.2012.20340.x. eprint: <https://onlinelibrary.wiley.com/doi/pdf/10.1111/j.1365-2966.2012.20340.x>. URL: <https://onlinelibrary.wiley.com/doi/abs/10.1111/j.1365-2966.2012.20340.x>.
- [138]Aldo Rodriguez-Puebla et al. “The Star-forming Main Sequence and the Contribution of Dust-obscured Star Formation since $z \sim 4$ from the Far-UV+IR Luminosity Functions.” In: 905.2, 171 (Dec. 2020), p. 171. DOI: 10.3847/1538-4357/abc7c2. arXiv: 2008.06514 [astro-ph.GA].
- [139]Johannes König, Alexander Merle, and Maximilian Totzauer. “keV sterile neutrino dark matter from singlet scalar decays: the most general case.” In: 2016.11, 038 (Nov. 2016), p. 038. DOI: 10.1088/1475-7516/2016/11/038. arXiv: 1609.01289 [hep-ph].
- [140]Aurel Schneider. “Astrophysical constraints on resonantly produced sterile neutrino dark matter.” In: 2016.4, 059 (Apr. 2016), p. 059. DOI: 10.1088/1475-7516/2016/04/059. arXiv: 1601.07553 [astro-ph.CO].
- [141]Alexander Merle. “keV sterile neutrino Dark Matter.” In: *arXiv e-prints*, arXiv:1702.08430 (Feb. 2017), arXiv:1702.08430. arXiv: 1702.08430 [hep-ph].
- [142]Vid Iri et al. “First Constraints on Fuzzy Dark Matter from Lyman- α Forest Data and Hydrodynamical Simulations.” In: 119.3, 031302 (July 2017), p. 031302. DOI: 10.1103/PhysRevLett.119.031302. arXiv: 1703.04683 [astro-ph.CO].
- [143]Shi Xiangdong and G. M. Fuller. “New dark matter candidate: nonthermal sterile neutrinos.” In: 82.14 (Apr. 1999), pp. 2832–2835.
- [144]Tejaswi Venumadhav et al. “Sterile neutrino dark matter: Weak interactions in the strong coupling epoch.” In: 94.4, 043515 (Aug. 2016), p. 043515. DOI: 10.1103/PhysRevD.94.043515. arXiv: 1507.06655 [astro-ph.CO].
- [145]Alexander Merle and Maximilian Totzauer. “keV sterile neutrino dark matter from singlet scalar decays: basic concepts and subtle features.” In: 2015.6, 011 (June 2015), p. 011. DOI: 10.1088/1475-7516/2015/06/011. arXiv: 1502.01011 [hep-ph].
- [146]Tanja Rindler-Daller and Paul R. Shapiro. “Complex Scalar Field Dark Matter on Galactic Scales.” In: *Modern Physics Letters A* 29.2, 1430002 (Jan. 2014), p. 1430002. DOI: 10.1142/S021773231430002X. arXiv: 1312.1734 [astro-ph.CO].
- [147]Francis-Yan Cyr-Racine et al. “ETHOSan effective theory of structure formation: From dark particle physics to the matter distribution of the Universe.” In: 93.12, 123527 (June 2016), p. 123527. DOI: 10.1103/PhysRevD.93.123527. arXiv: 1512.05344 [astro-ph.CO].
- [148]Mark R. Lovell. “Toward a General Parameterization of the Warm Dark Matter Halo Mass Function.” In: 897.2, 147 (July 2020), p. 147. DOI: 10.3847/1538-4357/ab982a. arXiv: 2003.01125 [astro-ph.CO].

- [149] Aurel Schneider et al. “Non-linear evolution of cosmological structures in warm dark matter models.” In: 424.1 (July 2012), pp. 684–698. DOI: 10.1111/j.1365-2966.2012.21252.x. arXiv: 1112.0330 [astro-ph.CO].
- [150] A. Rodríguez-Puebla, V. Avila-Reese, and N. Drory. “The Galaxy-Halo/Subhalo Connection: Mass Relations and Implications for Some Satellite Occupational Distributions.” In: 767.1, 92 (Apr. 2013), p. 92. DOI: 10.1088/0004-637X/767/1/92. arXiv: 1302.0005 [astro-ph.CO].
- [151] L. Y. Aaron Yung et al. “Semi-analytic forecasts for JWST - I. UV luminosity functions at $z = 4-10$.” In: 483.3 (Mar. 2019), pp. 2983–3006. DOI: 10.1093/mnras/sty3241. arXiv: 1803.09761 [astro-ph.GA].
- [152] JWST User Documentation. <https://jwst-docs.stsci.edu/>. Accessed: 2022-05-25.
- [153] Gabriel B. Brammer et al. “THE NUMBER DENSITY AND MASS DENSITY OF STAR-FORMING AND QUIESCENT GALAXIES AT $0.4 < z < 2.2$.” In: *The Astrophysical Journal* 739.1 (Aug. 2011), p. 24. DOI: 10.1088/0004-637x/739/1/24. URL: <https://doi.org/10.1088/0004-637x/739/1/24>.
- [154] Adam Muzzin et al. “THE EVOLUTION OF THE STELLAR MASS FUNCTIONS OF STAR-FORMING AND QUIESCENT GALAXIES TO $z = 4$ FROM THE COSMOS/ULTRAVISTA SURVEY.” In: *The Astrophysical Journal* 777.1 (Oct. 2013), p. 18. DOI: 10.1088/0004-637x/777/1/18. URL: <https://doi.org/10.1088/0004-637x/777/1/18>.
- [155] O. Ilbert et al. “Mass assembly in quiescent and star-forming galaxies since $z = 4$ from UltraVISTA.” In: 556, A55 (Aug. 2013), A55. DOI: 10.1051/0004-6361/201321100. arXiv: 1301.3157 [astro-ph.CO].
- [156] Adam R. Tomczak et al. “GALAXY STELLAR MASS FUNCTIONS FROM ZFOURGE/CANDELS: AN EXCESS OF LOW-MASS GALAXIES SINCE $z = 2$ AND THE RAPID BUILDUP OF QUIESCENT GALAXIES.” In: *The Astrophysical Journal* 783.2 (Feb. 2014), p. 85. DOI: 10.1088/0004-637x/783/2/85. URL: <https://doi.org/10.1088/0004-637x/783/2/85>.
- [157] I. Davidzon et al. “The COSMOS2015 galaxy stellar mass function . Thirteen billion years of stellar mass assembly in ten snapshots.” In: 605, A70 (Sept. 2017), A70. DOI: 10.1051/0004-6361/201730419. arXiv: 1701.02734 [astro-ph.GA].
- [158] Diana Khimey, Sownak Bose, and Sandro Tacchella. “Degeneracies between baryons and dark matter: the challenge of constraining the nature of dark matter with JWST.” In: 506.3 (Sept. 2021), pp. 4139–4150. DOI: 10.1093/mnras/stab2019. arXiv: 2010.10520 [astro-ph.GA].
- [159] Steven Weinberg. “The cosmological constant problem.” In: *Rev. Mod. Phys.* 61 (1 Jan. 1989), pp. 1–23. DOI: 10.1103/RevModPhys.61.1. URL: <https://link.aps.org/doi/10.1103/RevModPhys.61.1>.
- [160] Ivaylo Zlatev, Li-Min Wang, and Paul J. Steinhardt. “Quintessence, cosmic coincidence, and the cosmological constant.” In: *Phys. Rev. Lett.* 82 (1999), pp. 896–899. DOI: 10.1103/PhysRevLett.82.896. arXiv: astro-ph/9807002.

- [161]Raphael Bousso. “The Cosmological Constant Problem, Dark Energy, and the Landscape of String Theory.” In: [arXiv e-prints](#), arXiv:1203.0307 (Mar. 2012), arXiv:1203.0307. arXiv: 1203.0307 [astro-ph.CO].
- [162]P. J. E. Peebles. [Principles of Physical Cosmology](#). Princeton University Press, 1993.
- [163]J. P. Ostriker and Paul J. Steinhardt. “Cosmic Concordance.” In: [arXiv e-prints](#), astro-ph/9505066 (May 1995), astro-ph/9505066. arXiv: astro-ph/9505066 [astro-ph].
- [164]M. Davis and P. J. E. Peebles. “A survey of galaxy redshifts. V. The two-point position and velocity correlations.” In: [ApJ](#) 267 (Apr. 1983), pp. 465–482. DOI: 10.1086/160884.
- [165]J.P. Ostriker, P.J.E. Peebles, and A. Yahil. “The size and mass of galaxies, and the mass of the universe.” In: [Astrophys. J. Lett.](#) 193 (1974), pp. L1–L4. DOI: 10.1086/181617.
- [166]M. S. Roberts. “M 31 and a Brief History of Dark Matter.” In: [Frontiers of Astrophysics: A Celebration of NRAO’s 50th Anniversary](#). Ed. by A. H. Bridle, J. J. Condon, and G. C. Hunt. Vol. 395. Astronomical Society of the Pacific Conference Series. Aug. 2008, p. 283.
- [167]Vera C. Rubin. “One Hundred Years of Rotating Galaxies1.” In: [Publications of the Astronomical Society of the Pacific](#) 112.772 (June 2000), pp. 747–750. DOI: 10.1086/316573. URL: <https://doi.org/10.1086/316573>.
- [168]Gong-Bo Zhao et al. “Dynamical dark energy in light of the latest observations.” In: [Nature Astron.](#) 1.9 (2017), pp. 627–632. DOI: 10.1038/s41550-017-0216-z. arXiv: 1701.08165 [astro-ph.CO].
- [169]Paola Domínguez-Fernández et al. “Description of the evolution of inhomogeneities on a Dark Matter halo with the Vlasov equation.” In: [Gen. Rel. Grav.](#) 49.9 (2017), p. 123. DOI: 10.1007/s10714-017-2286-8. arXiv: 1703.03286 [gr-qc].
- [170]Adam G. Riess et al. “Observational evidence from supernovae for an accelerating universe and a cosmological constant.” In: [Astron. J.](#) 116 (1998), pp. 1009–1038. DOI: 10.1086/300499. arXiv: astro-ph/9805201.
- [171]A. Goobar et al. “The acceleration of the universe: Measurements of cosmological parameters from type Ia supernovae.” In: [Phys. Scripta T](#) 85 (2000), pp. 47–58. DOI: 10.1238/Physica.Topical.085a00047.
- [172]P.A.R. Ade et al. “Planck 2015 results. XIV. Dark energy and modified gravity.” In: [Astron. Astrophys.](#) 594 (2016), A14. DOI: 10.1051/0004-6361/201525814. arXiv: 1502.01590 [astro-ph.CO].
- [173]Eugenio Bianchi and Carlo Rovelli. “Why all these prejudices against a constant?” In: [arXiv e-prints](#), arXiv:1002.3966 (Feb. 2010), arXiv:1002.3966. arXiv: 1002.3966 [astro-ph.CO].
- [174]Timothy Clifton et al. “Modified Gravity and Cosmology.” In: [Phys. Rept.](#) 513 (2012), pp. 1–189. DOI: 10.1016/j.physrep.2012.01.001. arXiv: 1106.2476 [astro-ph.CO].

- [175] Luisa G. Jaime, Mariana Jaber, and Celia Escamilla-Rivera. “New parametrized equation of state for dark energy surveys.” In: *Phys. Rev. D* 98.8 (2018), p. 083530. DOI: 10.1103/PhysRevD.98.083530. arXiv: 1804.04284 [astro-ph.CO].
- [176] Celia Escamilla-Rivera, Maryi Alejandra Carvajal Quintero, and S. Capozziello. “A deep learning approach to cosmological dark energy models.” In: *JCAP* 03 (2020), p. 008. DOI: 10.1088/1475-7516/2020/03/008. arXiv: 1910.02788 [astro-ph.CO].
- [177] Paul J. Steinhardt, Li-Min Wang, and Ivaylo Zlatev. “Cosmological tracking solutions.” In: *Phys. Rev. D* 59 (1999), p. 123504. DOI: 10.1103/PhysRevD.59.123504. arXiv: astro-ph/9812313.
- [178] Pedro G. Ferreira and Michael Joyce. “Cosmology with a primordial scaling field.” In: *Phys. Rev. D* 58 (1998), p. 023503. DOI: 10.1103/PhysRevD.58.023503. arXiv: astro-ph/9711102.
- [179] Varun Sahni and Li-Min Wang. “A New cosmological model of quintessence and dark matter.” In: *Phys. Rev. D* 62 (2000), p. 103517. DOI: 10.1103/PhysRevD.62.103517. arXiv: astro-ph/9910097.
- [180] L. Arturo Urena-Lopez and Tonatiuh Matos. “A New cosmological tracker solution for quintessence.” In: *Phys. Rev. D* 62 (2000), p. 081302. DOI: 10.1103/PhysRevD.62.081302. arXiv: astro-ph/0003364.
- [181] Je-An Gu and W-Y.P. Hwang. “Can the quintessence be a complex scalar field?” In: *Phys. Lett. B* 517 (2001), pp. 1–6. DOI: 10.1016/S0370-2693(01)00975-3. arXiv: astro-ph/0105099.
- [182] E. A. Cornell and C. E. Wieman. “Nobel Lecture: Bose-Einstein condensation in a dilute gas, the first 70 years and some recent experiments.” In: *Rev. Mod. Phys.* 74 (3 Aug. 2002), pp. 875–893. DOI: 10.1103/RevModPhys.74.875. URL: <https://link.aps.org/doi/10.1103/RevModPhys.74.875>.
- [183] R. Ruffini and S. Bonazzola. “System of Self-Gravitating Particles in General Relativity and the Concept of an Equation of State.” In: *Phys. Rev.* 187 (1969), pp. 1767–1783.
- [184] Juan Barranco et al. “Are black holes a serious threat to scalar field dark matter models?” In: *Phys. Rev. D* 84 (2011), p. 083008. DOI: 10.1103/PhysRevD.84.083008. arXiv: 1108.0931 [gr-qc].
- [185] Miguel Alcubierre et al. “ ℓ -Boson stars.” In: *Class. Quant. Grav.* 35.19 (2018), 19LT01. DOI: 10.1088/1361-6382/aadcb6. arXiv: 1805.11488 [gr-qc].
- [186] Yi-Fu Cai et al. “Quintom Cosmology: Theoretical implications and observations.” In: *Physics Reports* 493 (Sept. 2009). DOI: 10.1016/j.physrep.2010.04.001.
- [187] Licia Verde, Tommaso Treu, and Adam G. Riess. “Tensions between the early and late Universe.” In: *Nature Astronomy* 3 (Sept. 2019), pp. 891–895. DOI: 10.1038/s41550-019-0902-0. arXiv: 1907.10625 [astro-ph.CO].

- [188]Edmund J. Copeland, M. Sami, and Shinji Tsujikawa. “Dynamics of dark energy.” In: Int. J. Mod. Phys. D 15 (2006), pp. 1753–1936. DOI: 10.1142/S021827180600942X. arXiv: hep-th/0603057 [hep-th].
- [189]Elías Castellanos et al. “Scalar Field as a Bose-Einstein Condensate?” In: JCAP 11 (2014), p. 034. DOI: 10.1088/1475-7516/2014/11/034. arXiv: 1310.3319 [gr-qc].
- [190]Elías Castellanos et al. “Scalar field as a Bose-Einstein condensate in a Schwarzschild–de Sitter spacetime.” In: Int. J. Mod. Phys. D 26.04 (2016), p. 1750032. DOI: 10.1142/S0218271817500328. arXiv: 1512.03118 [gr-qc].
- [191]D. M. Scolnic et al. “The Complete Light-curve Sample of Spectroscopically Confirmed SNe Ia from Pan-STARRS1 and Cosmological Constraints from the Combined Pantheon Sample.” In: Astrophys. J. 859.2 (2018), p. 101. DOI: 10.3847/1538-4357/aab9bb. arXiv: 1710.00845 [astro-ph.CO].
- [192]Rafael C Nunes et al. “Cosmological parameter analyses using transversal BAO data.” In: Monthly Notices of the Royal Astronomical Society 497.2 (July 2020), pp. 2133–2141. ISSN: 0035-8711. DOI: 10.1093/mnras/staa2036. eprint: <https://academic.oup.com/mnras/article-pdf/497/2/2133/33565883/staa2036.pdf>. URL: <https://doi.org/10.1093/mnras/staa2036>.
- [193]Michele Moresco et al. “A 6% measurement of the Hubble parameter at $z \sim 0.45$: direct evidence of the epoch of cosmic re-acceleration.” In: JCAP 05 (2016), p. 014. DOI: 10.1088/1475-7516/2016/05/014. arXiv: 1601.01701 [astro-ph.CO].
- [194]Juan Magana et al. “The Cardassian expansion revisited: constraints from updated Hubble parameter measurements and type Ia supernova data.” In: Mon. Not. Roy. Astron. Soc. 476.1 (2018), pp. 1036–1049. DOI: 10.1093/mnras/sty260. arXiv: 1706.09848 [astro-ph.CO].
- [195]Nisha Godani. “Wormhole solutions in $f(R, T)$ gravity.” In: 94, 101774 (July 2022), p. 101774. DOI: 10.1016/j.newast.2022.101774.
- [196]Francisco S. N. Lobo and Miguel A. Oliveira. “Wormhole geometries in $f(R)$ modified theories of gravity.” In: 80.10, 104012 (Nov. 2009), p. 104012. DOI: 10.1103/PhysRevD.80.104012. arXiv: 0909.5539 [gr-qc].
- [197]Christian G. Böhrer, Tiberiu Harko, and Francisco S. N. Lobo. “Wormhole geometries in modified teleparallel gravity and the energy conditions.” In: 85.4, 044033 (Feb. 2012), p. 044033. DOI: 10.1103/PhysRevD.85.044033. arXiv: 1110.5756 [gr-qc].
- [198]Ibrar Hussain et al. “Phantom traversable wormholes in modified teleparallel gravity.” In: Chinese Journal of Physics 77 (June 2022), pp. 1253–1268. DOI: 10.1016/j.cjph.2022.03.004.
- [199]H. M. Manjunatha and S. K. Narasimhamurthy. “The wormhole model with an exponential shape function in the Finslerian framework.” In: Chinese Journal of Physics 77 (June 2022), pp. 1561–1578. DOI: 10.1016/j.cjph.2021.11.031.

- [200]Soo-Jong Rey. “Axion dynamics in wormhole background.” In: 39.10 (May 1989), pp. 3185–3189. DOI: 10.1103/PhysRevD.39.3185.
- [201]Stefano Andriolo et al. “Axion wormholes with massive dilaton.” In: arXiv e-prints, arXiv:2205.01119 (May 2022), arXiv:2205.01119. arXiv: 2205.01119 [hep-th].
- [202]S. Krasnikov. “A Traversable wormhole.” In: Phys. Rev. D 62 (2000). [Erratum: Phys. Rev. D 76,109902(2007)], p. 084028. DOI: 10.1103/PhysRevD.62.084028, 10.1103/PhysRevD.76.109902. arXiv: gr-qc/9909016 [gr-qc].
- [203]Matt Visser, Sayan Kar, and Naresh Dadhich. “Traversable wormholes with arbitrarily small energy condition violations.” In: Phys. Rev. Lett. 90 (2003), p. 201102. DOI: 10.1103/PhysRevLett.90.201102. arXiv: gr-qc/0301003 [gr-qc].
- [204]Francisco S. N. Lobo. “Energy conditions, traversable wormholes and dust shells.” In: Gen. Rel. Grav. 37 (2005), pp. 2023–2038. DOI: 10.1007/s10714-005-0177-x. arXiv: gr-qc/0410087 [gr-qc].
- [205]Francisco S. N. Lobo. “Phantom energy traversable wormholes.” In: Phys. Rev. D 71 (2005), p. 084011. DOI: 10.1103/PhysRevD.71.084011. arXiv: gr-qc/0502099 [gr-qc].
- [206]Francisco S. N. Lobo. “Stability of phantom wormholes.” In: Phys. Rev. D 71 (2005), p. 124022. DOI: 10.1103/PhysRevD.71.124022. arXiv: gr-qc/0506001 [gr-qc].
- [207]John L. Friedman, Kristin Schleich, and Donald M. Witt. “Topological censorship.” In: Phys. Rev. Lett. 71 (1993). [Erratum: Phys. Rev. Lett. 75,1872(1995)], pp. 1486–1489. DOI: 10.1103/PhysRevLett.75.1872, 10.1103/PhysRevLett.71.1486. arXiv: gr-qc/9305017 [gr-qc].
- [208]C. Armendariz-Picon, Viatcheslav F. Mukhanov, and Paul J. Steinhardt. “A Dynamical solution to the problem of a small cosmological constant and late time cosmic acceleration.” In: Phys. Rev. Lett. 85 (2000), pp. 4438–4441. DOI: 10.1103/PhysRevLett.85.4438. arXiv: astro-ph/0004134 [astro-ph].
- [209]J. Garriga and A. Vilenkin. “Solutions to the cosmological constant problems.” In: Phys. Rev. D 64 (2001), p. 023517. DOI: 10.1103/PhysRevD.64.023517. arXiv: hep-th/0011262 [hep-th].
- [210]Dragan Huterer and Michael S. Turner. “Probing the dark energy: Methods and strategies.” In: Phys. Rev. D 64 (2001), p. 123527. DOI: 10.1103/PhysRevD.64.123527. arXiv: astro-ph/0012510 [astro-ph].
- [211]Celia Escamilla-Rivera et al. “Tension between SN and BAO: current status and future forecasts.” In: JCAP 1109 (2011), p. 003. DOI: 10.1088/1475-7516/2011/09/003. arXiv: 1103.2386 [astro-ph.CO].
- [212]Eyal A. Kazin et al. “The WiggleZ Dark Energy Survey: improved distance measurements to $z = 1$ with reconstruction of the baryonic acoustic feature.” In: Mon. Not. Roy. Astron. Soc. 441.4 (2014), pp. 3524–3542. DOI: 10.1093/mnras/stu778. arXiv: 1401.0358 [astro-ph.CO].

- [213]P. A. R. Ade et al. “Planck 2013 results. XVI. Cosmological parameters.” In: Astron. Astrophys. 571 (2014), A16. DOI: 10.1051/0004-6361/201321591. arXiv: 1303.5076 [astro-ph.CO].
- [214]H. G. Ellis. “Ether flow through a drainhole - a particle model in general relativity.” In: J. Math. Phys. 14 (1973), pp. 104–118. DOI: 10.1063/1.1666161.
- [215]K. A. Bronnikov. “Scalar-tensor theory and scalar charge.” In: Acta Phys. Polon. B4 (1973), pp. 251–266.
- [216]F. Abe. “Gravitational Microlensing by the Ellis Wormhole.” In: Astrophys. J. 725 (2010), pp. 787–793. DOI: 10.1088/0004-637X/725/1/787. arXiv: 1009.6084 [astro-ph.CO].
- [217]M. S. Morris and K. S. Thorne. “Wormholes in space-time and their use for interstellar travel: A tool for teaching general relativity.” In: Am. J. Phys. 56 (1988), pp. 395–412. DOI: 10.1119/1.15620.
- [218]Francisco S. N. Lobo. “Exotic solutions in General Relativity: Traversable wormholes and ‘warp drive’ spacetimes.” In: Classical and Quantum Gravity Research, 1-78, (2008), Nova Sci. Pub. ISBN 978-1-60456-366-5. 2007. arXiv: 0710.4474 [gr-qc].
- [219]Matt Visser. Lorentzian wormholes: From Einstein to Hawking. 1995. ISBN: 1563966530, 9781563966538.
- [220]Tonatiuh Matos and Dario Nunez. “Rotating scalar field wormhole.” In: Class. Quant. Grav. 23 (2006), pp. 4485–4496. DOI: 10.1088/0264-9381/23/13/012. arXiv: gr-qc/0508117 [gr-qc].
- [221]Edward Teo. “Rotating traversable wormholes.” In: Phys. Rev. D 58 (1998), p. 024014. DOI: 10.1103/PhysRevD.58.024014. arXiv: gr-qc/9803098 [gr-qc].
- [222]Vladimir Dzhunushaliev et al. “Wormhole solutions with a complex ghost scalar field and their instability.” In: Phys. Rev. D 97.2 (2018), p. 024002. DOI: 10.1103/PhysRevD.97.024002. arXiv: 1710.01884 [gr-qc].
- [223]Vladimir Dzhunushaliev et al. “Non-singular solutions to Einstein-Klein-Gordon equations with a phantom scalar field.” In: JHEP 07 (2008), p. 094. DOI: 10.1088/1126-6708/2008/07/094. arXiv: 0805.3211 [gr-qc].
- [224]Panagiota Kanti, Burkhard Kleihaus, and Jutta Kunz. “Wormholes in Dilatonic Einstein-Gauss-Bonnet Theory.” In: Phys. Rev. Lett. 107 (2011), p. 271101. DOI: 10.1103/PhysRevLett.107.271101.
- [225]Eloy Ayon-Beato, Fabrizio Canfora, and Jorge Zanelli. “Analytic self-gravitating Skyrmions, cosmological bounces and AdS wormholes.” In: Phys. Lett. B752 (2016), pp. 201–205. DOI: 10.1016/j.physletb.2015.11.065.

- [226]Matt Visser and Carlos Barcelo. “Energy conditions and their cosmological implications.” In: Proceedings, 3rd International Conference on Particle Physics and the Early Universe. 2000, pp. 98–112. DOI: 10.1142/9789812792129_0014. arXiv: gr-qc/0001099 [gr-qc].
- [227]Elisabetta Majerotto, Domenico Sapone, and Luca Amendola. “Supernovae Type Ia data favour negatively coupled phantom energy.” In: Submitted to: Phys. Rev. D (2004). arXiv: astro-ph/0410543 [astro-ph].
- [228]Richard H. Price. “Negative mass can be positively amusing.” In: American Journal of Physics 61.3 (1993), pp. 216–217. DOI: 10.1119/1.17293. eprint: <https://doi.org/10.1119/1.17293>. URL: <https://doi.org/10.1119/1.17293>.
- [229]Ignacio Olabarrieta et al. “Critical Behavior in the Gravitational Collapse of a Scalar Field with Angular Momentum in Spherical Symmetry.” In: Phys. Rev. D 76 (2007), p. 124014. DOI: 10.1103/PhysRevD.76.124014. arXiv: 0708.0513 [gr-qc].
- [230]John David Jackson. Classical Electrodynamics. Wiley, 1998. ISBN: 9780471309321.
- [231]J. A. Gonzalez, F. S. Guzman, and O. Sarbach. “Instability of wormholes supported by a ghost scalar field. I. Linear stability analysis.” In: Class. Quant. Grav. 26 (2009), p. 015010. DOI: 10.1088/0264-9381/26/1/015010. arXiv: 0806.0608 [gr-qc].
- [232]Charles W. Misner and David H. Sharp. “Relativistic Equations for Adiabatic, Spherically Symmetric Gravitational Collapse.” In: Physical Review 136.2B (Oct. 1964), pp. 571–576. DOI: 10.1103/PhysRev.136.B571.
- [233]J. A. Gonzalez, F. S. Guzman, and O. Sarbach. “Instability of wormholes supported by a ghost scalar field. II. Nonlinear evolution.” In: Class. Quant. Grav. 26 (2009), p. 015011. DOI: 10.1088/0264-9381/26/1/015011. arXiv: 0806.1370 [gr-qc].

Bibliography

- [1] Raul E. Angulo and Oliver Hahn. “Large-scale dark matter simulations.” In: Living Reviews in Computational Astrophysics 8.1, 1 (Dec. 2022), p. 1. DOI: 10.1007/s41115-021-00013-z. arXiv: 2112.05165 [astro-ph.CO].
- [2] Julio F. Navarro, Carlos S. Frenk, and Simon D. M. White. “The Structure of Cold Dark Matter Halos.” In: 462 (May 1996), p. 563. DOI: 10.1086/177173. arXiv: astro-ph/9508025 [astro-ph].
- [3] A. Burkert. “Fuzzy Dark Matter and Dark Matter Halo Cores.” In: 904.2, 161 (Dec. 2020), p. 161. DOI: 10.3847/1538-4357/abb242. arXiv: 2006.11111 [astro-ph.GA].
- [4] Andrea V. Macciò et al. “Creating a galaxy lacking dark matter in a dark matter-dominated universe.” In: 501.1 (Feb. 2021), pp. 693–700. DOI: 10.1093/mnras/staa3716. arXiv: 2010.02245 [astro-ph.GA].
- [5] Pieter van Dokkum et al. “A trail of dark-matter-free galaxies from a bullet-dwarf collision.” In: 605.7910 (May 2022), pp. 435–439. DOI: 10.1038/s41586-022-04665-6. arXiv: 2205.08552 [astro-ph.GA].
- [6] Lam Hui. “Wave Dark Matter.” In: 59 (Sept. 2021). DOI: 10.1146/annurev-astro-120920-010024. arXiv: 2101.11735 [astro-ph.CO].
- [7] Yong Shi et al. “A Cuspy Dark Matter Halo.” In: 909.1, 20 (Mar. 2021), p. 20. DOI: 10.3847/1538-4357/abd777. arXiv: 2101.01282 [astro-ph.GA].
- [8] Ivan de Martino et al. “Dark Matters on the Scale of Galaxies.” In: Universe 6.8 (Aug. 2020), p. 107. DOI: 10.3390/universe6080107. arXiv: 2007.15539 [astro-ph.CO].
- [9] Giuseppina Battaglia and Carlo Nipoti. “Stellar dynamics and dark matter in Local Group dwarf galaxies.” In: Nature Astronomy (May 2022). DOI: 10.1038/s41550-022-01638-7. arXiv: 2205.07821 [astro-ph.GA].
- [10] Vivian Poulin et al. “Early Dark Energy can Resolve the Hubble Tension.” In: 122.22, 221301 (June 2019), p. 221301. DOI: 10.1103/PhysRevLett.122.221301. arXiv: 1811.04083 [astro-ph.CO].

- [11] Luz Ángela Garca, Leonardo Castañeda, and Juan Manuel Tejeiro. “A novel early dark energy model.” In: 84, 101503 (Apr. 2021), p. 101503. DOI: 10.1016/j.newast.2020.101503.
- [12] Alon E. Faraggi and Marco Matone. “The geometrical origin of dark energy.” In: European Physical Journal C 80.11, 1094 (Nov. 2020), p. 1094. DOI: 10.1140/epjc/s10052-020-08665-6. arXiv: 2006.11935 [hep-th].
- [13] B. Czerny et al. “Dark Energy Constraints from Quasar Observations.” In: Acta Physica Polonica A 139.4 (Apr. 2021), pp. 389–393. DOI: 10.12693/APhysPolA.139.389. arXiv: 2011.12375 [astro-ph.CO].
- [14] P. Suresh Kumar, Pankaj, and Umesh Kumar Sharma. “Quintessence model of Tsallis holographic dark energy.” In: 96, 101829 (Oct. 2022), p. 101829. DOI: 10.1016/j.newast.2022.101829.
- [15] Arindam Das et al. “Two-component scalar and fermionic dark matter candidates in a generic $U(1)_X$ model.” In: Physics Letters B 829, 137117 (June 2022), p. 137117. DOI: 10.1016/j.physletb.2022.137117. arXiv: 2202.01443 [hep-ph].

List of Figures

3.1	Single scalar field representative cases of Table 3.1. Top panel: All solid lines correspond to the classical positive self-interaction fiducial cosmology [22]. The dashed lines are the reference CDM Universe, which happens to coincide in this plot to the Higgs and axion (GUT, Planck) cases. Bottom panel: Equations of state. While the positive self-interaction classical field undergoes three phases, the negative self-interaction case undergoes two and the Higgs field remains indistinguishable from standard cold dark matter.	33
3.2	Evolution of the density parameters of the Universe. All solid lines correspond to the scalar field dark matter model with two components and the dashed lines represent the rest of the density contributions. Top panel: Two scalar field model I. Bottom panel: Two scalar field model II.	34
3.3	Variability of our model, labeled as 2SFDM, with respect to Planck 2018 (PL18) and Riess et al (R19) H_0 priors in (a) the case I (Classical+Higgs) for $\eta = 0.25$ and (b) for $\eta = 0.75$. (c) The variability in the case II (axion+Higgs) for $\eta = 0.25$ and (d) for $\eta = 0.75$. The values for the free model parameters are in Table 3.1	36
3.4	Quantification (Eq. 3.43) of the shift on the slope of the variability (see Figure 3.3) of the models I and II. The maximum relative difference in the density fraction between $\eta = 0.25$ and $\eta = 0.75$ for the Classical + Higgs model computed with R19 relative to the density fraction of the two scalar field model, occurs at $a \sim 10^{-6}$ (red solid line); while for the axion + Higgs model this occurs earlier, at $a \sim 10^{-12}$ (blue dashed line). This behavior is the same for the density fraction when PL18 is used and shows that the model I is more sensitive to the current energy density fraction than the model II.	37

3.5	Constraints from z_{eq} and N_{eff} within 1σ for the two scalar field Model I. η is the fraction of the classical field with respect to the total dark matter components. The crosshatched region that appears on the right side of all figures, represents the values of the scalar field parameters not allowed by the z_{eq} constrain. The green and yellow bands are the allowed regions from the N_{eff} constrain, (3.48), at $a_{\text{n/p}}$ and a_{nuc} respectively. The red band is the region of the parameter space that is consistent with both the z_{eq} and N_{eff} , throughout BBN, constraints.	41
3.6	The Galaxy Stellar Mass Function (GSMF) at $z = 0$. The black solid line represents the GSMF as in the Eq. (3.64) [125]; the black dotted line, in contrast, shows the GSMF with the baryon suppression at EoR; the violet points are the observations of the GAMA project for $z < 0.06$ [137].	49
3.7	Stellar-to-halo mass relation modified according to equation 3.70 with the baryonic suppression (dashed lines) in comparison with the SHMR without the baryonic suppression [125]	50
3.8	short	55
3.9	short	56
3.10	short	57
3.11	short	58
4.1	Evolution of the w Eq. (4.32) as a function of the scale factor, a , in the quintessence model. The dashed vertical lines represent the valid interval of the solution; the left line is taken as the value $a_i = 0.1$ and the right limit a_e is defined as the scale factor when the fast oscillation regime ceases, Eq. (4.36).	74
4.2	Evolution of the fractions Ω_i of the energy density of each component of the Universe i as a function of the scale factor, a , in the quintessence model. Different components are represented with different line styles as labeled in the legend.	75
4.3	The 68% confidence level (C.L.), 95% CL. and 99.7% regions inferring from the parametric CSFDE (4.37) using CC (yellow C.L), Pantheon supernovae + BAO (red C.L) and the full sample (CC+SN+BAO) (green C.L).	76
4.4	Gravitational potential produced by a point mass $\sim -1/r$ (left panel) and by the exotic distribution presented in this work (right panel), see section 4.3.4. In both cases a test particle with vanishing angular momentum is considered.	82

4.5	Normalized density at the throat for a $\ell = 1$ wormhole. The first sphere represents the $m = \pm 1$ contribution while the center sphere corresponds to the $m = 0$ contribution.	88
4.6	Ghost field and the corresponding density for the original Ellis wormhole.	90
4.7	Kretschmann scalar and effective potential, $V_{eff} = L^2/R^2 + \kappa$ for a massive particle propagating on the reflection-symmetric Ellis wormhole.	91
4.8	Solitonic profile for the 0-wormhole, for $\Lambda \in [0.5, 4.0]$, and $\omega = 0$	100
4.9	Density profile for the 0-wormhole, for $\Lambda \in [0.5, 4.0]$ and $\omega = 0$	101
4.10	Metric coefficients for $\Lambda \in [0.5, 4.0]$ and $\omega = 0$	101
4.11	Ricci and Kretschmann scalars for $\Lambda \in [0.5, 4.0]$ and $\omega = 0$	102
4.12	Density profile, curvature scalar and metric function a for the 0-wormhole, $\Lambda = 0.7$ and $\omega = 0.1, 0.2, 0.3$	103
4.13	Metric function $a(r)$, density profile $\hat{\rho}$ and R_s, K scalars for $\ell \geq 0, \Lambda = 1.0$ and $\omega = 0$	104
4.14	Mass function $M(r)$ for the parameters $\ell \geq 0, \Lambda = 1$ and $\omega = 0$	105
4.15	Metric function a for different values of the parameters ℓ, ω and Λ	105
4.16	Embedding of the different ℓ -wormholes, for $\Lambda = 1.5, \omega = 0$. The complete embedding diagram is obtained by rotating this figure about the z axis. In the enlarged picture we underline the change of the value of the throat radius for the given values of ℓ	107
4.17	Effective potential for time-like (left panel) and null geodesics (right panel) for $L = \sqrt{\frac{1}{10}}$	108
4.18	Different $\ell = 0$ (top), $\ell = 1$ (middle) and $\ell = 2$ (bottom) geodesics for $\kappa = 1, \omega = 0, \Lambda = 1.5, L = \sqrt{1/10}$. On the left we plot the motion of the particle in the embedding surface of the wormhole and on the right the value of E and V_{eff}	109
4.19	Two different $\ell = 1$ geodesics for $\kappa = 0, L = \sqrt{1/10}, \omega = 0, \Lambda = 1.5$. We plot the motion with their corresponding E (right y-axis) and u^r (left y-axis) values.	110

List of Tables

3.1	Single and double scalar field models described in section 3.2.2. Top: Three single scalar field models with their free parameters and the validity intervals of m and λ parameters. The representative cases are the specific values of the parameters explored in this work. Bottom: Three possible double scalar field models with the corresponding combinations at the description. The k constrain is referred to the minimum fraction of the energy density of the lightest field at the present ($a = 1$) with respect to the total dark matter density. The viability of the models is reported in the last column with two different meanings in the viability term for the single models: the (i) column refers to the BBN+ z_{eq} analysis described on section 3.2.4, while the column (ii) denotes the viability from a relic density point of view for the scalar field models reported at the cited works.	27
3.2	Values of β and M_{hm} of Eq. (3.72) given by [6] for several non-cold dark matter models taken from [48]. The γ parameter was fixed as $\gamma = 5$	53
4.1	Background best fits values for Eq. (4.37). For CC, Pantheon+BAO and CC+Pantheon+BAO.	79
4.2	Central values of the field χ_ℓ and metric functions R and a for several values of $\Lambda = 0.5, 0.7, 1.0, 4.0$ and $\ell = 0, 1, 2$ with $\omega = 0$	96
4.3	Central values of the field χ_ℓ and metric functions R and a for several values of ω and $\ell = 0, 1, 2$ with $\Lambda = 0.7$	97
4.4	Total mass values for ℓ -wormholes with $\Lambda = 1$, $\omega = 0$ and $\ell = 0, 1, 2, 3$	98

Glossary

This section is useful to all the definitions used in this Thesis work.

- ALP Axion-like particles. They are generally light, weakly interacting and have a coupling to electromagnetism.
- BAO Baryon Acoustic Oscillations. A pattern of imprints in the density distribution of the clusters of galaxies.
- BBN Big Bang Nucleosynthesis. Predicts the amount of light nuclei during the early Universe. It depends critically on the density of baryons at the time of nucleosynthesis.
- CANDELS-W Cosmic Assembly Near-infrared Deep Extragalactic Legacy / Wide survey.
- CC Cosmic Chronometers sample. Measurements obtained by comparing the stellar evolution of galaxies with low star formation that provide model independent measurements for H , the Hubble parameter.
- CDM Cold Dark Matter (see DM). Called cold because it moves slowly compared with the speed of light.
- CP CP symmetry. The combination of Charge symmetry and Parity symmetry.
- CRESST Cryogenic Rare Event Search with Superconducting Thermometers. Searches dark matter using detectors which are operated at extremely low temperatures.
- CSFDE Complex Scalar Field Dark Energy. A model of complex scalar field that mimics dark energy.
- DAMA An observatory whose main activity field is the investigation on Dark Matter particles in the galactic halo.
- DFSZ Dine-Fischler-Srednicki-Zhitnitsky axion.

- DM Dark Matter, called dark because it does not interact with any force except the gravitational. It constitutes the 27% amount of content in the Universe.
- EoR Epoch of Reionization. The period in the history of the Universe during which the predominantly neutral intergalactic medium was ionized.
- ETHOS Effective Theory of structure formation. An alternative self-interacting dark matter model.
- FLRW Friedman-Lemaître-Robertson-Walker metric. Used to describe the cosmic spacetime based on the cosmological principle.
- FUV Far UV Luminosity Function. Represents a useful tool to quantify the effects of the cluster environment on star formation from the “passive” galaxies.
- GSMF Galaxy Stellar Mass Function. Describe the number density of galaxies as a function of their stellar mass.
- GUT Grand Unified Theory. An extension of the SM that can address several of its issues.
- HMF Halo Mass Function. Describe the number density of dark matter haloes as a function of their mass.
- HUDF Hubble Ultra Deep Field. The view of nearly 10 000 galaxies.
- IceCube IceCube Neutrino Observatory. A detector designed to observe the cosmos from deep within the South Pole ice.
- ISM Interstellar medium. The matter and radiation that exist in the space between the star systems in a galaxy.
- JWST James Webb Space Telescope. Launched on 2021, will find the first galaxies that formed in the early universe.
- KGE Klein Gordon equation. The first relativistic wave equation.
- KSVZ Kim-Shifman-Vainshtein-Zakharov axion.
- ΛCDM Lambda Cold Dark Matter. The standard model of cosmology

- LSW Light-Shining-through-Walls experiment. The search experiments for weakly interacting slim particles (WIMPs) with the smallest model dependence.
- M_{vir} Virial Mass. The mass of a gravitationally bound system such a dark matter halo.
- MCMC Markov Chain Monte Carlo. Methods for sampling from probability distributions using Markov chains.
- N_{eff} Effective number of neutrino species. A parametrisation of the relativistic energy density of the Universe in units of one neutrino in the instantaneous decoupling limit.
- nCDM non Cold Dark Matter models. A set of models motivated by particle physics theories.
- OHD Observational Hubble-Parameter Data (see CC).
- OSQAR Optical Search for QED Vacuum Bifringence, Axions and Photon Regeneration. An experiment at CERN that searches for axions.
- PandaX Particle and Astrophysical Xenon Experiments. A series of experimental projects that utilizes Xenon detectors to search for elusive dark matter particles.
- PL18 Planck Collaboration 2018 prior of H_0 . Based on the Λ CDM model.
- PQ PecceiQuinn mechanism. A proposal for the resolution of the strong CP problem.
- PQWW Peccei-Quinn-Weinberg-Wilczek axion.
- QCD Quantum Chromodynamics. The theory of the strong interaction between quarks mediated by gluons.
- QFT Quantum Field Theory. A fundamental theory that describes all particles of the Standard Model of particle physics.
- R19 Riess 2019 prior of H_0 . Based on the measurement of the Cepheid amplitudes.
- SFDM Scalar Field Dark Matter. Model that assumes the existence of a scalar field with a $\sim 10^{-22}$ eV that can have observable consequences in the formation of cosmological structure.

- SFG Star-forming Galaxies. Trace the prime formation epoch of today's massive disk and elliptical galaxies.
- SFH Galaxy Star Formation Histories. Describe how stars formed over time and space.
- SFR Star Formation Rate. Describes the total mass of stars formed per year.
- SHAM Sub-Halo Abundance Matching. A technique used to connect galaxies to their host dark matter haloes.
- SM Standard Model of particle physics. Our best understanding of how the baryonic particles and three of the forces are related to each other.
- SNeIa Supernovae Type Ia. An observational category of Supernovae, a very luminous stellar explosion that presents silicon lines and no helium that have very homogeneous spectral and photometric properties.
- WIMP Weakly Interacting Massive Particle. The candidate for particle dark matter from the Λ CDM cosmology.
- z_{eq} Redshift at the epoch of matter-radiation equality.

